Circulation and water properties under the landfast ice in the southeastern Laptev Sea

Master's Thesis

University of Bremen

Postgraduate Programme Environmental Physics

Marie Schlenker

Date of birth: May 26, 1992

Matriculation number: 2634650

Supervisors: Dr. Markus Janout, Prof. Dr. Torsten Kanzow

1. Examiner: Prof. Dr. Torsten Kanzow

2. Examiner: Prof. Dr. Monika Rhein

Submission: Bremen, October 27, 2017

Abstract

The vast and shallow region under the landfast ice in the southeastern Laptev Sea has been scarcely explored due to its remoteness and restricted accessibility. Therefore, the understanding of the winter circulation on the inner Laptev Sea shelf is largely incomplete. Oceanographic moorings and conductivity-temperature-depth (CTD) surveys from winter expeditions in 1998/99, 2008, 2009, and 2012 are analyzed to characterize the under-ice circulation and water properties on the shelf, especially with respect to spatial and temporal variability. Satellite-based sea ice concentration data and meteorological reanalysis data are used to interpret the observed hydrographic conditions in the context of the physical processes which determine the circulation under the landfast ice on the southeastern Laptev Sea shelf in winter. The results of this study suggest that the circulation and water properties on the southeastern Laptev Sea shelf are strongly influenced by the annual freeze-thaw cycle. The presence of an immobile landfast ice cover in winter has been identified to largely decouple the water column on the inner shelf from atmospheric forcing. Landfast ice also provides an additional boundary layer to the water column that likely interacts with tidal dynamics, possibly contributing to the observed amplification of the dominant semidiurnal M2 tide and damping of the semidiurnal S2 tide during the ice-covered season. Pronounced spatial differences of hydrographic conditions have been observed under the landfast ice, which are likely influenced by the presence of immobile landfast ice, polynya openings, as well as preconditioning of the inner Laptev Sea shelf during the previous summer by the variable extent of the Lena River freshwater plume and possible heat accumulation in the interior water column. Observed positive temperature anomalies in the bottom layer and in the surface layer just above the pycnocline on the inner Laptev Sea shelf may represent storage of overwintered heat due to the pronounced stratification under the landfast ice. Additionally, the winter circulation and hydrography in the southeastern Laptev Sea have been identified to exhibit considerable variability on short timescales. Detailed oceanographic time series have shown extreme semidiurnal fluctuations of salinity and temperature of approximately 15 psu and 0.5 °C in the pycnocline near the landfast ice edge. These fluctuations have been linked to the complex interactions of enhanced lateral and vertical gradients of water properties with tidal dynamics, wind forcing, and thermohaline forcing in response to a polynya event in April 2012.

Table of contents

1. Introduction

The Arctic region is currently undergoing significant climatic induced changes, including rapidly rising water temperatures, decreasing sea ice cover, destabilization of landfast ice, and sea level rise, possibly with major implications for global climate through changes in ocean circulation and marine ecosystems, as well as for human activities (Hinzmann et al. 2005). These alterations clearly manifest themselves in the sensitive Arctic shelf environments (Kassens et al. 1999). The vast and shallow Siberian shelves comprise a large part of the total Arctic shelf area (see Fig. 1) and significantly influence the hydrographic and bio-chemical conditions of the Arctic Ocean through sea ice processes and river water influxes (Pavlov and Pavlov 1999, Wegner et al. 2017). The seasonally ice covered region has been identified as a major ice formation and export site of the Arctic Ocean (Alexandrov et al. 2000, Kern et al. 2005, Rosén et al. 2015). Moreover, it is characterized by enormous freshwater input from the Eurasian continent by some of the largest rivers on Earth (Dai and Trenberth 2002), which amounts to more than 80 % of the total Arctic Ocean freshwater input (Peterson et al. 2002, Holland et al. 2006). Nevertheless, the Siberian shelves are among the least studied regions on Earth due to their remoteness and restricted accessibility (Janout and Lenn 2014).

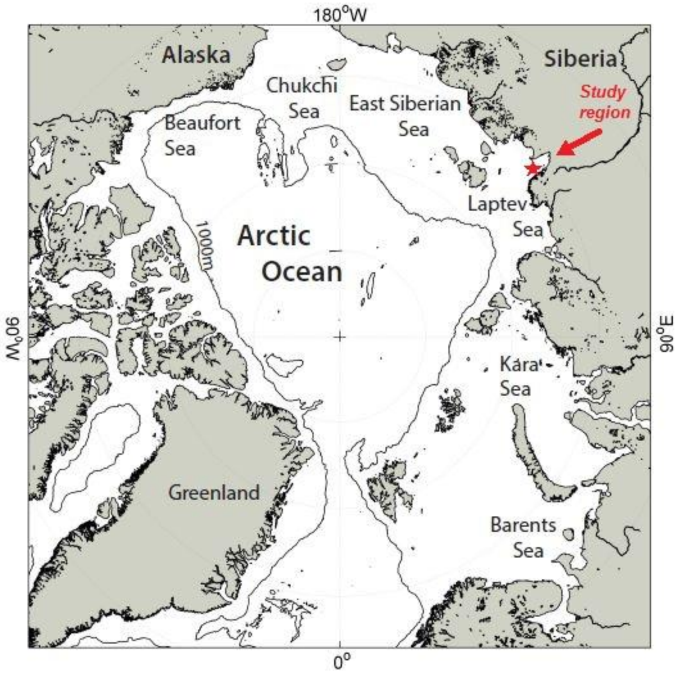

Fig. 1: Map of the Arctic Ocean and its shelf seas including the 1000 m bathymetry contour based on the International Bathymetric Chart of the Arctic Ocean (IBCAO) (Jakobsson et al. 2008). The study region is highlighted with a red star.

Among the Siberian shelves, the Laptev Sea, located between the Kara Sea and the East Siberian Sea (see Fig. 1), represents one of the most important sites of net ice production and export in the Arctic Ocean (Dmitrenko et al. 2009, Krumpen et al. 2011, Rosén et al. 2015) and forms the beginning of the wind-driven Transpolar Drift System, which transports sea ice across the Arctic Ocean towards Fram Strait (Pfirman et al. 1997, Mysak 2001). From October to June, large areas of the Laptev Sea are ice-covered (Bareiss and Görgen 2005).

The inner Laptev Sea shelf is characterized by the presence of an extensive landfast ice cover in winter, i.e. sea ice that is immobile and attached to the coast or the sea floor (Bareiss and Görgen 2005, Itkin et al. 2015, Selyuzhenok et al. 2015), which develops over the time period from October to January (Selyuzhenok et al. 2015). Flaw polynyas, large, persistent areas of open water and thin ice created by offshore winds, frequently form along the landfast ice edge (Bareiss and Görgen 2005), which is located at relatively shallow water depths between 25 and 30 m (Dmitrenko et al. 2005). These stretches of open water are part of the system of flaw polynyas known as the Great Siberian Polynya and can be up to 200 km wide (Dmitrenko et al. 2005, Dmitrenko et al. 2010a). While the landfast ice cover has been described to act as an immobile lid which effectively decouples the inner shelf from the atmosphere through inhibiting heat and momentum transfer (Itkin et al. 2015, Weingarter et al. 2017), flaw polynyas have been identified as regions of significant ocean-atmosphere interaction (Smith et al. 1990, Krumpen et al. 2011). Extremely low air temperatures and associated surface heat loss within a flaw polynya significantly impact the energy budget of the underlying water column (Gutjahr et al. 2016) and lead to enhanced thermodynamic ice formation at the surface (Dmitrenko et al. 2010a). The newly formed ice crystals, known as frazil ice, are transported toward the downwind edge of the polynya, where they accumulate and form a thin layer of ice and water slurry called grease ice, which thickens and finally consolidates as it drifts further offshore (Martin and Kauffman 1981). Salt ions are excluded from the almost pure ice matrix and are released into the underlying shelf water in a process called brine rejection, which causes a local salinity increase in the upper water column and consequently weakens the vertical density stratification (Ivanov and Golovin 2007). Therefore, hydrographic conditions and physical processes on the Laptev Sea shelf are strongly influenced by seasonal sea ice formation and dynamics (Dmitrenko et al. 2002, Bareiss and Görgen 2005, Dmitrenko et al. 2005, Krumpen et al. 2011, Janout et al. 2013, Janout et al. 2016, Janout et al. 2017).

In addition, oceanographic conditions on the inner Laptev Sea shelf, comprising the shallower southern region proximal to the Lena Delta with an average water depth of about 20 to 30 m (Dmitrenko et al. 2008), are significantly impacted by the powerful Lena River freshwater discharge, which controls stratification and influences coastal landfast ice processes (Bareiss et al. 1999, Dmitrenko et al. 2010b, Janout and Lenn 2014, Janout et al. 2016, Fofonova et al. 2015). Moreover, the Lena River transports sediment, suspended particulate matter, and colored dissolved organic matter onto the Laptev Sea shelf, which regulates light and nutrient availability, and consequently biological productivity in this region (Pfirman et al. 1997, Stedmon et al. 2011, Wegner et al. 2013). The Lena River discharge amounts to roughly 539 km³ annually and exhibits a strong seasonal variability with a peak in June and very moderate discharge during winter (Dmitrenko et al. 2005, Dmitrenko et al. 2008, Thibodeau et al. 2014, Fofonova et al. 2015).

Previous studies focusing on the oceanic current regime on the Laptev Sea shelf are scarce. In particular, the circulation under the vast landfast ice cover of the inner shelf has been neglected in previous research due to limited field observations. Consequently, the understanding of the local hydrography of the shelf in winter is largely incomplete. Diagnostic hydrodynamic calculations by Pavlov and Pavlov (1999) suggest that the circulation in the Laptev Sea is mainly driven by the large-scale surface salinity distribution, with winter currents velocities generally below 5 – 8 cm/s. Modeled geostrophic currents on the inner Laptev Sea shelf, close to the Lena River Delta, are directed to the north, implying an offshore winter circulation regime in this area (Pavlov and Pavlov 1999). In addition to the prominent local characteristics of Lena River freshwater discharge and sea ice dynamics, wind forcing as well as tidal dynamics, have been investigated as possible processes influencing the under-ice circulation in the Laptev Sea (Dmitrenko et al. 2002, Dmitrenko et al. 2012, Janout et al. 2013, Janout and Lenn 2014, Fofonova et al. 2014, Fofonova et al. 2015, Janout et al. 2016).

Wind forcing over the Laptev Sea is determined by the balance between the sea level pressure associated with the Siberian High and the Icelandic Low, which mainly control the atmospheric circulation over the Siberian Arctic (Johnson and Polyakov 2001). During anticyclonic circulation phases, the Siberian High is well developed and the Icelandic Low is suppressed, resulting in prevailing winds over the Laptev Sea oriented towards the East Siberian Sea. In contrast, cyclonic circulation phases are associated with a weak Siberian High and a strong Icelandic Low, leading to prevailing winds over the Laptev Sea tending towards the Eurasian Basin of the Arctic Ocean (Johnson and Polyakov 2001). Dmitrenko et al. (2010c) have discussed the role of intrusions of warmer and more saline Atlantic-derived waters to the Laptev Sea shelf, which may occur as a result of offshore, upwelling-favorable wind conditions and have provided some indications for wind-driven under-ice transport. These findings are complemented by the observations of Janout et al. (2013), who identified a series of onshore bottom-intensified flow events along a relic submarine river valley in the Laptev Sea during upwelling-favorable winds and ice drift in winter. Janout et al. (2013) have highlighted the importance of wind-driven under-ice currents and have suggested a simplified two-dimensional two-layered ocean, where near bottom, barotropic response flow compensates for offshore surface Ekman transport. However, the relative importance of advection for the hydrographic conditions and physical processes on the inner Laptev Sea is still not clear and needs further investigation.

Tidal oscillations are the response of the oceans to the gravitational pull of celestial bodies other than the Earth, especially the Sun and the Moon (e.g. Schwiderski 1980). Tidal processes play an important role in the dynamics of the shelf circulation in the Laptev Sea in all seasons (Dmitrenko et al. 2002). Due to its shallow character and topographic features, the inner Laptev Sea shelf is very sensitive to tidally-induced mixing through dissipation of turbulent kinetic energy (Janout and Lenn 2014, Fofonova et al. 2014, Fofonova et al. 2015). Tidal signals can be interpreted as the superposition of periodic tidal components with frequencies associated with the movement of celestial bodies exerting the force (Schwiderski 1980). Contribution from the principal lunar semidiurnal tidal constituent, M2, has been identified to be the most important on the Laptev Sea shelf, followed by the principal solar semidiurnal tidal constituent, S2 (Chen et al. 2009, Lenn et al. 2011, Janout and Lenn 2014). While recent studies have focused on the influence of tides for the Laptev Sea shelf in summer (Fofonova et al. 2014, Fofonova et al. 2015), the impact of tidal dynamics on the winter circulation on the inner Laptev Sea shelf is still largely unexplored. Arctic tides have been identified to be sensitive to the presence of an ice cover (Kowalik and Proshutinsky 1994, Kagan et al. 2008, Lenn et al. 2011). Dmitrenko et al. (2002) have found an amplification of M2 tidal currents in the pycnocline under the landfast ice. This finding is supported by the results of Janout and Lenn (2014), which indicate a general enhancement of M2 tides under the sea ice cover throughout the Laptev Sea shelf. Janout and Lenn (2014) have inferred that reductions in the sea ice extent may significantly impact tidal processes and water column structure in the Laptev Sea, leading to decreasing predictability of hydrographic conditions, especially on the inner shelf. Therefore, further investigations into the interactions of sea ice cover and oceanic current regime are necessary to understand the impacts of a changing climate.

The aim of this study is to contribute to the understanding of the under-ice hydrography and oceanic current regime of the vast and largely unexplored region under the landfast ice on the southeastern Laptev Sea shelf, especially with respect to spatial and temporal variability. Oceanographic data obtained under the landfast ice on the inner Laptev Sea shelf during various winter expeditions conducted within the framework of the joint Russian-German research project “Laptev Sea System” in 1998/99, 2008, 2009, and 2012, respectively, (see Fig. 2) forms the basis of this investigation. The inner Laptev Sea shelf is strongly influenced by the annual freeze-thaw cycle, which controls the phasing and duration of the Lena River discharge and landfast ice (Dmitrenko et al. 2002, Selyuzhenok et al. 2015). Consequently, the circulation and hydrography under the landfast ice is expected to exhibit considerable variations between different seasons. To investigate the oceanographic seasonality on the southeastern Laptev Sea shelf, a yearlong current velocity record measured under the landfast ice in 1998/99 (see Fig. 2) complemented with satellite-based sea ice concentration data (see Cavalieri et al. 2008) is analyzed with respect to changes of the characteristics of the current regime over the annual freeze-thaw cycle. Tidal harmonic analysis and comparisons of the non-tidal residual current signal to ECMWF near-surface wind reanalysis data (see Berrisford et al. 2011, Dee et al. 2011) are performed to determine the influence of different drivers of the oceanic current regime over the course of the seasonal cycle. As the freshwater influx from the Lena River Delta and the presence of the landfast ice cover are anticipated to significantly influence the circulation on the inner Laptev Sea shelf in winter, spatial variations of the under-ice current regime and water properties with respect to the distance from the Lena River Delta and the landfast ice edge are examined in detail with the help of detailed oceanographic time series from short-term moorings as well as ship-based CTD measurements at various locations on the southeastern Laptev Sea shelf obtained in winter 2008, 2009, and 2012, respectively (see Fig. 2). Additionally, oceanographic conditions under the landfast ice on the southeastern Laptev Sea shelf are expected to exhibit pronounced temporal variability within the ice-covered season associated with tidal dynamics, advective processes of non-tidal origin, and polynya activity. In order to provide some insights into the interactions between different forcing mechanisms of the under-ice circulation, detailed short-term time series of water properties and current velocities obtained under the landfast ice in winter 2012 (see Fig. 2) are analyzed with respect to cause-and-effect relationships between different physical processes and observed oceanographic conditions on the southeastern Laptev Sea shelf in winter.

2. Data and methods

This section introduces the datasets and methods which are applied in this study to investigate the circulation and water properties under landfast ice in the southeastern Laptev Sea.

2.1 Data

Analyzed datasets include oceanographic data, sea ice concentration data, and meteorological data.

2.1.1 Oceanographic data

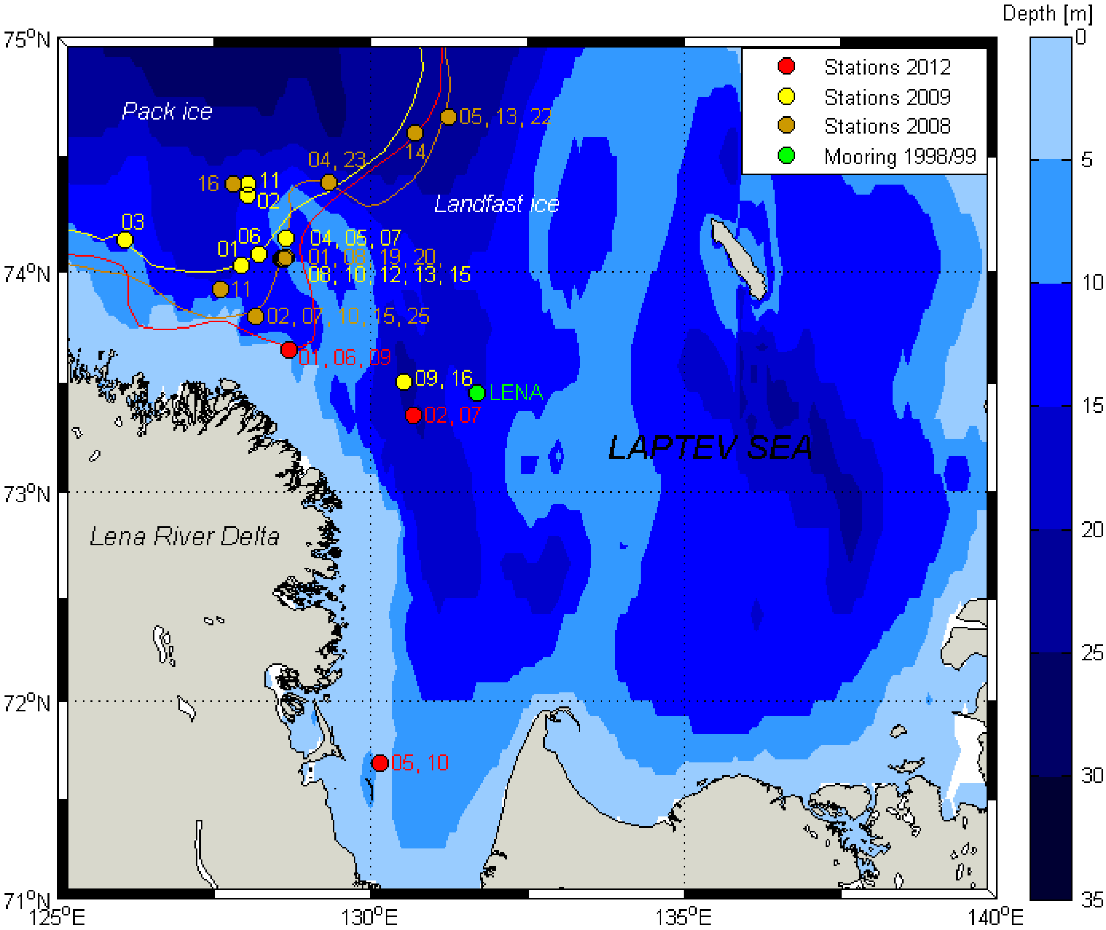

Fig. 2: Map of study region, including information on bathymetry, the location of the landfast ice edge, and the location of oceanographic measurements analyzed in this study. The bathymetry is based on the International Bathymetric Chart of the Arctic Ocean (IBCAO) (Jakobsson et al. 2008). Red circles indicate the position of the three ice camps (North, Central, South) at which oceanographic datasets were obtained during TRANSDRIFT XX in winter 2012. Yellow and brown circles show the locations of oceanographic stations during TRANSDRIFT XV in winter 2009 and TRANSDRIFT XIII in winter 2008, respectively. The green circle shows the location of the yearlong mooring LENA deployed during 1998/99. The red, yellow, and brown lines indicate the position of the landfast ice edge based on operational sea ice charts provided by the Arctic and Antarctic Research Institute (AARI) (Mahoney et al. 2008, Selyuzhenok et al. 2015) for the first week of April in 2012, 2009, and 2008, respectively. For better legibility, the position of the landfast ice edge in 1998/99 is omitted as Mooring LENA is located at considerable distance from the landfast ice edge.

This study focuses on the analysis of oceanographic datasets collected under the landfast ice during several expeditions within the framework of the joint Russian-German research project “Laptev Sea System” to investigate the characteristics of the circulation and hydrography on the inner Laptev Sea shelf during the ice-covered season. More specifically, current velocity data gathered from a yearlong mooring deployed east of the Lena Delta in 1998/99 as well as temperature, salinity, and current velocity data obtained at three different ice camps during the winter expedition TRANSDRIFT XX in 2012 are analyzed in detail (see Fig. 2). Comparisons with oceanographic datasets from the winter expeditions TRANSDRIFT XV and XIII in 2009 and 2008, respectively, are used to establish a broader context with regard to general features of the circulation under the landfast ice in the Laptev Sea. It should be noted that the expeditions were conducted with varying research objectives and that oceanographic data acquisition was not specifically designed to study the under-ice circulation on the shelf. Some of the datasets have already been partly employed in other scientific studies associated with different research foci (see Dmitrenko et al. 2002, Dmitrenko et al. 2010a, Dmitrenko et al. 2010c, Dmitrenko et al. 2012, Kirillov et al. 2013, Wegner et al. 2017). Nevertheless, the analyzed datasets constitute a unique source of information about the hydrography and current regime under the vast landfast ice cover of the Laptev Sea shelf, a major Arctic shelf with significant influence on the entire Arctic Ocean.

2.1.1.1 Mooring LENA, 1998/99

The oceanographic bottom station LENA was deployed on the Laptev Sea shelf northeast of the Lena River Delta at the geographic position 73°27'36.0"N, 131°42'39.6"E at a water depth of approximately(~) 24 m during leg 1b of the cruise ARK-XIV on August 2, 1998 (see Fig. 2). It was recovered in the following year, on August 30, 1999, during the expedition TRANSDRIFT VII. The mooring was equipped with a 300 kHz upward looking Teledyne-RDI Workhorse Sentinel Acoustic Doppler Current Profiler (ADCP), which measured vertical profiles of water current velocities using the Doppler effect of sound waves, which are transmitted at a constant frequency into the water column and scattered back with a slightly different frequency from particles moving with the water column (Brumley et al. 1991, Joseph 2014). The ADCP was located close to the seafloor and measured current velocity profiles in 30 min time-averaged ensembles with a vertical bin size of 1.5 m and 30 pings per ensemble. Reliable data was obtained for the depth interval from ~ 8.5 m to 20.5 m. The initial accuracy of the current velocity measurements is ±0.5 % of the velocity and ±0.5 cm s^{-1}. The standard compass accuracy is ±2°.

2.1.1.2 TRANSDRIFT XX, 2012

During the winter expedition TRANSDRIFT XX, from March 19 to April 24, 2012, three helicopter-based ice camps were installed on the landfast ice cover in the Laptev Sea: Camp North (stations TI1201, TI1206, TI1209), Camp Central (stations TI1202, TI1207), and Camp South (stations TI1205, TI12010) (see Fig. 2). At Camp North and Camp Central, two autonomous short-term oceanographic moorings were deployed under the landfast ice. The design of the moorings was typical of ice-covered regions. Figure 3 shows the layout of the two short-term moorings. The anchor and rope with the attached instruments were lowered through a drill hole with a large diameter. The upper end of the rope was fixed on the ice surface.

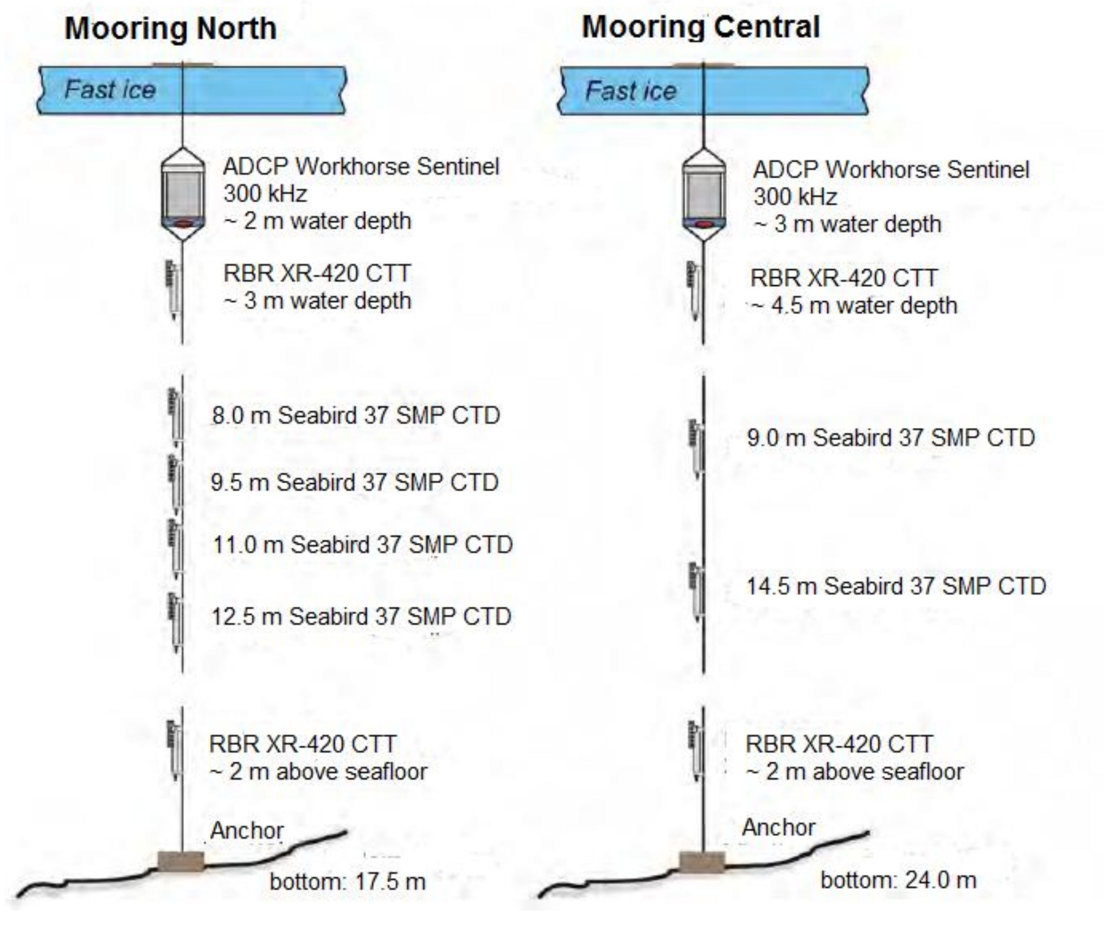

Fig. 3: Scheme of short-term moorings deployed under the landfast ice at Camp North (station TI1201) and Camp Central (station TI1202) during TRANSDRIFT XX in winter 2012.

The mooring at Camp North, henceforth Mooring North, was deployed at the geographical position 73°38’34.6’’N, 128°43’40.0’’E at a water depth of ~ 17.5 m close to the landfast ice edge on March 26, 2012 and retrieved on April 17, 2012 (see Fig. 2). The mooring was equipped with a 300 kHz downward looking Teledyne-RDI Workhorse Sentinel ADCP, two RBR XR-420 Conductivity-Temperature-Turbidity (CTT) units, and four Seabird Electronics (SBE) 37 SMP Conductivity-Temperature-Depth (CTD) sensors (see Fig. 3). All sensors were calibrated prior to and recalibrated after the expedition. The ADCP was positioned at ~ 2 m water depth and measured current velocity profiles in 15 min time-averaged ensembles with a vertical bin size of 0.5 m and 350 pings per ensemble. The depth interval covered by the ADCP ranged from ~ 4.5 m to the deepest reliable measurements at ~ 14 m. The accuracy of the current velocity measurements is ±0.5 % of the velocity and ±0.5 cm s^{-1}. The standard compass accuracy is ±2°. CTD instruments measure the hydrographic properties conductivity, temperature, and pressure by default. Depth measurements are derived from observations of hydrostatic pressure. Seawater salinity is inferred from electrical conductivity (Topham and Perkin 1988). The deployed RBR XR-420 CTT units measure the parameter turbidity instead of hydrostatic pressure. The CTT units were located at ~ 3 m and 15.5 m water depth, respectively. The sampling interval was programmed to one minute for the upper RBR instrument and to two minutes for the lower RBR instrument. According to the calibration by the manufacturer prior to the expedition, the accuracy of the temperature obtained by the RBR units is ±0.002 °C and the accuracy of the conductivity is ±0.003 mS cm^{-1}. The SBE 37 SMP CTD sensors were mounted at water depths of ~ 8.0 m, 9.5 m, 11.0 m, and 12.5 m, respectively, and operated at a sampling interval of one minute. The accuracies of the SBE 37 SMP CTD sensors are ±0.002 °C for the temperature, ±0.003 mS cm^{-1} for the conductivity, and ±0.1 % of the full scale range for the pressure. The instruments at the mooring at Camp North operated without failure, except for the SBE 37 SMP CTD unit at ~ 12.5 m water depth, which measured extremely low conductivity values for the time period from the initial deployment to March 29, which are assumed to be unreliable.

The mooring at Camp Central, henceforth Mooring Central, was deployed east of the Lena River Delta at the geographical position 73°20’29.9’’N, 130°40’13.8’’E at a water depth of ~ 24 m on March 27 and recovered on April 12. The mooring was equipped with a 300 kHz downward looking Teledyne-RDI Workhorse Sentinel ADCP, two RBR XR-420 CTT units, and two SBE 37 SMP CTD sensors (see Fig. 3). All sensors were calibrated prior to and recalibrated after the expedition. Accuracies of the equipment are the same as denoted for Mooring North. The ADCP was mounted at ~ 3 m water depth and recorded current velocity profiles in 15 min time-averaged ensembles with a vertical bin size of 0.5 m and 400 pings per ensemble, covering the depth interval from ~ 4 m to 14 m. The CTD sensors operated at sampling intervals of 1 min and were positioned at water depths of ~ 4.5 m, 9 m, 14.5 m, and 22 m, respectively (see Fig. 3). The conductivity measurements of the two SBE 37 SMP CTD sensors at 9 m and 14.5 m failed, most likely due to accumulation of slush-ice in the conductivity cell. Hence, the conductivity data obtained from these two sensors are rejected in the data analysis. All other instruments operated without failures.

In addition to the short-term moorings, episodically repeated CTD profile measurements under the landfast ice were carried out at all three ice camps (see Fig. 2). The holes in the ice were drilled with a motor drill. To reduce measurement errors caused by ice crushing during drilling and sensor cooling due to very low air temperatures, the CTD instrument was given some time to adjust in the water and measurements were taken repeatedly. A pumped SEACAT Profiler SBE 19plus equipped was used to obtain measurements at ~ 10-15 cm vertical intervals. According to the calibration by the manufacturer prior to the expedition, the accuracies of the temperature and recalculated salinity measurements are ±0.002 °C and ±0.001 psu, respectively. Between March 26 and April 19, seven oceanographic stations were operated at the three different ice camps (see Table 1). Due to the extreme fluctuations in salinity and temperature over very short vertical distances, the observations from station TI1205 are assumed to be unreliable.

Table 1: Station list for CTD measurements obtained during TRANSDRIFT XX in winter 2012.

Station	Camp	Date	Longitude	Latitude	Depth [m]
TI1201	North	03/26/2012	128.678°E	73.657°N	17.5
TI1202	Central	03/27/2012	130.670°E	73.358°N	24.0
TI1205	South	04/04/2012	130.152°E	71.693°N	10.5
TI1206	North	04/10/2012	128.678°E	73.657°N	17.5
TI1207	Central	04/12/2012	130.670°E	73.358°N	24.0
TI1209	North	04/17/2012	128.678°E	73.657°N	17.5
TI1210	South	04/19/2012	130.152°E	71.693°N	10.5

2.1.1.3 TRANSDRIFT XV, 2009

During the winter expedition TRANSDRIFT XV, from March 15 to April 28, 2009, oceanographic measurements were conducted in the vicinity of the landfast ice edge to study the influence of polynyas on the hydrography and current regime of the inner Laptev Sea shelf. Two autonomous short-term moorings were installed under the landfast ice, which were both equipped with a 300 kHz downward looking Teledyne-RDI Workhorse Sentinel ADCP and four SBE 37 SM CTD sensors (see Fig. 4). All sensors were calibrated prior to and recalibrated after the expedition. Information on the installation process and the main characteristics of the deployed equipment has been provided in section 2.1.1.2. The first oceanographic mooring was deployed at Camp POLYNYA I at the geographical position 74°01'59.7''N, 127°56'05.6''E at a water depth of ~ 26.1 m on March 24 as part of station TI0901 (see Fig. 2). Due to ice rifting the mooring was recovered on April 2 and re-installed as Camp POLYNYA III at station TI0908 at the geographical position 74°03'28.5''N, 128°33'56.1''E at a water depth of ~ 23.4 m for the time period from April 8 to April 23 (see Fig. 2). The second mooring, initially deployed at station TI0904, was lost as a result of ice rifting.

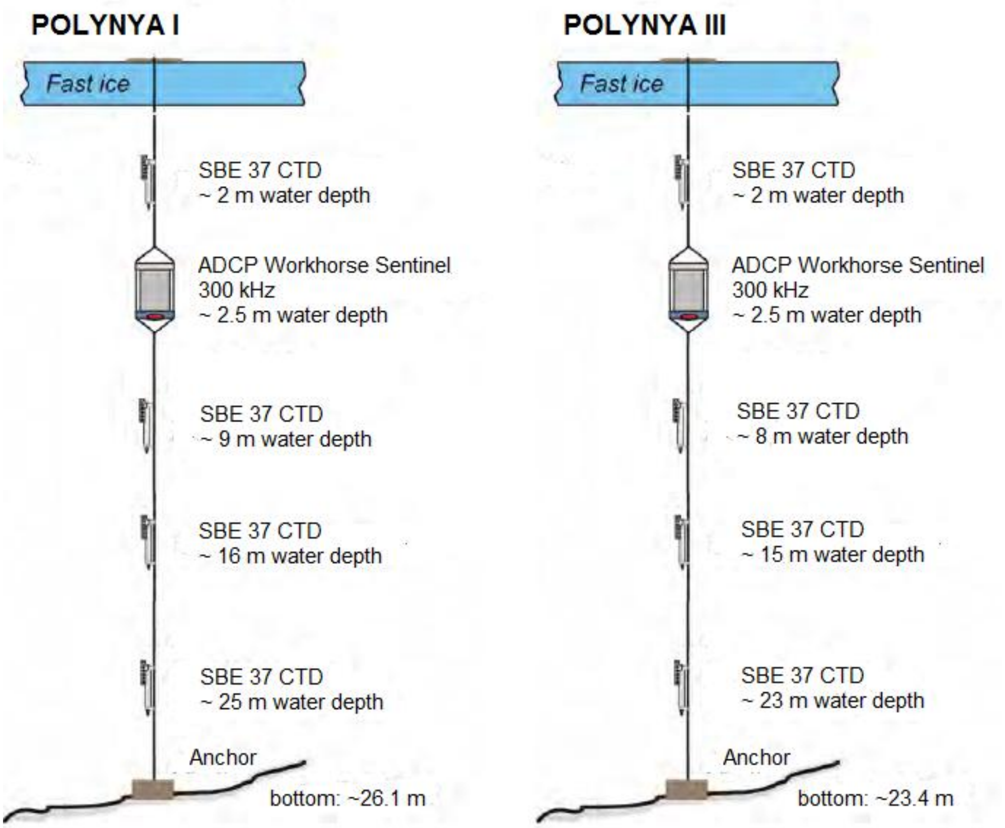

Fig. 4: Scheme of short-term moorings POLYNYA I (station TI0901) and POLYNYA III (station TI0908) deployed under the landfast ice during TRANSDRIFT XV in winter 2009.

Figure 4 shows the layout of the sub-ice bottom stations at Camp POLYNYA I and III. This study focuses on the current velocity measurements obtained at the two moorings. The accuracy of the current velocity measurements by the ADCPs is 0.5 % and ±0.5 cm s^{-1}. The current direction measurement accuracy is ±2°. At both stations, the ADCP was positioned at ~ 2.5 m water depth and measured current velocity profiles in 25 min time-averaged ensembles with a vertical bin size of 1 m and 100 pings per ensemble. The depth interval covered by the ADCP ranged from ~ 5.7 m to the deepest reliable measurements at ~ 20.7 m at Camp POLYNYA I, and from ~ 5.7 m to 19.7 m at Camp POLYNYA III.

Additionally, repeated vertical CTD measurements were carried out with a SBE 19plus probe in close vicinity of the landfast ice edge (see Fig. 2), using the same process as described in section 2.1.1.2. In total, 29 measurements were obtained at 15 different oceanographic stations (see Table 2). The accuracies of the temperature and salinity measurements are ±0.005 °C and ±0.001 ‰, respectively, according to the calibration by the manufacturer prior to the expedition.

Table 2: Station list for CTD measurements obtained during TRANSDRIFT XV in winter 2009.

Station	Camp	Date	Longitude	Latitude	Depth [m]
TI0901	POLYNYA I	03/24/2009	127.935°E	74.033°N	26.1
TI0902	-	03/26/2009	128.027°E	74.334°N	32.6
TI0903	-	03/26/2009	126.057°E	74.141°N	17.1
TI0904	POLYNYA II	03/27/2009	128.634°E	74.151°N	22.6
TI0905	POLYNYA II	04/01/2009	128.634°E	74.151°N	22.6
TI0906	POLYNYA I	04/02/2009	128.197°E	74.081°N	25.9
TI0907	POLYNYA II	04/03/2009	128.635°E	74.151°N	22.6
TI0908	POLYNYA III	04/08/2009	128.575°E	74.055°N	23.4
TI0909	-	04/14/2009	130.526°E	73.512°N	-
TI0910	POLYNYA III	04/14/2009	128.565°E	74.058°N	23.8
TI0911	-	04/15/2009	128.020°E	74.381°N	33.7
TI0912	POLYNYA III	04/15/2009	128.565°E	74.058°N	23.8
TI0913	POLYNYA III	04/21/2009	128.564°E	74.058°N	23.8
TI0915	POLYNYA III	04/23/2009	128.566°E	74.058°N	23.8
TI0916	-	04/23/2009	130.522°E	73.513°N	24.5

2.1.1.4 TRANSDRIFT XIII, 2008

During the expedition TRANSDRIFT XIII, from April 5 to May 5, 2008, five sub-ice oceanographic bottom stations were successfully deployed and recovered in close vicinity of the landfast ice edge (see Fig. 2), which were all equipped with a 300 kHz downward looking Teledyne-RDI Workhorse Sentinel ADCP and one or two SBE 37 CTD sensors. All sensors were calibrated prior to and recalibrated after the expedition. Information on the installation process and the main characteristics of the equipment can be found in section 2.1.1.2. This study focuses on current velocity measurements obtained at the five moorings in winter 2008. The deployed moorings had a similar layout, which is depicted in Figure 5. The ADCPs were mounted ~ 1 m under the ice cover and obtained current velocity profiles in 25 min time-averaged ensembles with a vertical bin size of 1 min and 60 pings per ensemble. The accuracy of the current velocity measurements by the ADCP is 0.5 % and ±0.5 cm s^{-1}. The current direction measurement accuracy is ±2°. Table 3 provides a list of the deployed sub-ice bottom stations, including their exact location, associated water depth, and the mounted equipment.

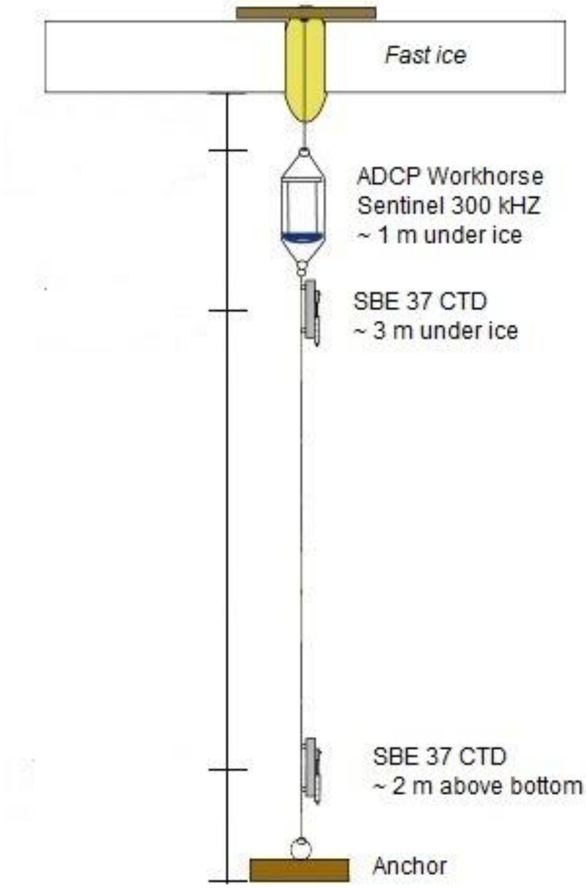

Fig. 5: Scheme of short-term moorings M08-1 (station TI0801), M08-2 (station TI0802), M08-3 (station TI0804), M08-4 (station TI0805), and M08-5 (station TI0808) deployed under the landfast ice during TRANSDRIFT XIII in winter 2008.

Repeated vertical CTD measurements were carried out with a SBE 19plus probe in close vicinity of the landfast ice edge (see Fig. 2) using the same process as described in section 2.1.1.2. In total, 60 measurements were obtained at 17 different oceanographic stations (see Table 4). The CTD probe was calibrated by the manufacturer prior to the expedition and initial accuracies of the temperature and salinity measurements are ±0.005 °C and ±0.001 ‰, respectively.

Table 3: List of sub-ice moorings deployed during TRANSDRIFT XIII in winter 2008.

Camp	Station	Date	Longitude	Latitude	Depth [m]	Equipment (and position in water column)
M08-1	TI0801	04/10/2008	128°37’52.1’’E	74°03’59.0’’N	24	ADCP (~2.5 m), two CTDs (~3 m , ~20 m)
M08-2	TI0802	04/11/2008	128°09'45.2"E	73°48'19.0"N	21	ADCP (~2 m), two CTDs (~3 m, ~20 m)
M08-3	TI0804	04/12/2008	129°19'10.2"E	74°23'21.3"N	19.8	ADCP (~2 m), two CTDs (~10 m, ~17 m)
M08-4	TI0805	04/14/2008	131°14'40.4"E	74°40'21.1"N	18	ADCP (~2 m), two CTDs (~3 m, ~17m)
M08-5	TI0808	04/16/2008	128°36'27.9"E	74°03'19.5"N	22.4	ADCP (~3 m), CTD (~17 m)

Table 4: Station list for CTD measurements obtained during TRANSDRIFT XIII in winter 2008.

Station	Camp	Date	Longitude	Latitude	Depth [m]
TI0801	M08-1	04/10/2008	128.631°E	74.066°N	24
TI0802	M08-2	04/11/2008	128.163°E	73.805°N	21
TI0804	M08-3	04/12/2008	129.320°E	74.389°N	19.8
TI0805	M08-4	04/14/2008	131.245°E	74.673°N	18
TI0807	M08-2	04/14/2008	128.163°E	73.805°N	-
TI0808	M08-5	04/16/2008	128.608°E	74.055°N	22.4
TI0810	M08-2	04/19/2008	128.162°E	73.805°N	21
TI0811	-	04/19/2008	127.581°E	73.928°N	24.7
TI0813	M08-4	04/21/2008	131.245°E	74.673°N	18.8
TI0814	-	04/21/2008	130.715°E	74.604°N	28.4
TI0815	M08-2	04/24/2008	128.162°E	73.805°N	20.7
TI0816	-	04/24/2008	127.786°E	74.381°N	33.8
TI0819	M08-5	04/28/2008	128.607°E	74.055°N	-
TI0820	M08-1	04/28/2008	128.631°E	74.066°N	22.9
TI0822	M08-4	04/29/2008	131.245°E	74.673°N	18.6
TI0823	M08-3	04/29/2008	129.320°E	74.390°N	20
TI0825	M08-2	05/04/2008	128.162°E	73.805°N	21.3

2.1.2 Sea ice concentration data

To investigate the link between oceanographic conditions and polynya activity, daily satellite-based sea ice concentration data provided by the National Snow and Ice Data Center on a polar stereographic grid with a cell size of 25 km x 25 km is used in this study. Information on sea ice concentration is derived from brightness temperature data obtained from the Nimbus-7 Scanning Multichannel Microwave Radiometer (SMMR), the Defense Meteorological Satellite Program (DMSP) F8, F11, and F13 Special Sensor Microwave Imager/Sounder (SSM/IS), and the F17 Special Sensor Microwave Imager/Sounder (SSM/IS) (Cavalieri et al. 2008). The brightness temperature is a measure of the emitted radiance received by the satellite, which is related to the kinematic temperature and emissivity properties of the emitting surface. Differences in the emissivity properties of areas of open water and ice-covered areas are used to infer sea ice concentrations (Spreen et al. 2008).

2.1.3 Meteorological data

To examine the relationship between hydrographic conditions, polynya activity, and meteorological conditions, the horizontal and meridional components of the wind, measured 10 m above sea level, are extracted at 6-hour time steps from the ERA-Interim global atmospheric reanalysis dataset provided on the European Centre for Medium Range Weather Forecasts (ECMWF) Public Database web interface for the southeastern Laptev Sea for the time period covered by the oceanographic datasets. Reanalysis data are based on a fixed data assimilation scheme combining observations from various sources onto a regularly spaced grid with the help of models that ingest all available observations at a fixed time step over the period being analyzed. This method provides a dynamically consistent estimate of the meteorological state of the system at each time step (Dee et al. 2011). The data assimilation system which is used to produce the ERA-Interim dataset is based on a 2006 release of the ECMWF's Integrated Forecast Model (IFS Cy31r2) and includes a 4-dimensional variational analysis with a 12-hour analysis window. The dataset has a horizontal spatial resolution of ~ 80 km on 60 vertical levels from the surface up to 0.1 hPa. Detailed information on the ERA-Interim dataset is provided by Dee et al. (2011) and Berrisford et al. (2011). The advantages and disadvantages of choosing the ERA-Interim dataset versus other reanalysis datasets for studies in the Arctic region have been discussed in previous studies, for example by Francis (2002), Jakobson et al. (2012), Lindsay et al. (2014), and Chaudhuri et al. (2014). In this study, the ERA-Interim reanalysis dataset is chosen for analysis because it has been found to show a good overall alignment with meteorological field observations. However, 10 m surface winds are likely to be slightly overestimated in the ERA-Interim dataset (Francis 2002, Chaudhuri et al. 2014).

2.2 Methods

The described oceanographic datasets are analyzed with respect to general patterns of the circulation and water properties under the landfast ice in the southeastern Laptev Sea, as well as their respective spatial and temporal variability. Information on sea ice concentrations and wind velocities, measured 10 m above sea level, are used for interpretation of the observed variations of the under-ice hydrography and current regime.

All data is subject to careful screening for potentially incorrect measurements, and unreliable data is excluded from further analysis in order to obtain scientifically meaningful results. Data processing and analysis is performed using the numerical computing environment MATLAB.

2.2.1 Current velocity records

In order to identify the main characteristics of the under-ice oceanic current regime at the different mooring locations, information about current velocities are condensed by averaging over depth and time and by identifying the respective principal current ellipses. Moreover, the obtained current velocity records are dismantled into tidal and non-tidal components and compared to sea ice concentration and near-surface wind data in order to obtain information about the main drivers of the under-ice circulation.

2.2.1.1 Current direction and magnitude

Current velocity records acquired at the different mooring locations include information on zonal and meridional current velocities at different water depths at regular time intervals over the respective observation periods. To provide an overview of the temporal changes of current directions and magnitudes, current velocities obtained at different water depths at the same point in time are averaged over the entire depth range, resulting in depth-averaged current velocity time series.

The resulting depth-averaged current velocity records are used as input for the identification of the respective principal current ellipse with the help of the MATLAB function PRINCAX, developed by Signell (2000) and based on Emery and Thompson (1998). The principal current ellipse is characterized by the orientation and the magnitude of its major and minor axes (see Fig. 6). It provides information on the main direction and magnitude of current variability at the respective mooring locations. The orientation of the current ellipse is provided in degrees to north (see Fig. 6).

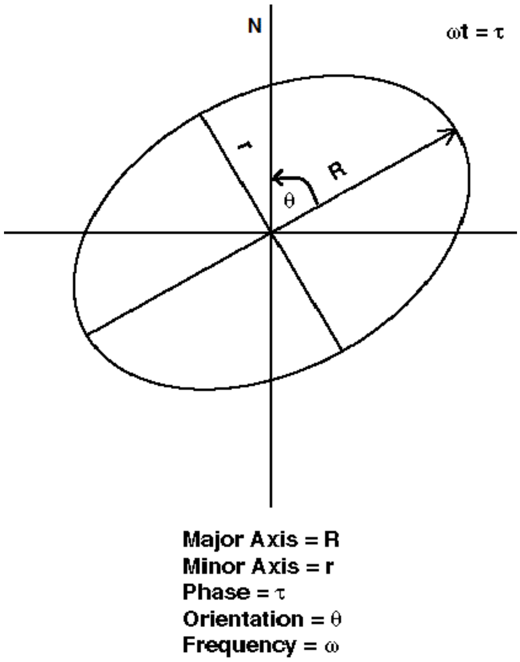

Fig. 6: Scheme of principal current ellipse (Naval Postgraduate School 2017, modified). The orientation of the principal current ellipse is specified as the angle between the major axis and geographic north.

In order to acquire information on spatial variations of the oceanic current regime with depth, observed current velocities at different water depths are averaged over time, resulting in vertical profiles of mean current velocities. For the yearlong current velocity record obtained at Mooring LENA, the time series is divided into different seasons, based on satellite-derived sea ice concentration data, and mean current velocities are computed for the individual periods to investigate seasonal variability. To study the response of the oceanic current regime to a polynya event in April 2012, current velocities obtained for different depths at Mooring North are extracted and averaged for the respective time period.

Error estimates for the mean current velocities at the different water depths are based on the formulation of the standard error of the mean, SE_μ:

$$SE_\mu = \frac{\sigma_x}{\sqrt{n}}$$

, where σ_x is the population standard deviation and n is the number of independent observations (Thomson and Emery 2014). Since the population standard deviation, σ_x, and the number of independent observations, n, are unknown, they have to be estimated.

In order to obtain an estimate of the population standard deviation, σ_x, the sample standard deviation, s, of the respective current velocity record is calculated with the help of the standard statistics toolbox of MATLAB. To obtain an estimate of the number of independent observations, the dependency between consecutive measurements within the respective current velocity time series needs to be investigated. The autocorrelation function, which is based on a lagged correlation of a function with itself, is used to infer the number of dependent consecutive measurements within the respective time series (Thomson and Emery 2014). In this study, autocorrelation functions are calculated with the help of MATLAB's standard statistics toolbox. Below a threshold value of 0.1 for the autocorrelation, measurements are assumed to be independent of one another. Based on this assumption, the number of consecutive dependent measurements for the different moorings is depicted in Table 5. To obtain the number of independent measurements, these values are divided by the total number of individual measurements in the respective time series.

Table 5: Number of consecutive dependent current velocity measurements in the records obtained at the different oceanographic moorings analyzed in this study. Results are based on the computation of the respective autocorrelation function and the assumption that below a threshold value of 0.1 for the autocorrelation measurements are independent of one another.

Mooring	Number of consecutive dependent measurements
LENA	40
ice-covered season	60
break-up season	33
ice-free season	39
Central	15
North	16
polynya event	15
POLYNYA I	14
POLYNYA III	35
M08-1	10
M08-2	14
M08-3	11
M08-4	10
M08-5	9

2.2.1.2 Tidal harmonic analysis

Tides are the periodic rise and fall of the sea surface due to the spatially varying gravitational attraction forces of celestial bodies other than the Earth, especially of the Sun and the Moon, as the Earth rotates on its axis (e.g. Schwiderski 1980). The tidally forced elevation of the sea surface results in a current response, which can significantly affect the oceanic current regime. In the case of tides in coastal seas, the influence of the tide-generating forces on the oceanic current regime is largely indirect, as coastal tides are driven by ocean tides (Bowden 1983).

Nevertheless, tidal variability is often the largest signal in an oceanographic time series in coastal waters (Schwiderski 1980). In order to separate tidal from non-tidal components of the signal, classical tidal harmonic analysis can be performed. The method is based on the modeling of the tidal forcing as the sum of a finite set of sinusoids at specific frequencies associated with the movement of celestial bodies exerting the gravitational force (Schwiderski 1980, Pawlowicz et al. 2002). A detailed discussion of tidal harmonic analysis can be found in Godin (1972).

In this study, T_TIDE, a package for tidal harmonic analysis with error estimates implemented in MATLAB, is used to analyze the tidal signal in the current velocity records obtained at Mooring LENA, Mooring Central, and Mooring North (see Fig. 2). It provides information about the ratio of the tidal variability to the total variability in the respective time series. Moreover, it identifies the tidal constituents present in the data record, including their frequency, amplitude, and phase, as well as the associated 95 % confidence intervals and the signal-to-noise ratio. The results are presented in the form of tidal current ellipses for each constituent, characterized by the magnitude of the major and minor axes, the orientation of the ellipse (provided in degrees to north), and the constituent phase (see Fig. 6). Based on this information, a prediction of associated tidal current velocities is created. Detailed information on the T_TIDE package is provided by Pawlowicz et al. (2002).

In order to obtain an overview of the tidal influence on the oceanic current regime at the different moorings, the respective depth-averaged current velocity time series are used as input for the tidal harmonic analysis. Furthermore, more detailed investigations are performed in order to acquire information on the vertical structure of the tidal influence as well as temporal changes of the tidal influence. In the case of Mooring Central and Mooring North, tidal harmonic analysis is performed using current velocity data obtained at individual water depths as input, resulting in vertical profiles of the tidal influence. The yearlong current velocity record at Mooring LENA is divided into 29-day overlapping time segments, necessary to resolve a lunar month, to identify temporal changes in the tidal dynamics. Tidal harmonic analysis is performed using current velocity information obtained at individual water depths over the individual time segments as input, yielding a time series of the vertical structure of the tidal influence at Mooring LENA.

2.2.1.3 Residual currents

Since tidal variability can only account for part of the total variability in the observed current velocity records at the different moorings, zonal and meridional components of the residual currents are calculated as the difference between the original depth-averaged time series and the predicted tidal signal. In order to identify the drivers of the residual current regime, resulting current velocity time series are compared to near-surface wind components (see Berrisford et al. 2011, Dee et al. 2011) as well as satellite-derived sea ice concentration data (see Cavalieri et al. 2008). To facilitate the comparison, a 24-hour low-pass Butterworth filter is applied to the residual current velocity records, removing potential leftover tidal signals (Roberts and Roberts 1978).

2.2.2 Salinity and temperature measurements

In order to provide an overview of the water properties under the landfast ice on the southeastern Laptev Sea shelf, vertical salinity and temperature profiles obtained at different measurement locations during the winters 2008, 2009, and 2012 are analyzed with respect to the main characteristics of the water column structure as well as spatial and temporal changes of the hydrographic conditions. Moreover, temperature and salinity time series obtained at Mooring North in winter 2012 are used for the detailed investigation of the temporal variability of water properties in the vicinity of the landfast ice edge and its relationship to the oceanic current regime.

2.2.2.1 Vertical salinity and temperature profiles

In order condense information on the general vertical structure of hydrographic conditions under the landfast ice on the inner Laptev Sea shelf, CTD casts are averaged if more than one reliable CTD profile was measured at the same station. Furthermore, information about salinity and temperature distributions are presented in 1 m depth-averaged intervals. Vertical salinity and temperature profiles obtained at the same location at different points in time are displayed as individual pieces of information to enable the investigation of temporal changes of the vertical distribution of water properties.

Dmitrenko et al. (2010a) have identified supercooling of water masses, i.e. the lowering of the water temperature below the freezing point without ice formation, near the landfast ice edge in the southeastern Laptev Sea. Furthermore, temperature inversions in the bottom layer, which significantly exceed the respective freezing points of seawater, have been discussed to occur on the inner Laptev Sea shelf (Dmitrenko et al. 2010c). Therefore, temperature profiles analyzed in this study are compared to the respective freezing temperatures of seawater at the associated in-situ salinities in order to identify potentially supercooled as well as anomalously warm water masses. Freezing temperatures are calculated with the help of a standard algorithm by Fofonoff and Millard (1983) implemented in MATLAB by Greene (2012).

2.2.2.2 Salinity and temperature time series

Detailed salinity and temperature records obtained at Mooring North and Mooring Central in winter 2012 are analyzed with respect to temporal changes in the water properties under the landfast ice the southeastern Laptev Sea shelf. The salinity and temperature time series are compared to information on current velocities to investigate the relationship between observed water properties and the oceanic current regime under the landfast ice. Since the hydrographic conditions at Mooring North indicate great temporal variability, information on the temporal development of the vertical structure of the water column is highly desirable. Salinity and temperature observations from the individual CTD sensors at ~ 3 m, 8 m, 9.5 m, 11 m, 12.5 m, and 15.5 m water depth are linearly interpolated using a standard interpolation tool in MATLAB, resulting in a time series of vertical distribution of salinity and temperature at Mooring North.

2.2.2.3 Brunt-Väisälä frequency

The Brunt-Väisälä frequency, or buoyancy frequency, is the natural frequency of oscillation of a parcel of water when displaced vertically from its level of equilibrium. It can be used as a measure of the stability of the water column and is approximated by

$$N \cong \sqrt{-\frac{g}{\rho_0}\frac{d\rho}{dz}}$$

, where g = 9.81 m s^{-1} is the acceleration due to gravity, $\frac{d\rho}{dz} \leq 0$ is the vertical in-situ density gradient (z-direction upward) and ρ_0 is a reference density (Thomson and Emery 2014). If $N^2 > 0$, a vertically displaced water parcel will be accelerated towards its initial position, resulting in vertical oscillations of the water parcel. In this case, the vertical stratification of the water column is said to be stable. If $N^2 < 0$, a vertically displaced water parcel is accelerated away from its initial position and the stratification is unstable (Bowden 1983).

In this study, the Brunt-Väisälä frequency is calculated with the help of the CSIRO Seawater Library implemented in MATLAB (Morgan and Pender 2003). The temperature and salinity time series obtained from the individual CTD sensors at Mooring North are used as input to the MATLAB function, resulting in a time series of Brunt-Väisälä frequency squared (N^2) at the respective mid-depths. The results are displayed as a time series of linearly interpolated profiles of N^2, showing the temporal development of the stratification of the water column.

3. Results

The results of this study include an overview of the general characteristics of the current regime and its seasonal variability on the inner Laptev Sea shelf based on observations of current velocities from the yearlong Mooring LENA, deployed on the Laptev Sea shelf northeast of the Lena River Delta from August 2, 1998 to August 30, 1999 (see Fig. 2). The current regime under the landfast ice during the ice-covered season is investigated in detail with the help of current velocity data measured at several short-term oceanographic moorings, deployed on the inner Laptev Sea shelf in 2008, 2009, and 2012, respectively (see Fig. 2). Moreover, the under-ice hydrography is assessed with respect to its temporal and spatial variability using vertical salinity and temperature profiles, as well as salinity and temperature time series obtained from various ship-based CTD casts and oceanographic moorings under the landfast ice in 2008, 2009, and 2012, respectively (see Fig. 2). In particular, short-term temporal variability of water properties at Mooring North deployed in the vicinity of the landfast ice edge (see Fig. 2) in winter 2012 is examined in detail with respect to interactions between tidal dynamics, wind-driven, and density-driven advective processes.

3.1 Annual cycle of the current regime

An outstanding characteristic of oceanic currents is the temporal and spatial variability of their velocity and direction (Joseph 2014). For a comprehensive understanding of the hydrography and circulation under the landfast ice in the Laptev Sea, it is - hence - necessary to first obtain an overall picture of the general characteristics of the current regime and its temporal and spatial variability before specific physical processes can be investigated in greater detail. Current velocity data obtained at the yearlong Mooring LENA, deployed northeast of the Lena River Delta (see Fig. 2) from August 2, 1998 to August 30, 1999, is analyzed to provide an overview of the general features of the current regime on the inner Laptev Sea shelf and its seasonal variability. Satellite-based sea ice concentration data, provided by the National Snow and Ice Data Center (see Cavalieri et al. 2008), is used to describe the annual freeze-thaw cycle on the inner Laptev Sea shelf (see Fig. 7 a), which controls the phasing and duration of landfast ice (Selyuzhenok et al. 2015).

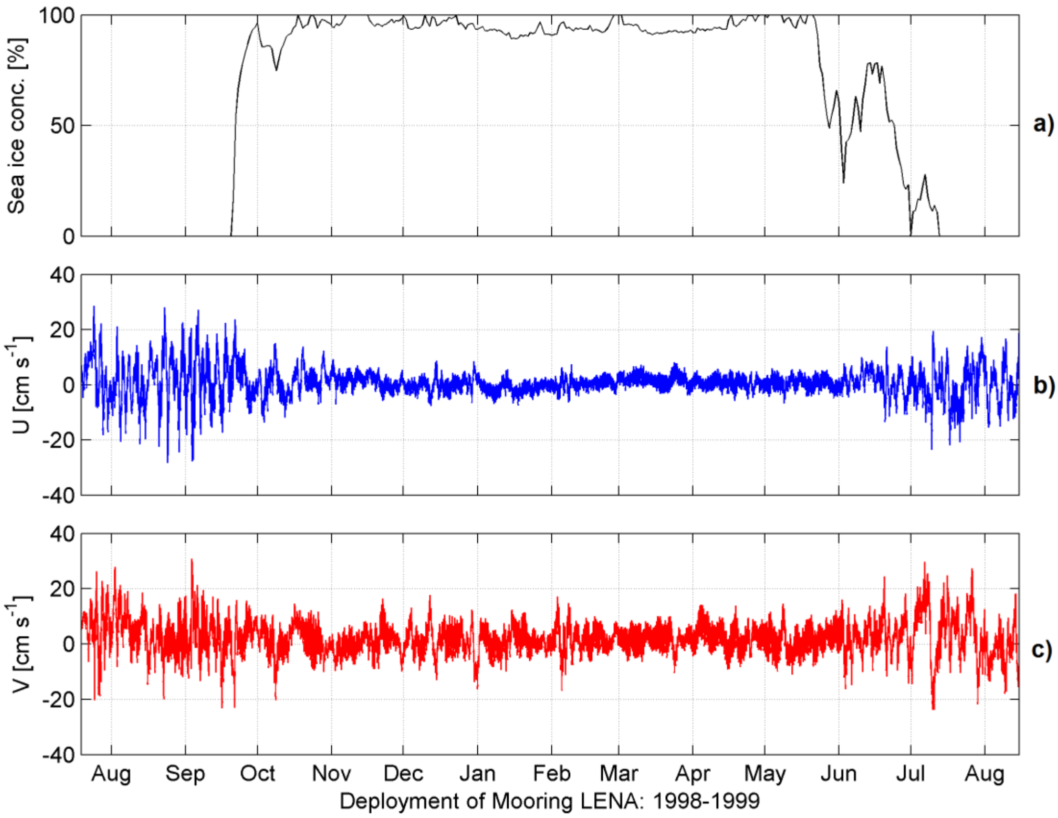

Fig. 7: Time series of satellite-based sea ice concentration (a, black line) for the location and deployment period of Mooring LENA, provided by the National Snow and Ice Data Center (Cavalieri et al. 2008), as well as depth-averaged zonal (b, blue line) and meridional (c, red line) current velocities obtained at Mooring LENA between August 2, 1998 and August 30, 1999.

In August and September 1998, the inner Laptev Sea shelf was ice-free. The onset of freeze-up occurred on October 4, 1998, and was followed by rapid growth of the sea ice cover in early October to over 90 % sea ice concentration by mid October. The ice-covered season lasted until the beginning of June 1999, when the ice cover started to decline. The break-up phase occurred from early June to the end of July 1999, by when the seasonal ice cover vanished completely. However, the general decrease of the sea ice concentration during the break-up phase was repeatedly interrupted by phases of increasing sea ice concentration, suggesting greater complexity of the break-up of the sea ice cover compared to the rapid freeze-up. The break-up phase was followed by the open water season, which began in August 1999 (see Fig. 7 a). For further analysis, the described annual cycle of satellite-based sea ice concentrations is used to divide the yearlong record at Mooring LENA into three different seasons. Ice-covered, break-up, and ice-free season are differentiated. Due to its short duration of less than two weeks, the freeze-up phase is assigned to the ice-covered season. Figure 7 b) and c) present the depth-averaged time series of zonal and meridional current velocities measured at Mooring LENA between August 2, 1998 and August 30, 1999. Current velocities exhibit considerable seasonal variations. In general, zonal current velocities vary between ~ -28 cm s^{-1} and 29 cm s^{-1} (see Fig. 7 b), and meridional current velocities vary between ~ -24 cm s^{-1} and 31 cm s^{-1} (see Fig. 7 c). The most striking characteristic of the record is the strong seasonality of current velocities, which manifests itself in significantly smaller current velocities during the ice-covered season from early October to early June (see Fig. 7). The depth-averaged current velocity time series is used to identify the orientation and magnitude of the principal current ellipse at Mooring LENA. For the ice-covered season, the major axis of the principal current ellipse exhibits an orientation of 155.2° (to north), i.e. towards southeast, and a magnitude of ~ 5.1 cm s^{-1}. The minor axis has a magnitude of ~ 2.5 cm s^{-1}. For the ice-free season, the principal current ellipse exhibits an orientation of 121.5°, with magnitudes of the major and minor axes of ~ 9.2 cm s^{-1} and 7.4 cm s^{-1}, respectively. Therefore, variability of oceanic currents at Mooring LENA is predominantly associated with a southeast-northwest direction during the ice-covered season, while the observed current regime is more variable in direction during the ice-free season. The pronounced seasonal differences are also apparent in the vertical profiles of time-averaged current velocities for the ice-covered, break-up, and ice-free seasons (see Fig. 8, 9, 10).

The vertical profile of current velocities at Mooring LENA averaged over the ice-covered season from early October to early June indicates the dominance of weak northeastward to northward currents under the landfast ice in the depth interval from ~ 8.5 m to 20.5 m (see Fig. 8). Due to biased measurements caused by disturbance of the sound reflection near the ice-ocean interface, information on current velocities in the upper water layer cannot be provided. In general, mean zonal current velocities exhibit only small variations between ~ 0.1 cm s^{-1} and 0.9 cm s^{-1}, with estimated standard errors of around ±0.3 cm s^{-1} (see Fig. 8 a). Mean meridional current velocities are slightly higher and exhibit greater vertical variability. The respective vertical profile shows an increase of mean meridional current velocities from ~ 1.5 cm s^{-1} at 8.5 m depth to its maximum of ~ 2.3 cm s^{-1} at 11 m depth and then a decrease to ~ 0.5 cm s^{-1} at 20.5 m depth, with standard errors varying between ~ ±0.4 cm s^{-1} and ±0.5 cm s^{-1} (see Fig. 8 b).

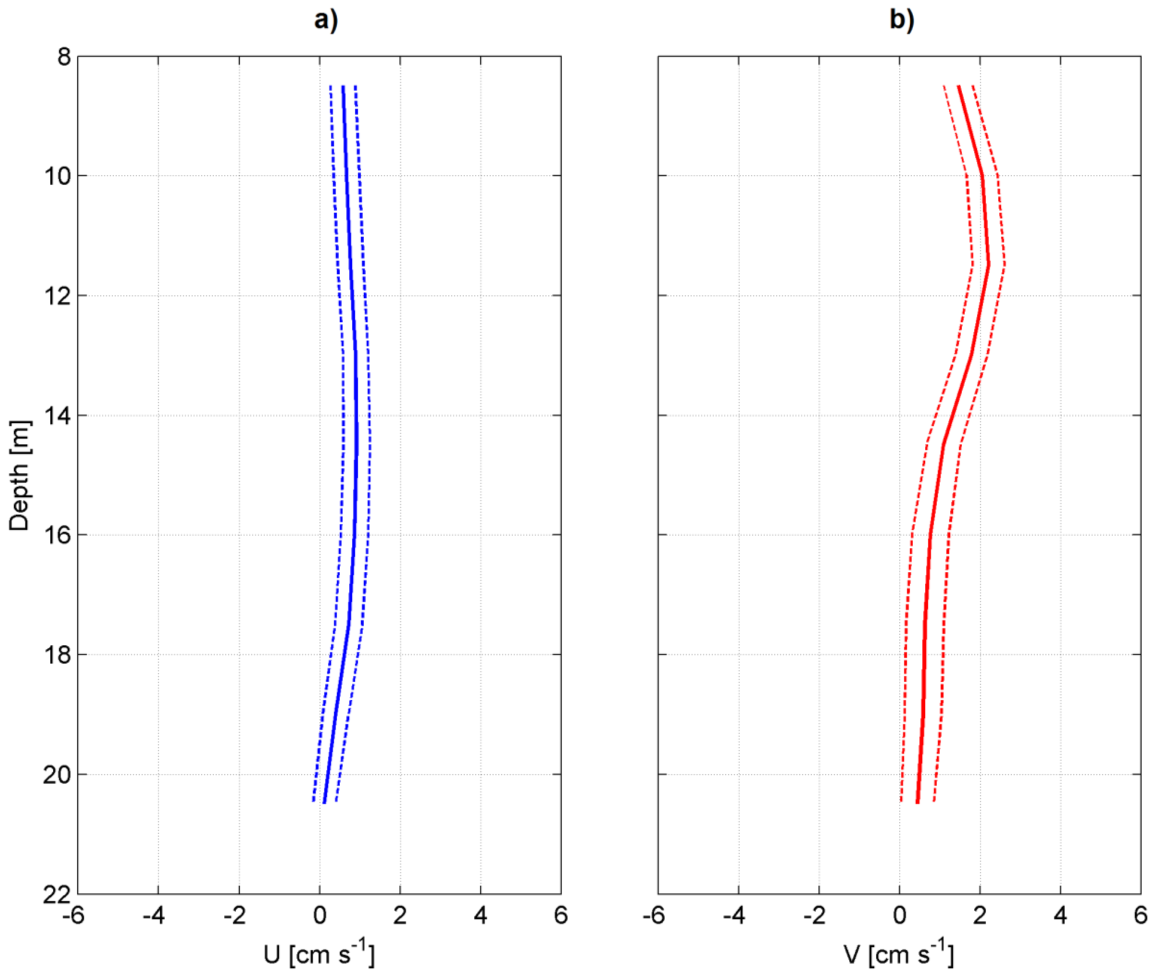

Fig. 8: Vertical profile of time-averaged zonal (a, blue line) and meridional (b, red line) current velocities obtained at Mooring LENA for the depth interval from ~ 8.5 m to 20.5 m during the ice-covered season (October 5, 1998 to June 4, 1999).

In comparison to the ice-covered season, the vertical profile of time-averaged current velocities at Mooring LENA for the break-up season from early June to the end of July shows significantly higher meridional current velocities and stronger vertical variability in the depth interval from ~ 8.5 m to 20.5 m (see Fig. 9). The mean current vector turns throughout the water column from a northeastward direction at 8.5 m depth to a northwestward direction near the seafloor at 20.5 m depth. Mean zonal current velocities decrease continuously with depth from ~ 1.2 cm s^{-1} at 8.5 m depth to 0 cm s^{-1} at ~ 17 m depth and to ~ -1.5 cm s^{-1} at 20.5 m depth. Standard errors associated with mean zonal current velocities range from ~ ±0.8 cm s^{-1} to ±1.0 cm s^{-1} (see Fig. 9 a). Mean meridional current velocities decrease slightly from ~ 5 cm s^{-1} to 4.6 cm s^{-1} in the depth interval from 8.5 m to 11.5 m, followed by a stronger decrease from ~ 4.6 cm s^{-1} to 2.0 cm s^{-1} in the depth interval from 11.5 m to 16 m. Below this depth, mean meridional current velocities remain nearly constant until 20.5 m depth. Standard errors associated with mean meridional current velocities are in the range of ~ ±1.0 cm s^{-1} to ±1.4 cm s^{-1} (see Fig. 9 b).

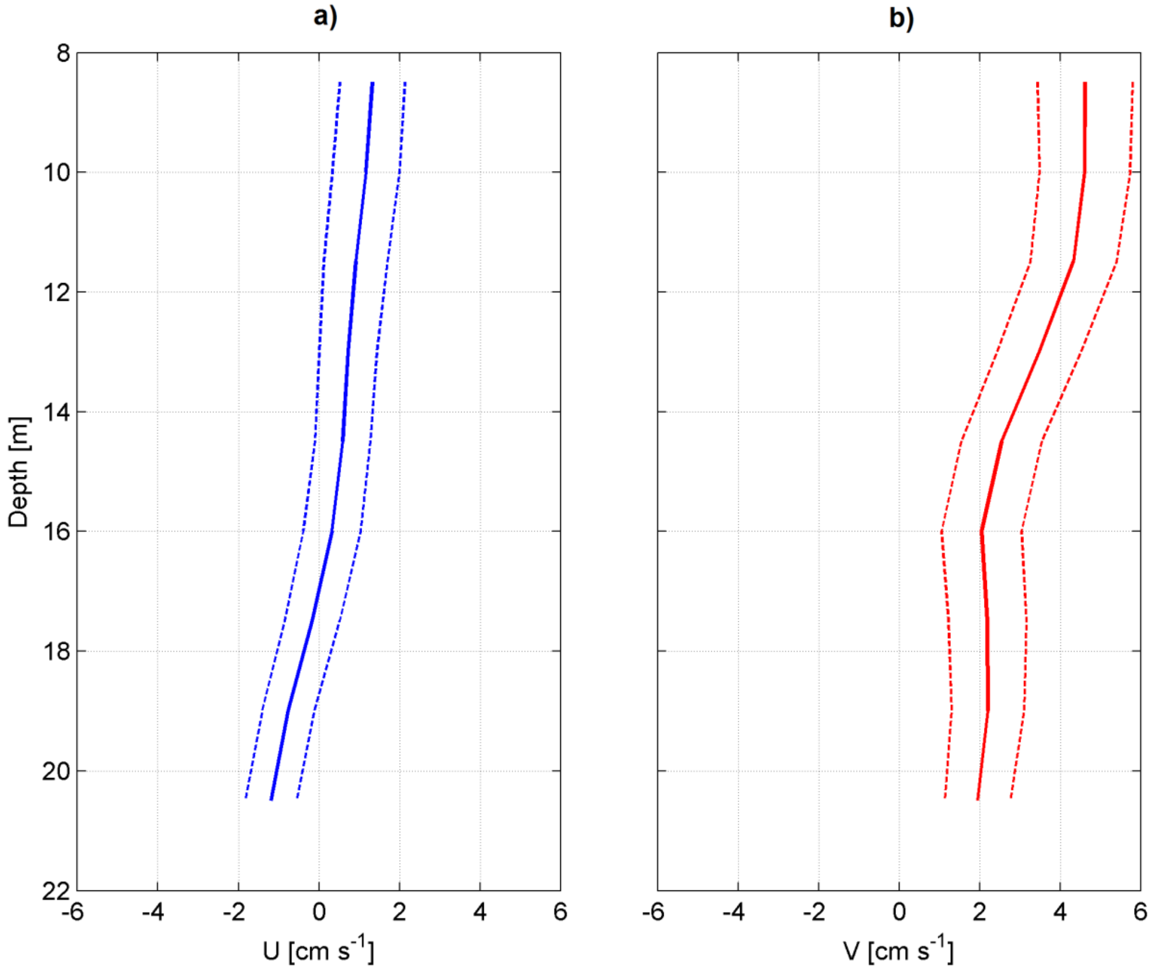

Fig. 9: Vertical profile of time-averaged zonal (a, blue line) and meridional (b, red line) current velocities obtained at Mooring LENA for the depth interval from ~ 8.5 m to 20.5 m during the break-up season (June 5, 1999 to July 31, 1999). Dashed lines indicate the respective standard error of the mean.

The vertical profile of current velocities at Mooring LENA averaged over the ice-free season from the beginning of August to early October (see Fig. 10) indicates similar current magnitudes as described for the break-up season. However, the mean current vector turns from a northwestward direction at 8.5 m depth to a northeastward direction near the seafloor at 20.5 m depth, which is opposite to change of the mean current vector during the break-up season. Mean zonal current velocities increase from ~ -0.4 cm s^{-1} at 8.5 m depth to the maximum of ~ 1.2 cm s^{-1} at 17 m depth, followed by a slight decrease to 1 cm s^{-1} at 20.5 m depth, with standard errors of ~ ±0.9 cm s^{-1} to ±1.1 cm s^{-1} (see Fig. 10 a). The vertical structure of observed mean meridional current velocities is similar to the results obtained during the break-up season. In the depth interval from 8.5 m to 10 m, mean meridional current velocities exhibit a nearly constant value of ~ 3.2 cm s^{-1}, followed by a decrease from ~ 3.2 cm s^{-1} to 2.4 cm s^{-1} in the depth interval from 10 m to 13 m. Below this depth, mean meridional current velocities decrease only slightly to ~ 2.2 cm s^{-1}. Standard errors associated with mean meridional current velocities range from ~ ±0.8 cm s^{-1} to ±1.2 cm s^{-1} (see Fig. 10 b).

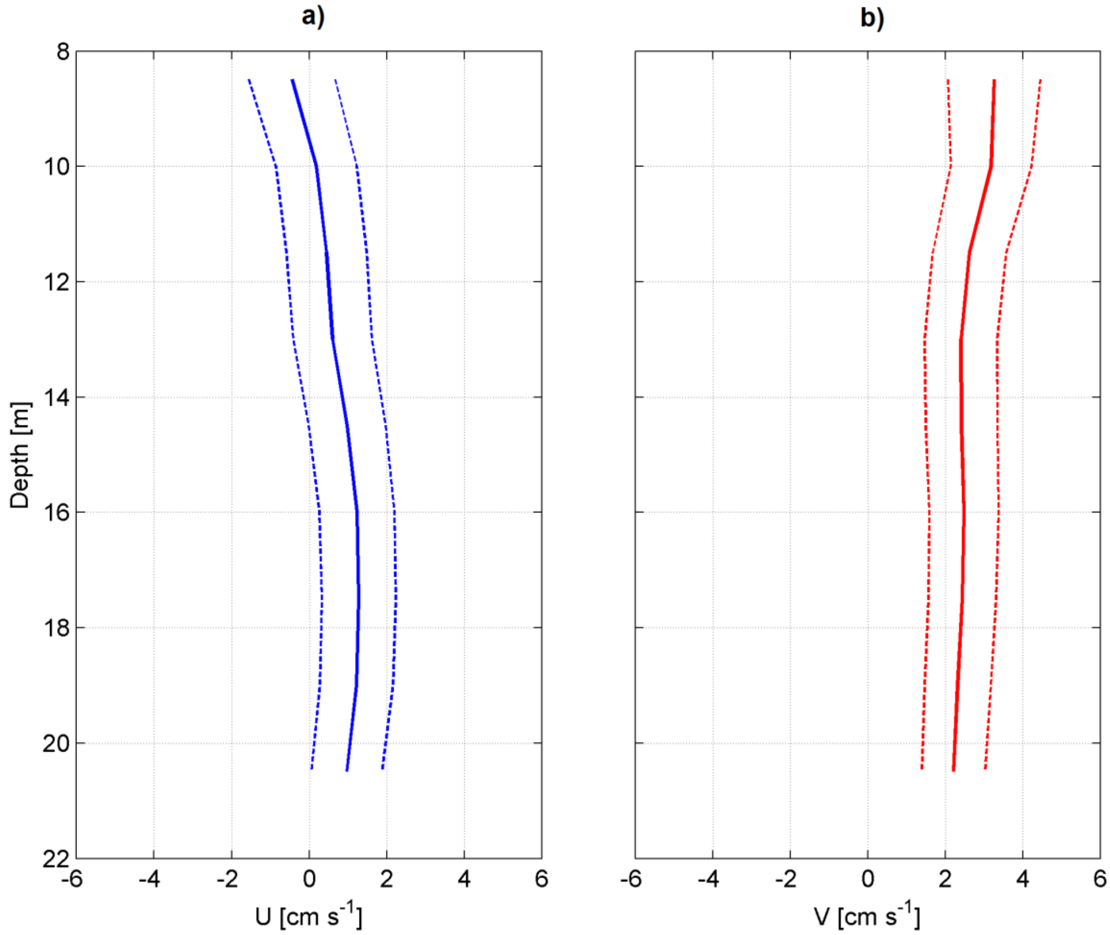

Fig. 10: Vertical profile of time-averaged zonal (a, blue line) and meridional (b, red line) current velocities obtained at Mooring LENA for the depth interval from ~ 8.5 m to 20.5 m during the ice-free season (August 2, 1998 to October 4, 1998, and August 1, 1999 to August 30, 1999). Dashed lines indicate the respective standard error of the mean.

Beside the pronounced seasonal cycle, strong variability on shorter timescales can also be identified in the current velocity record obtained at Mooring LENA (see Fig. 7 b, c). Alternating current directions over ~ 12-hour cycles suggest a strong influence of semidiurnal tides. Furthermore, variability on timescales of days to weeks is also clearly apparent in the depth-averaged current velocity records, especially during the ice-free season (see Fig. 7). Tidal harmonic analysis is performed to investigate the pronounced tidal variability at Mooring LENA in detail. Tidal variability explains ~ 19.4 % of the total variability in the yearlong, depth-averaged current velocity record. In total, 46 different significant tidal constituents are identified in the time series. Table 6 depicts the frequency, major and minor axes of the tidal ellipse, ellipse orientation, constituent phase, and signal-to-noise ratio of the most important tidal constituents, based on the following criteria: (a) a signal-to-noise ratio of over 2, and (b) a tidal velocity along the major axis of over 1 cm s^{-1}. For the major and minor axes, ellipse orientation, and constituent phase, the respective 95 % confidence intervals are provided. The dominant tidal constituent observed at Mooring LENA is M2, the principal lunar semidiurnal component, followed by S2, the principal solar semidiurnal component, supporting the findings from the depth-averaged current velocity record (see Fig. 7 b, c). The associated tidal current ellipses indicate a distinct predominance of tidal variability along the respective major axis. The M2 tidal current ellipse is characterized by a major axis with a magnitude of 3.4 cm s^{-1} (±0.1 cm s^{-1}) and an orientation of 114.6° (±1.9°), i.e. towards east. The major axis of the S2 tidal current ellipse has a magnitude of 1.6 cm s^{-1} (±0.1 cm s^{-1}) and an orientation of 122.5° (±4.3°), i.e. towards southeast. Other important tidal constituents are H1 and H2 in the vicinity of M2 described by Horn (1960), which have been discussed to be created by M2 itself, as well as the low-frequency constituents MM, the lunar monthly component, SA, the solar annual component, SSA, the solar semiannual component, and MSF, the lunisolar synodic fortnightly component (see Table 6). Detailed information on the different tidal constituents is provided by Godin (1972).

Table 6: Results of tidal harmonic analysis based on depth-averaged current velocity record obtained at Mooring LENA between August 2, 1998 and August 30, 1999. Information on frequency, major and minor axes of the tidal ellipse, ellipse orientation, constituent phase, and signal-to-noise ratio for all identified significant tidal constituents with a signal-to-noise ratio of over 2 and a tidal velocity along the major axis of over 1 cm s^{-1}. For the major and minor axes, ellipse orientation, and constituent phase, the respective 95 % confidence intervals are provided.

Tidal constituent	**Frequency [cycles h^{-1}]**	**Major axis [cm s^{-1}]**	**Minor axis [cm s^{-1}]**	**Ellipse orientation [°]**	**Constituent phase [° relative to Greenwich]**	**Signal-to-noise ratio**
M2	0.0805114	3.4 ± 0.1	0.3 ± 0.1	114.6 ± 1.9	168.9 ± 2.0	820
S2	0.0833333	1.6 ± 0.1	0.1 ± 0.1	122.5 ± 4.3	267.6 ± 4.1	210
H1	0.0803973	1.1 ± 0.1	-0.1 ± 0.1	99.6 ± 5.4	204.0 ± 5.9	99
H2	0.0806255	1.1 ± 0.1	-0.5 ± 0.1	105.1 ± 5.7	272.0 ± 6.1	77
MM	0.0015122	1.2 ± 0.6	0.2 ± 0.7	97.8 ± 32.7	139.3 ± 36.8	4.3
SA	0.0001141	1.1 ± 0.6	-0.2 ± 0.6	88.2 ± 35.1	145.6 ± 44.0	3.5
SSA	0.0002282	1.1 ± 0.6	-0.5 ± 0.5	155.8 ± 49.6	317.8 ± 50.8	3.5
MSF	0.0028219	1.0 ± 0.6	-0.1 ± 0.7	173.4 ± 39.9	187.7 ± 39.6	3.1
Total variability explained by tidal signal: 19.4 %						

Based on the results of the tidal harmonic analysis, the time series of depth-averaged tidal current velocities at Mooring LENA is inferred for the time period from August 2, 1998 to August 30, 1999 (see Fig. 11). The prediction of the tidal current velocities takes into account the magnitude, phase, and orientation of all identified significant tidal constituents. Inferred zonal and meridional current velocities range from ~ - 6 cm s^{-1} to 6 cm s^{-1} and from ~ -7 cm s^{-1} to 7 cm s^{-1}, respectively. Although the peak amplitudes of both current velocity components are similar, the variability of the zonal and meridional components associated with tidal forcing on various timescales is significantly different. The meridional velocity component exhibits considerably stronger variations on short timescales than the zonal component. Strongly alternating northwestward and southeastward currents over ~ 12-hour cycles clearly demonstrate the dominance of semidiurnal tidal variability at Mooring LENA. However, the semidiurnal tidal signal is significantly modulated by various lower-frequency components. Especially, fortnightly variations of current velocities have a strong influence on the characteristics of the predicted tidal record (see Fig. 11; Table 6).

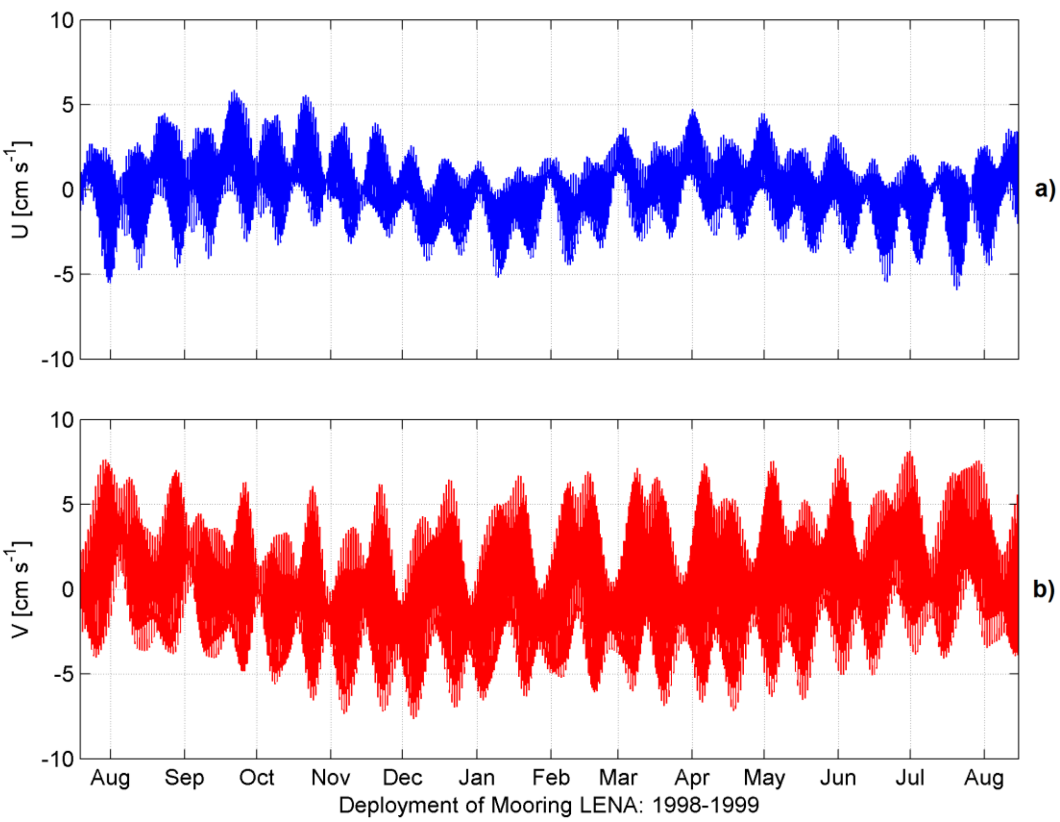

Fig. 11: Time series of inferred zonal (a, blue line) and meridional (b, red line) tidal current velocities based on the results of the tidal harmonic analysis of the depth-averaged current record from Mooring LENA (see Fig. 7) for the time period from August 2, 1998 to August 30, 1999.

The results of the tidal harmonic analysis for the depth-averaged current velocity record provide a first overview of tidal dynamics at Mooring LENA. However, by using the full length of the yearlong, depth-averaged current velocity record as input for the tidal analysis, information on the spatial and temporal variations of the tidal signal is lost. To examine the tidal influence at Mooring LENA for different water depths, tidal harmonic analysis is performed for current velocity data obtained from individual depth bins. Moreover, the analysis is performed over 29-day overlapping segments, necessary to resolve a lunar month, to identify temporal changes in the tidal dynamics (see Fig. 12).

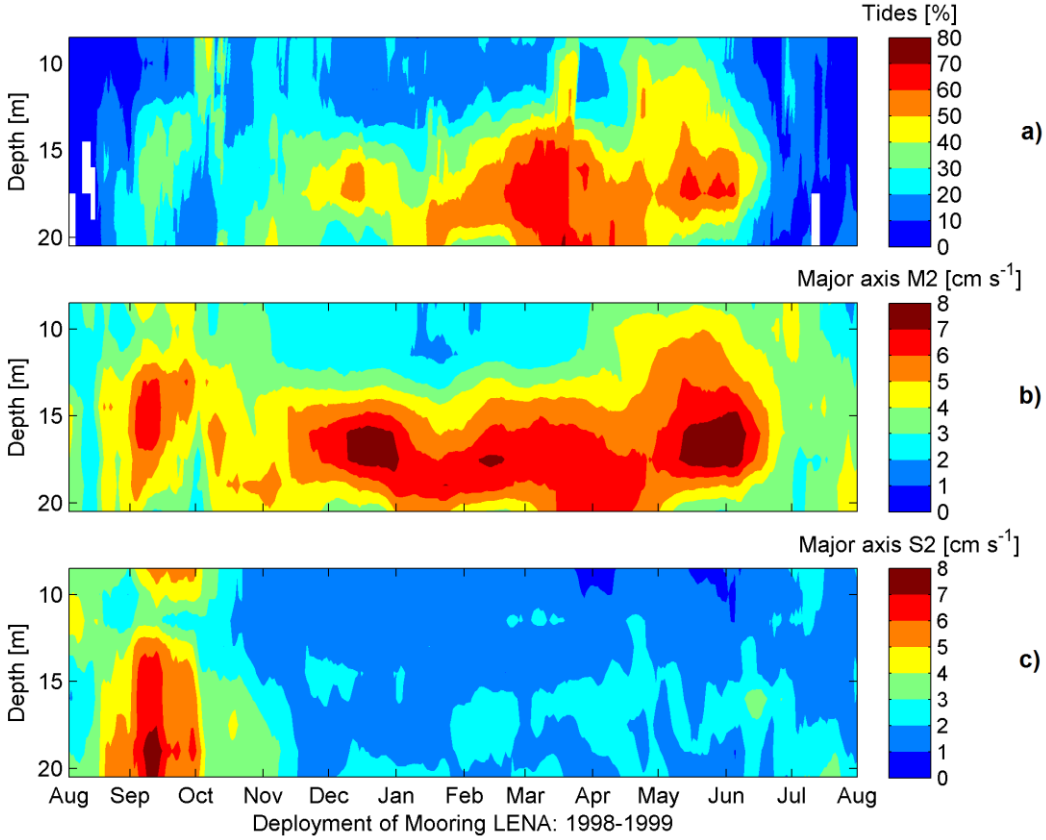

Fig. 12: Results of 29-day overlapping tidal harmonic analysis for the current velocity record obtained at Mooring LENA for the depth interval from ~ 8.5 m to 20.5 m between August 1998 and August 1999. a) Ratio of tidal variability to total variability of the current velocity record. Magnitude of the major axis of the tidal current ellipse associated with the dominant tidal constituents M2 (b) and S2 (c).

Figure 12 a) shows the ratio of the tidal variability to the total variability of the current velocity record at Mooring LENA for the depth interval from ~ 8.5 m to 20.5 m over the annual cycle. The influence of tides varies significantly with depth and season. The ratio of tidal variability to total variability ranges from less than 1 % to ~ 70 %. In general, the influence of tides on the current regime is strongest during the ice-covered season. The vertical structure of the water column shows a distinct difference in the importance of tides between the upper water layer, extending down to ~ 12 to 15 m depth, and the lower water layer during this season. Tidal variability plays a significantly greater role in the lower water layer than in the upper water layer. Differences in the ratio of tidal variability to total variability for the upper and lower water layers are up to ~ 50 %. However, the influence of tides on the total variability of the velocity record decreases close to the seafloor. It should be noted that the influence of tides near the ice-ocean interface is unknown due to a lack of reliable observations in the depth interval from 0 m to 8.5 m. The tidal influence on the total variability of the current velocity record is considerably smaller during early winter compared to late winter. For the time period from initial freeze-up to end of December, the contribution of tidal variability is mainly in the range from ~ 10 % to 30 %. In contrast, contributions of ~ 40 % to over 60 % are common in the lower water column during late winter. During the break-up season, the influence of tides on the total variability diminishes significantly and tidal variability explains less than 10 % of the total variability in the water column during the ice-free season (see Fig. 12 a). Figure 12 b) depicts the time series of current velocities along the major axis of the tidal ellipse identified with the help of tidal harmonic analysis for the tidal principal lunar semidiurnal component, M2, at Mooring LENA in the depth interval from ~ 8.5 m to 20.5 m. Tidal current velocities associated with M2 tides exhibit pronounced temporal and vertical variability. Predicted current magnitudes range from ~ 2 cm s^{-1} to 7 cm s^{-1}. The temporal and spatial patterns of M2 current velocities are very similar to the described general characteristics of the ratio of tidal variability to total variability (see Fig. 12 a, b), indicating that the tidal principal lunar semidiurnal constituent has a dominant influence of the observed total tidal variability. Current velocities along the major axis of M2 are generally higher during the ice-covered season compared to the ice-free season. During the open water period, M2 current velocities vary between ~ 2 cm s^{-1} and 4 cm s^{-1}. In winter, M2 current velocities range from ~ 1 cm s^{-1} to 8 cm s^{-1} and exhibit pronounced vertical variability. In general, vertical maxima of M2 tides are centered at ~ 15 m to 19 m water depth and have magnitudes of ~ 4 cm s^{-1} to 8 cm s^{-1}, which decrease towards the seafloor as well as towards the surface. From a temporal perspective, maxima of M2 tides occur in October and January (see Fig. 12 b). The current velocities along the major axis of the tidal ellipse for the tidal principal solar semidiurnal component, S2 (see Fig. 12 c), show a significantly different seasonal pattern compared to the total tidal variability and the M2 constituent. Tidal current velocities associated with the S2 constituent range from ~ 1 cm s^{-1} to 8 cm s^{-1}. The highest velocities can be observed for the period from mid September to mid October. In contrast, the lowest S2 current velocities occur from December to August with values generally below ~ 2 cm s^{-1}. In general, the influence of S2 seems to be stronger in the lower water column, beneath ~ 12 m water depth (see Fig. 12 c). However, the contrast between the velocities in the upper and lower water layer is not as pronounced as for M2 tides (see Fig. 12 b, c).

Since tidal variability can only account for part of the total variability in the observed current velocity records at Mooring LENA (see Fig. 12 a), residual currents are estimated as the difference between the original depth-averaged time series (see Fig. 7 b, c) and the predicted tidal signal (see Fig. 11) in order to investigate possible drivers of current variability other than tides. Especially during the ice-free season, other physical processes seem to play an important role for the oceanic current regime (see Fig. 7). Figure 13 depicts the depth-averaged time series of residual current velocities at Mooring LENA over the annual cycle. It should be noted that the record still exhibits some semidiurnal variability, indicating that the influence of tides is not completely removed by the tidal harmonic analysis. However, the magnitude of the semidiurnal variability is small compared to variability on other timescales. The strongest variability of residual currents occurs during the ice-free season. Zonal and meridional current velocities range from ~ -30 cm s^{-1} to 26 c cm s^{-1} and from ~ -24 cm s^{-1} to 29 cm s^{-1}, respectively, during this season. In comparison, zonal and meridional current velocities during the ice-covered season generally vary between ~ -10 cm s^{-1} and 10 cm s^{-1}, and ~ -15 cm s^{-1} and 15 cm s^{-1}, respectively, except for the freeze-up period in October, which is associated with significantly higher variations in current velocities (see Fig. 13). The observed pattern indicates that the influence of non-tidal advective processes on the oceanic current regime in winter is limited, possibly due to the presence of the landfast ice cover, which may decouple the water column from atmospheric forcing (Itkin et al. 2015). Pronounced interaction between winds and the open water surface could be a potential driver of the higher residual current velocities observed at Mooring LENA during the ice-free season.

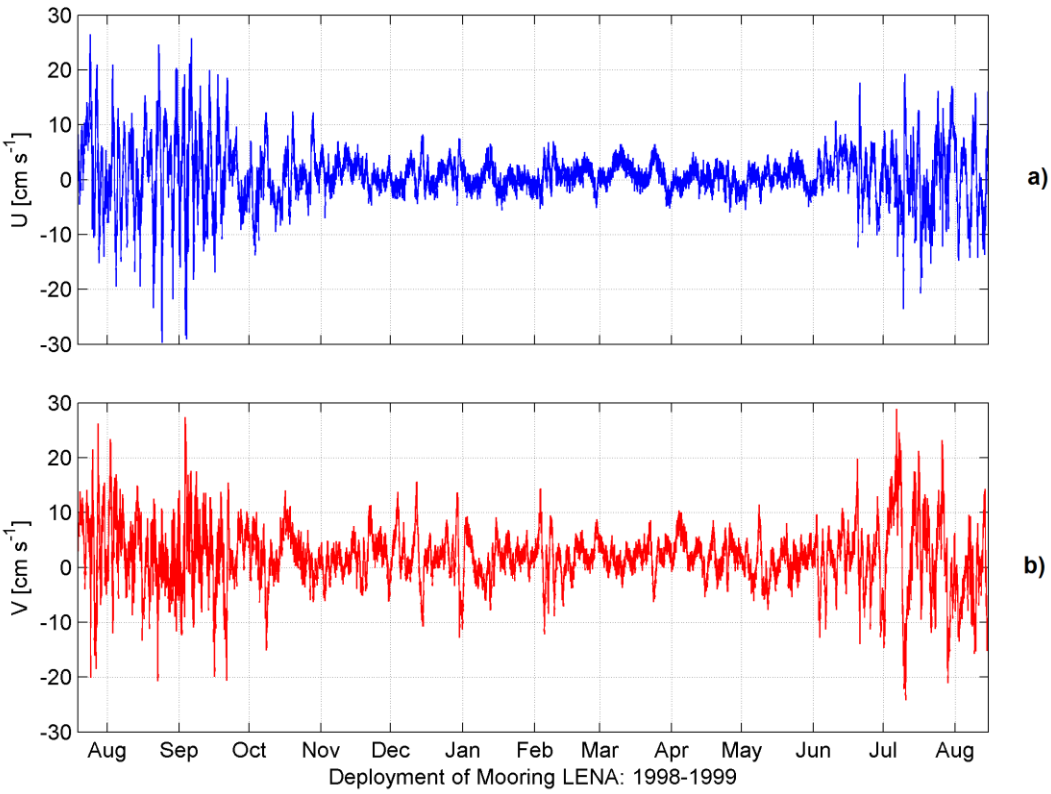

Fig. 13: Time series of the depth-averaged residual zonal (a, blue line) and meridional (b, red line) current velocities at Mooring LENA for the time period from August 2, 1998 to August 30, 1999 calculated as the difference of the depth-averaged current velocities (see Fig. 7) and the inferred tidal current velocities (see Fig. 11).

To investigate the relationship between near-surface winds and oceanic current response during the ice-free season, zonal and meridional components of the wind, 10 m above sea level, derived from the ECMWF ERA-Interim reanalysis dataset at the geographic position 73°30'N, 131°20'E, near Mooring LENA, are compared to the depth-averaged residual current velocities at Mooring LENA for the ice-free period in 1998 (see Fig. 14). To facilitate comparison of the datasets, a 24-hour low-pass Butterworth filter is applied to the residual current velocity record, removing the leftover tidal signal. Zonal wind velocities range from ~ -14 m s^{-1} to 10 m s^{-1} for the period of investigation (see Fig. 14 a). Meridional wind velocities exhibit variations between ~ -12 m s^{-1} and 9 m s^{-1} (see Fig 14 b). Pronounced variability can be identified on timescales of approximately two to seven days. Winds generally tend to fluctuate between southeastward and northwestward directions. On average, northwestward winds dominate the record. Overall, a close relationship between the prevailing winds and the oceanic currents at Mooring LENA can be observed during the ice-free season. Peaks of the wind strength tend to slightly precede peaks of residual current velocities, supporting a cause-and-effect relationship. However, the analyzed wind and current velocity records also indicate differences in the response of oceanic currents at similar wind forcing (see Fig. 14), indicating that winds cannot be the only driver of the oceanic current regime.

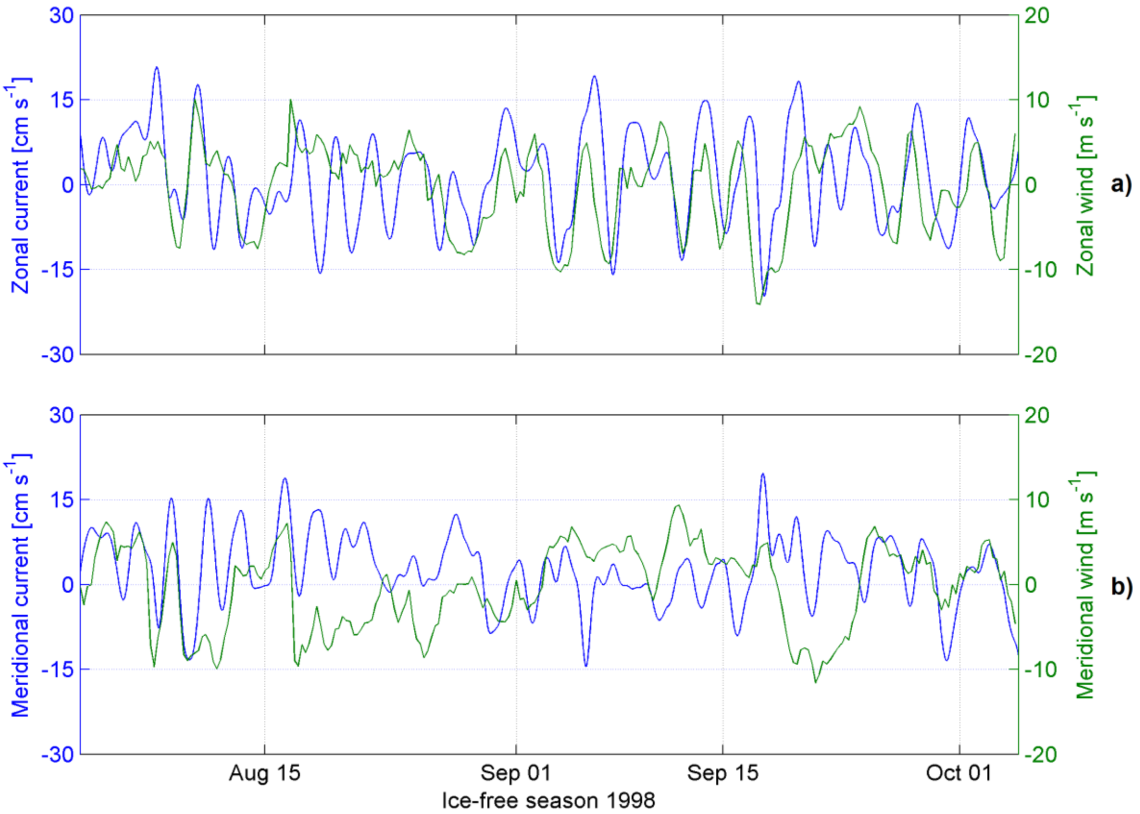

Fig. 14: Time series of depth-averaged, 24-hour low-pass Butterworth filtered residual zonal (a) and meridional (b) current velocities (blue line) at Mooring LENA for the ice-free season in 1998 compared to the time series of zonal (a) and meridional (b) 10 m wind velocities (green line) derived from the ECMWF ERA-Interim reanalysis dataset at the geographic position 73°30’N, 131°20’E, near Mooring LENA (Dee et al. 2011, Berrisford et al. 2011).

Near-surface winds and oceanic current response at Mooring LENA are also compared to each other for the ice-covered season to identify differences of the wind influence on the oceanic current regime over the annual cycle. Figure 15 shows the zonal and meridional 10 m wind components, derived from the ECMWF ERA-Interim reanalysis dataset at the geographic position 73°30’N, 131°20’E, near Mooring LENA, as well as the depth-averaged, low-pass-filtered residual current velocities at Mooring LENA for the ice-covered season. Zonal wind velocities vary between ~ -13 m s^{-1} and 13 m s^{-1} (see Fig. 15 a), while meridional wind velocities range from ~ -10 m s^{-1} to 11 m s^{-1} (see Fig. 15 b). Hence, the magnitudes of wind velocities during the ice-covered season are similar to the ones identified for the ice-free season. The mean wind direction in winter is also to the northwest. Moreover, the timescales of wind variability are also comparable for the different seasons (see Fig. 14, 15). However, the wind influence on the oceanic current regime is considerably weaker during the ice-covered season. While there are some indications that wind forcing induces changes in the current response during freeze-up phase and early winter, the relationship between wind forcing and residual currents in late winter is negligible (see Fig. 15), indicating that other physical processes (e.g. salinity differences; see Pavlov and Pavlov 1999) likely play a more important role for the oceanic current regime during this time period.

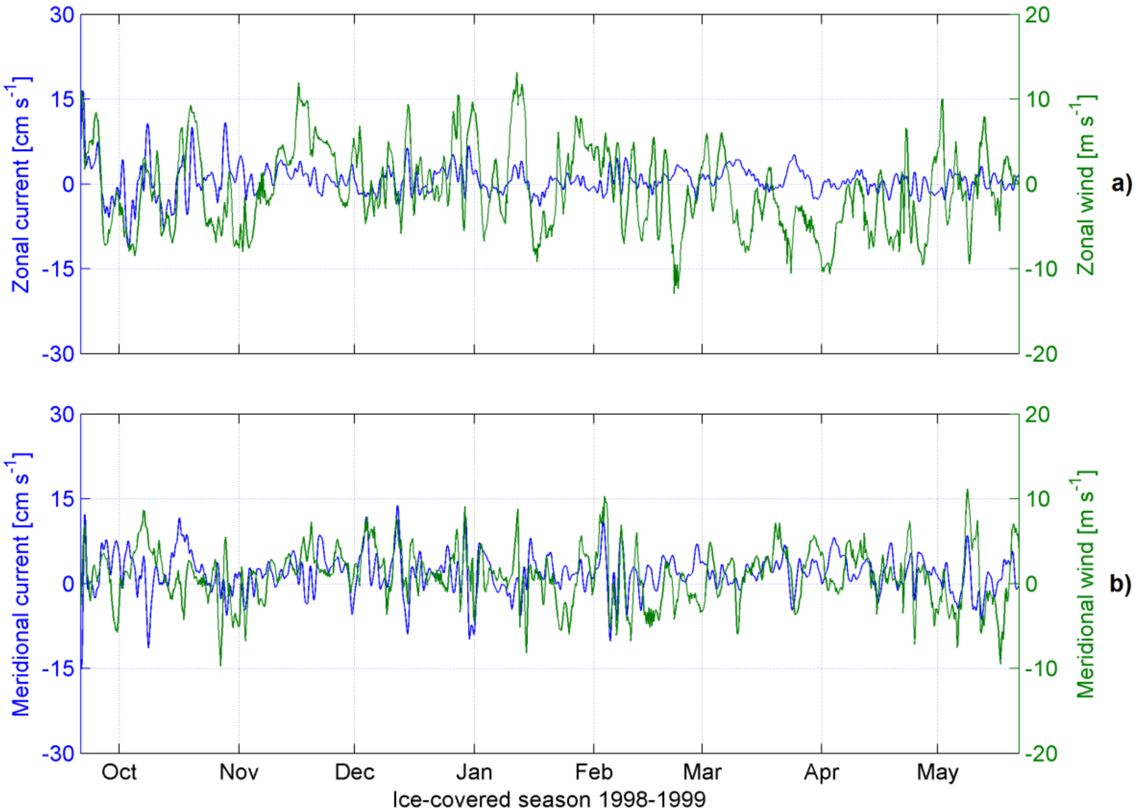

Fig. 15: Time series of depth-averaged, 24-hour low-pass Butterworth filtered residual zonal (a) and meridional (b) current velocities (blue line) at Mooring LENA for the ice-covered season in 1998/99 compared to the time series of zonal (a) and meridional (b) 10 m wind velocities (green line) derived from the ECMWF ERA-Interim reanalysis dataset at the geographic position 73°30'N, 131°20'E, near Mooring LENA (Dee et al. 2011, Berrisford et al. 2011).

In summary, the current regime at Mooring LENA exhibits significant variations over the annual freeze-thaw cycle. Three different periods can be identified, namely the ice-covered, the break-up, and the ice-free season. During the ice-covered season, the oceanic current regime is mainly influenced by tidal dynamics. Wind-driven advection is largely prevented by the landfast ice cover. In contrast, tidal dynamics lose importance during the break-up season and explain less than 10 % of the variability of current velocities during the ice-free season.

Wind forcing is of great importance during the ice-free season, resulting in significantly higher current velocities and greater variability than during the ice-covered season.

3.2 Current regime under the landfast ice

Since the current knowledge about the circulation on the Laptev Sea shelf during the ice-covered season is very limited, this section aims at providing a more detailed insight into the characteristics of the under-ice oceanic current regime using current velocity data obtained from short-term moorings deployed in 2008, 2009, and 2012, respectively (see Fig. 2). Since the oceanographic data acquired during TRANSDRFIT XIII and TRANSDRIFT XV in 2008 and 2009, respectively, have already been partly analyzed in previous studies by Dmitrenko et al. (2010a), Dmitrenko et al. (2010c), Dmitrenko et al. (2012) and Kirillov et al. (2013), particular attention is paid to the oceanographic moorings deployed at two different ice camps during the winter expedition TRANSDRIFT XX in March and April 2012, which provide a new and particularly detailed source of information about the under-ice circulation on the inner Laptev Sea shelf. Comparisons with oceanographic datasets from the winter expeditions TRANSDRIFT XV and XIII are used to establish a broader context with regard to general features of the circulation under the landfast ice in the Laptev Sea.

3.2.1 Current regime in winter 2012

Within the framework of TRANSDRIFT XX in March and April 2012, under-ice current velocity records were obtained at two different locations, Camp North (station TI1201) and Camp Central (station TI1202). While Camp North was located close to the landfast ice edge, similar to the short-term moorings deployed in 2008 and 2009, Camp Central was installed further southeast at greater distance to the landfast ice edge and the Lena River Delta (see Fig. 2). Observed current velocity records at the two moorings are analyzed in the context of the results derived from Mooring LENA for the ice-covered season (see section 3.1). Furthermore, similarities and differences between the current velocity records of the two locations themselves are examined in order to provide a spatial perspective to the investigation of the under-ice oceanic current regime on the southeastern Laptev Sea shelf.

3.2.1.1 Mooring Central

The depth-averaged current velocity record for Mooring Central, deployed east of the Lena River Delta at a water depth of ~ 24 m, provides information on the predominant current velocities and direction under the landfast ice for the depth interval from ~ 4 m to 14 m during the time period from March 28, 2012 to April 12, 2012 (see Fig. 16). Zonal current velocities range from ~ -12 cm s^{-1} to 16 cm s^{-1}. Meridional current velocities vary between ~ -9 cm s^{-1} to 20 cm s^{-1}. The time series exhibits pronounced semidiurnal variability, indicating that tides play a major role for the under-ice current regime. This finding is in line with the results obtained from the yearlong current velocity record from Mooring LENA described in the previous section. Furthermore, the depth-averaged current velocities at Mooring Central also vary considerably over longer time periods of ~ 4 to 5 days (see Fig. 16). The principal current ellipse calculated from the depth-averaged current velocity record at Mooring Central indicates pronounced variability along the major axis, which has a magnitude of ~ 9.1 cm s^{-1} and exhibits an orientation of 133.4°, i.e. towards southeast. In contrast, the minor axis of the principal current ellipse has a significantly smaller magnitude of ~ 2.3 cm s^{-1}. This finding also supports the strong influence of tidal currents on the oceanic current regime at Mooring Central.

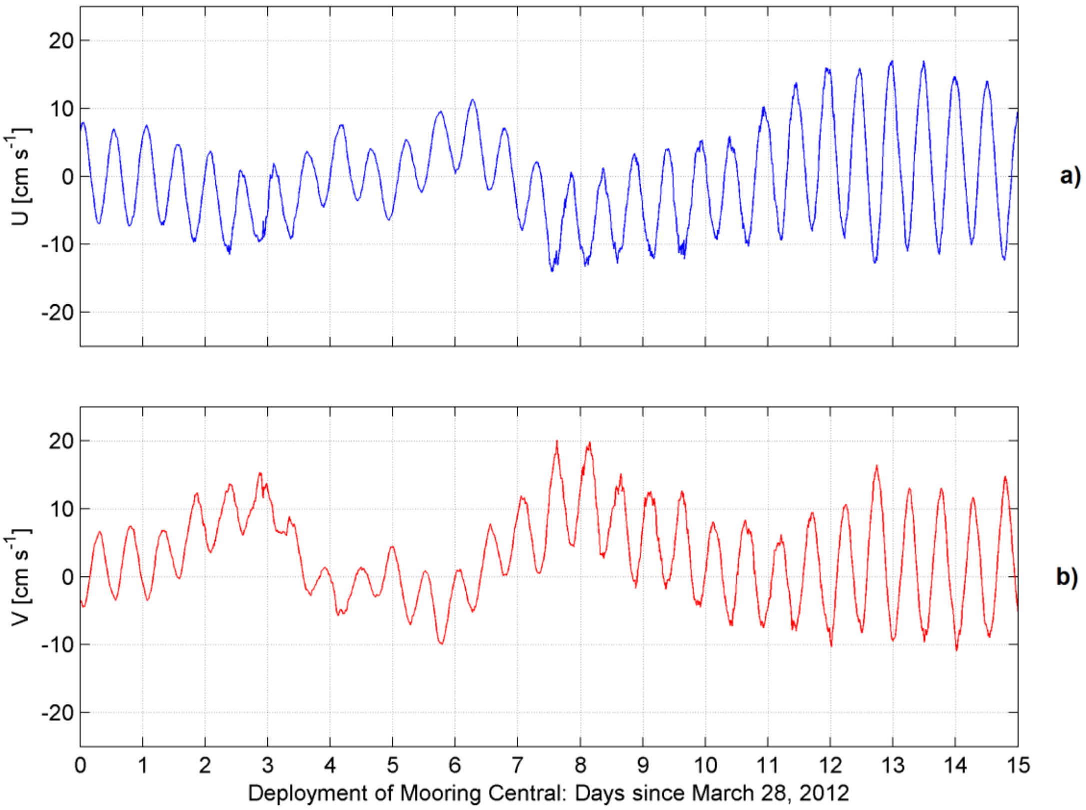

Fig. 16: Time series of depth-averaged zonal (a, blue line) and meridional (b, red line) current velocities obtained at Mooring Central between March 28 (day 0) and April 12 (day 15), 2012.

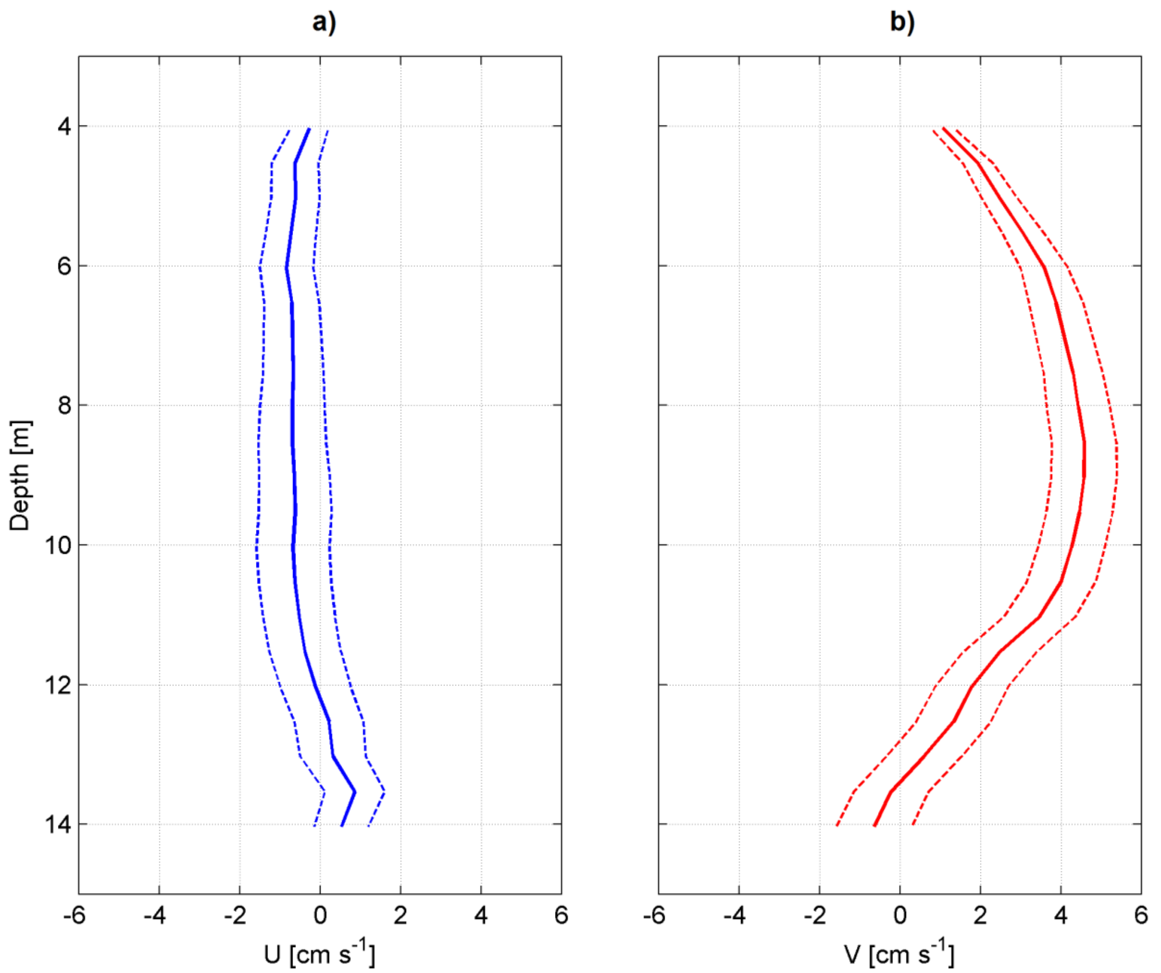

Fig. 17: Vertical profile of time-averaged zonal (a, blue line) and meridional (b, red line) current velocities obtained at Mooring Central for the depth interval from ~ 4 m to 14 m between March 28 and April 12, 2012. Dashed lines indicate the respective standard error of the mean.

The vertical profile of mean current velocities at Mooring Central, based on averaging of current velocity information from individual depth bins over the time period from March 28, 2012 to April 12, 2012, indicate a dominant northward current direction under the landfast ice (see Fig. 17). This finding is in line with the observations from Mooring LENA (see Fig. 8), which suggest the occurrence of northeastward to northward currents under the landfast ice. However, the magnitude of observed mean current velocities at Mooring Central is significantly higher than the magnitude of mean current velocities obtained at Mooring LENA for the ice-covered season. It should be noted that reliable oceanographic data from the two moorings cover different depths intervals. Only a small overlap from ~ 8.5 m to 14 m water depth exists, which complicates the comparison of the vertical structure of the under-ice current regime. The vertical profile of mean meridional current velocities at Mooring Central exhibits a parabolic shape, increasing from ~ 1.0 cm s^{-1} at 4 m water depth to the maximum value of ~ 4.6 cm s^{-1} at 9 m water depth, and then decreasing to -0.2 cm s^{-1} at 13.5 m water depth. Standard errors associated with the mean meridional current velocity vary between ~ ±0.3 cm s^{-1} and ±0.9 cm s^{-1} (see Fig. 17 b). Mean zonal current velocities vary only slightly between ~ -0.8 cm s^{-1} and 0.8 cm s^{-1} throughout the water column, with standard errors ranging from ~ ±0.5 cm s^{-1} to ±0.9 cm s^{-1}. For the depth interval from ~ 4.5 m to 10.5 m nearly constant zonal velocities are observed, exhibiting values between ~ -0.6 cm s^{-1} and -0.8 cm s^{-1}. Above and below this depth range zonal velocities increase slightly (see Fig. 17 a). Overall, the strongest currents can be observed at ~ 9 m depth.

Since tidal currents seem to play an important role for the under-ice current regime at Mooring Central (see Fig. 16), tidal harmonic analysis is performed to investigate the tidal influence in greater detail. The results indicate that tidal variability explains 64.2 % of the total variability in the two-week, depth-averaged current velocity record, supporting the findings from Mooring LENA, which also suggest a strong tidal influence on the variability of the oceanic current regime under the landfast ice. Overall, seven significant tidal constituents with a signal-to-noise ratio of over 2 are identified in the current velocity record at Mooring Central (see Table 7). The results of the tidal analysis indicate that M2, the principal lunar semidiurnal component, is the dominant tidal constituent in the record, followed by S2, the principal solar semidiurnal component, and MSF, the lunisolar fortnightly component. These tidal constituents are also important components of the tidal signal in the yearlong record obtained at Mooring LENA (see Table 6). Tidal current ellipses associated with these components indicate a strong predominance of tidal variability along the respective major axis. The M2 tidal current ellipse exhibits a major axis with a magnitude of ~ 9.7 cm s^{-1} (±0.9 cm s^{-1}) and an orientation of 140.1° (±5.7°), i.e. towards southeast. The S2 and MSF tidal current ellipses are characterized by major axes with magnitudes of 3.8 cm s^{-1} (±0.8 cm s^{-1}) and 1.6 cm s^{-1} (±0.3 cm s^{-1}), and are rotated by 144.9° (±14.0°) and 151.8° (±16.4°), respectively. Other significant tidal constituents in the current velocity record include 2MS6 and 2SM6, referring to the sixth-diurnal shallow water components, K1, the lunar diurnal component, and M3, the lunar third-diurnal shallow water component (see Godin (1972) for further information on tidal constituents). However, these tidal constituents account for a significantly smaller amount of the tidal variability in the record (see Table 7). It should be noted that due to the short record length of two weeks, low-frequency components, which are important in the yearlong record obtained at Mooring LENA (see Table 6), cannot be resolved at Mooring Central.

Table 7: Results of tidal harmonic analysis based on depth-averaged current velocity record obtained at Mooring Central between March 28 and April 12, 2012. Information on frequency, major and minor axes of the tidal ellipse, ellipse orientation, constituent phase, and signal-to-noise ratio for all identified significant tidal constituents with a signal-to-noise ratio of over 2. For the major and minor axes, ellipse orientation, and constituent phase, the respective 95 % confidence intervals are provided.

Tidal constituent	Frequency [cycles h^{-1}]	Major axis [cm s^{-1}]	Minor axis [cm s^{-1}]	Ellipse orientation [°]	Constituent phase [° relative to Greenwich]	Signal-to-noise ratio
M2	0.0805114	9.7 ± 0.9	-1.2 ± 0.9	140.1 ± 5.7	44.4 ± 4.9	120
S2	0.0833333	3.8 ± 0.8	0.3 ± 0.9	144.9 ± 14.0	161.7 ± 14.1	24
MSF	0.0028219	1.6 ± 0.3	0.0 ± 0.5	151.8 ± 16.4	338.3 ± 11.1	24
2MS6	0.2443561	0.2 ± 0.1	0.0 ± 0.1	119.0 ± 37.3	346.0 ± 30.0	5.1
2SM6	0.2471781	0.2 ± 0.1	-0.1 ± 0.1	110.3 ± 82.7	134.1 ± 71.0	3.6
K1	0.0417807	0.6 ± 0.4	-0.3 ± 0.3	128.8 ± 48.9	75.8 ± 63.7	2.6
M3	0.1207671	0.2 ± 0.1	-0.4 ± 0.1	177.9 ± 48.0	332.1 ± 73.4	2
Total variability explained by tidal signal: 64.2 %						

Based on the results of the tidal harmonic analysis, the time series of depth-averaged tidal current velocities at Mooring Central can be calculated, taking into account the magnitude, phase, and orientation of all identified significant tidal constituents (see Fig. 18). Predicted zonal and meridional current velocities range from ~ -10 cm s^{-1} to 12 cm s^{-1} and from ~ -8 cm s^{-1} to 8 cm s^{-1}, respectively. Pronounced variability of semidiurnal frequency can be observed in the record, which is associated with alternating northwestward and southeastward current directions. The tidal signal is also strongly influenced by lower-frequency modulation, which is likely associated with the lunisolar fortnightly constituent, MSF. However, the two-week prediction of current velocities at Mooring Central cannot resolve the complete fortnightly cycle (see Fig. 18). The timescales of temporal variability in the predicted current velocity record at Mooring Central correspond to the findings from Mooring LENA. However, the magnitudes of tidal current velocities, especially with regard to the zonal component, are significantly higher for the prediction obtained from Mooring Central (see Fig. 11, 18).

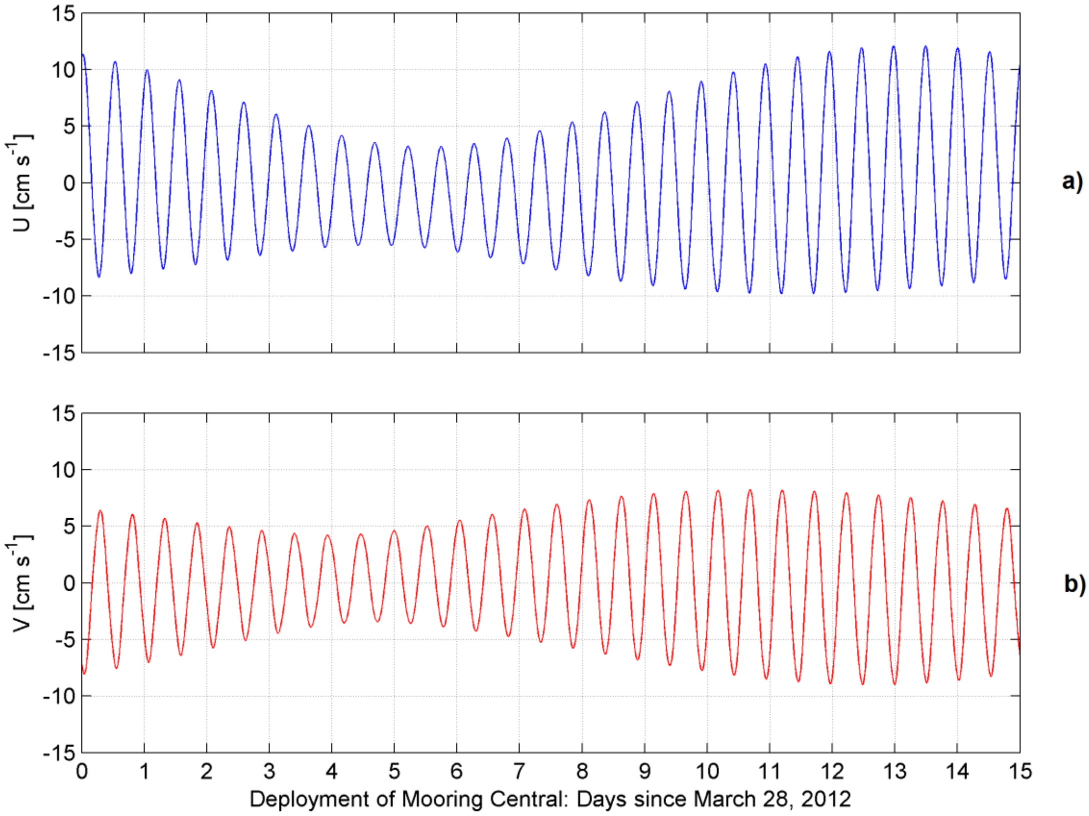

Fig. 18: Time series of inferred zonal (a, blue line) and meridional (b, red line) tidal current velocities based on the results of the tidal harmonic analysis of the depth-averaged current record from Mooring Central (see Fig. 16) for the time period from March 28 (day 0) to April 12 (day 15), 2012.

In order to examine the vertical structure of the tidal influence at Mooring Central, tidal harmonic analysis is performed for current velocity data obtained from individual depth bins. Figure 19 a) depicts the percentage of the total variability that is explained by tidal variability as a function of water depth. The influence of tides on observed current velocities at Mooring Central varies between ~ 50 % and 66 %. The ratio of tidal variability to total variability decreases from ~ 53 % at 4 m water depth to the minimum of ~ 50 % at 5.5 m. Below this depth, a nearly linear increase to the maximum of ~ 66 % at 10 m water depth occurs, followed by a decrease to ~ 57 % at 14 m water depth (see Fig. 19 a). The observed vertical structure of the tidal influence at Mooring Central is similar to the observations from Mooring LENA in March and April, which also suggest decreasing tidal influence towards the ice-ocean and ocean-seafloor boundary layers. However, the maximum of the tidal influence is located at different depths. The profile of current velocities along the major axis of M2 (see Fig. 19 b) shows a similar vertical structure as the magnitude of the tidal influence. It indicates an increase of M2 velocity from ~ 4.3 cm s^{-1} at 4 m water depth to ~ 12.4 cm s^{-1} at

10 m water depth. In the depth interval from ~ 10 m to 12.5 m, the M2 velocity stays nearly constant and then decreases to ~ 10.3 cm s^{-1} at 14 m depth (see Fig. 19 b). In comparison to these findings, M2 velocities observed at Mooring LENA in March and April are significantly smaller and do not exceed ~ 6 cm s^{-1} (see Fig. 12 b).

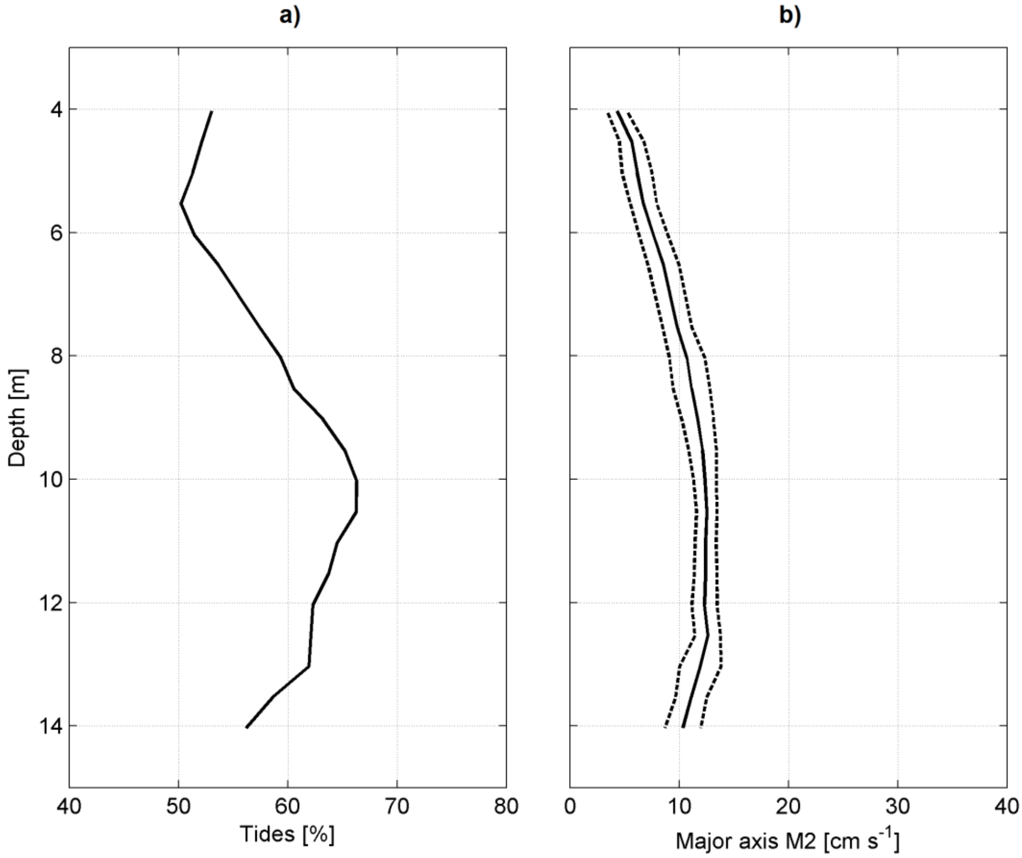

Fig. 19: Results of tidal harmonic analysis for the current velocity record obtained at Mooring Central for the depth interval from ~ 4 m to 14 m between March 28 and April 12, 2012. a) Ratio of tidal variability to total variability of the current velocity record. b) Magnitude of the major axis of the tidal current ellipse associated with the dominant tidal constituent M2. Dashed lines indicate the respective 95 % confidence intervals.

Since tidal variability can only account for ~ 50 % to 65 % of the total variability in the observed current velocity record at Mooring Central (see Fig. 19 a), residual currents are calculated as the difference between the original depth-averaged time series (see Fig. 16) and the predicted tidal signal (see Fig. 18) in order to investigate possible drivers of variability other than tides. Figure 20 shows the resulting time series of depth-averaged residual current velocities. Since depicted current velocities still exhibit variability on ~ 12-hour cycles, the influence of tides at Mooring Central is not completely removed by the tidal harmonic analysis. The short length of the current velocity record likely contributes to this finding. However, it is still possible to identify important features of the residual current regime. For the investigated time period, zonal and meridional residual current velocities range from ~ -7 cm s^{-1} to 7 cm s^{-1} and from -6 cm s^{-1} to 13 cm s^{-1}, respectively (see Fig. 20). These values are within the ranges identified for the residual current regime at Mooring LENA during the ice-covered season (see Fig. 13). Residual current velocities at Mooring Central exhibit pronounced variability over time periods of ~ 4 to 5 days, which demonstrates that non-tidal variability is significantly influences the oceanic current regime under the landfast ice. The most striking features of the record are the strong northwestward residual currents in the time periods from March 29 (day 1) to March 31 (day 3) and from April 3 (day 6) to April 6 (day 9), which are intersected by a period of southeastward residual currents (see Fig. 20).

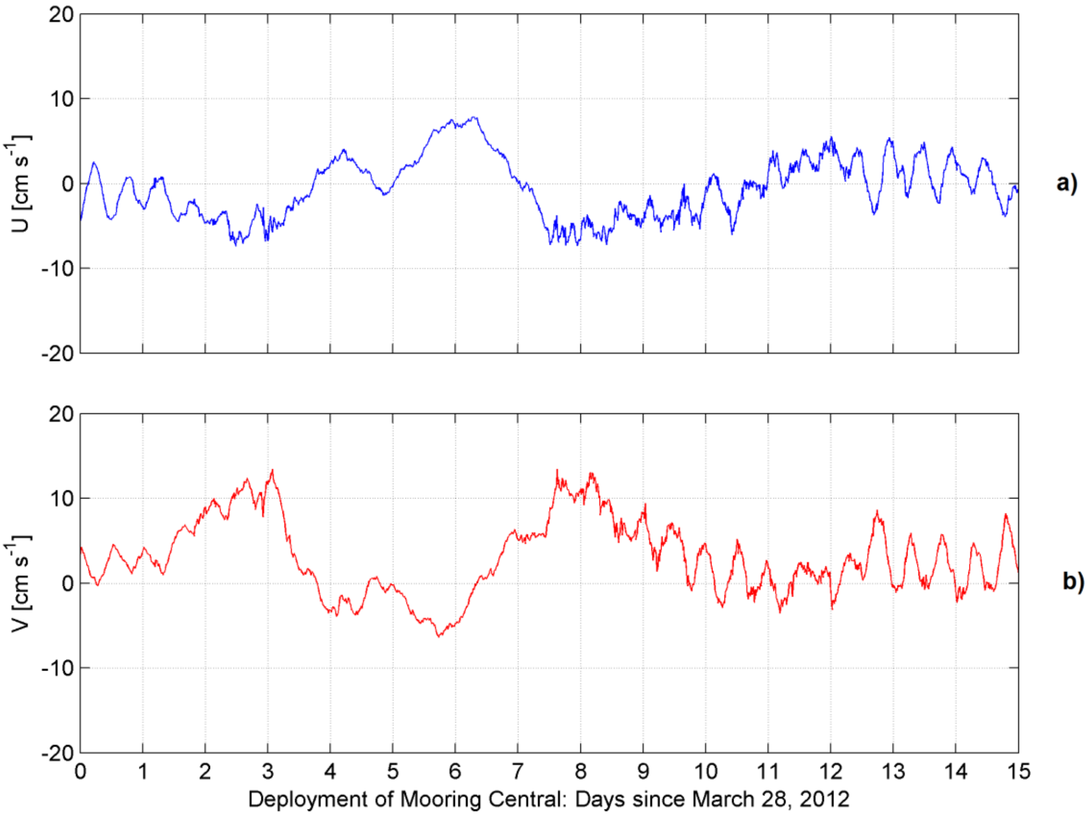

Fig. 20: Time series of the depth-averaged residual zonal (a, blue line) and meridional (b, red line) current velocities at Mooring Central for the time period from March 28 (day 0) to April 12 (day 15), 2012 calculated as the difference of the depth-averaged current velocities (see Fig. 16) and the inferred tidal current velocities (see Fig. 18).

Daily satellite-based sea ice concentration data provided by the National Snow and Ice Data Center indicates the opening of a flaw polynya along the landfast ice edge for the period from April 3 to April 8 (see Fig. 21), which coincides with the second occurrence of strong northward currents (see Fig. 20). The large-scale wind field, observed 10 m above sea level over the Arctic Ocean, derived from the ECMWF ERA-Interim reanalysis dataset, shows that the opening of the flaw polynya is associated with prolonged northwestward winds over the inner Laptev Sea shelf (see Fig. 22).

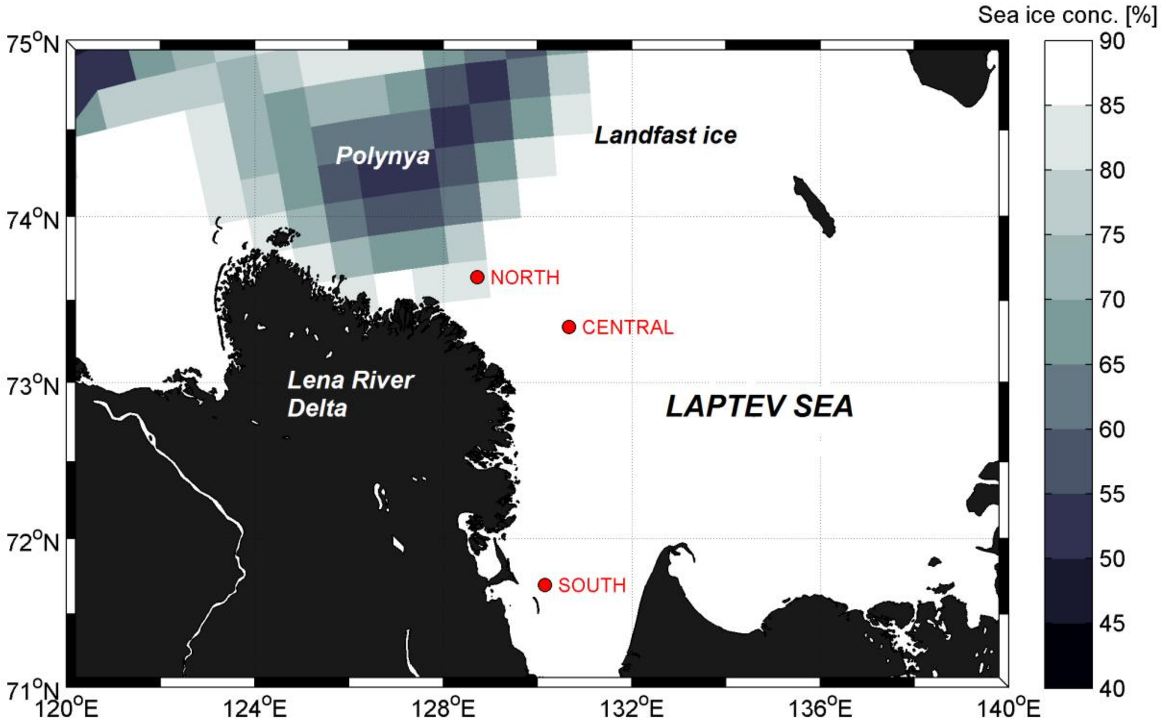

Fig. 21: Map of the sea ice concentration in the southeastern Laptev Sea on April 6, 2012, showing the maximum extent of the flaw polynya, which opened between April 3 and April 8, 2012. Satellite-based sea ice concentration data is provided by the National Snow and Ice Data Center (Cavalieri et al. 2008). Red circles indicate the position of the three ice camps installed during TRANSDRIFT XX in winter 2012.

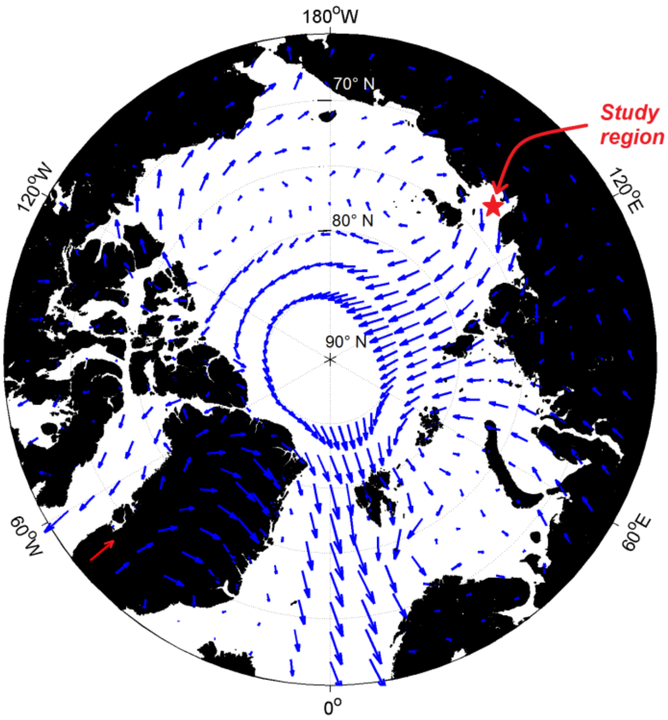

Fig. 22: Map of the time-averaged, large-scale 10 m wind field over the Arctic Ocean for the week from April 1 to April 8, 2012, derived from the ECMWF ERA-Interim reanalysis dataset (Dee et al. 2011, Berrisford et al. 2011). The red arrow represents a wind vector of magnitude 10 m s^{-1}, which can be used as a scale for the wind vectors. The red star indicates the location of the study region. Prolonged northwestward winds can be observed at this location, contributing to the opening of a flaw polynya along the landfast ice edge on the inner Laptev Sea shelf (see Fig. 21).

In order to investigate the influence of the near-surface wind on the oceanic current regime at Mooring Central in more detail, zonal and meridional components of the wind, 10 m above sea level, for the geographic position 73°30’N, 131°20’E, near Mooring Central, are compared to the depth-averaged, low-pass-filtered residual current velocities at Mooring Central for the period from March 28 to April 11, 2012 (see Fig. 23). Wind velocities generally range from ~ -8 m s^{-1} to 2 m s^{-1} for the zonal component and from ~ -5 m s^{-1} to 8 m s^{-1} for the meridional component. The comparison indicates that estimated residual current velocities are largely uncorrelated with the 10 m wind velocities, except for the meridional component during the opening of the flaw polynya (day 6 to day 11). Therefore, the direct effect of near-surface winds on the oceanic current regime at Mooring Central seems to be negligible, with the exception of the time period of the polynya opening. This finding corresponds to the weak relationship between near-surface winds and residual currents observed at Mooring LENA in March and April (see Fig. 15). Consequently, other physical processes (e.g. salinity differences; see Pavlov and Pavlov 1999) are likely the driver of the under-ice residual current regime at Mooring Central.

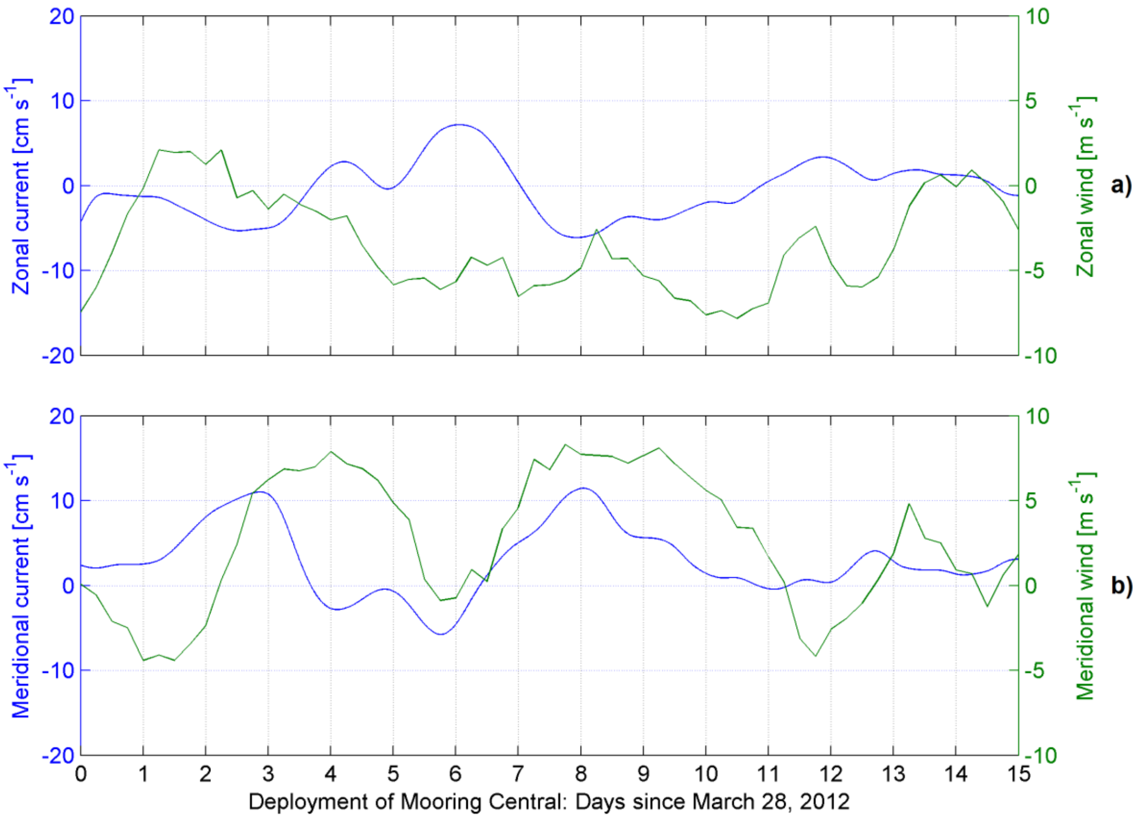

Fig. 23: Time series of depth-averaged, 24-hour low-pass Butterworth filtered residual zonal (a) and meridional (b) current velocities (blue line) at Mooring Central for the time period from March 28 to April 12, 2012 compared to the time series of zonal (a) and meridional (b) 10 m wind velocities (green line) derived from the ECMWF ERA-Interim reanalysis dataset at the geographic position 73°30’N, 131°20’E, near Mooring Central (Dee et al. 2011, Berrisford et al. 2011).

3.2.1.2 Mooring North

The depth-averaged current velocity record for Mooring North, deployed in the vicinity of the landfast ice edge at a water depth of ~ 17 m, provides information on the predominant current velocities and directions under the landfast ice for the depth interval from ~ 4.5 m to 13.5 m during the time period from March 27, 2012 to April 17, 2012 (see Fig. 24).

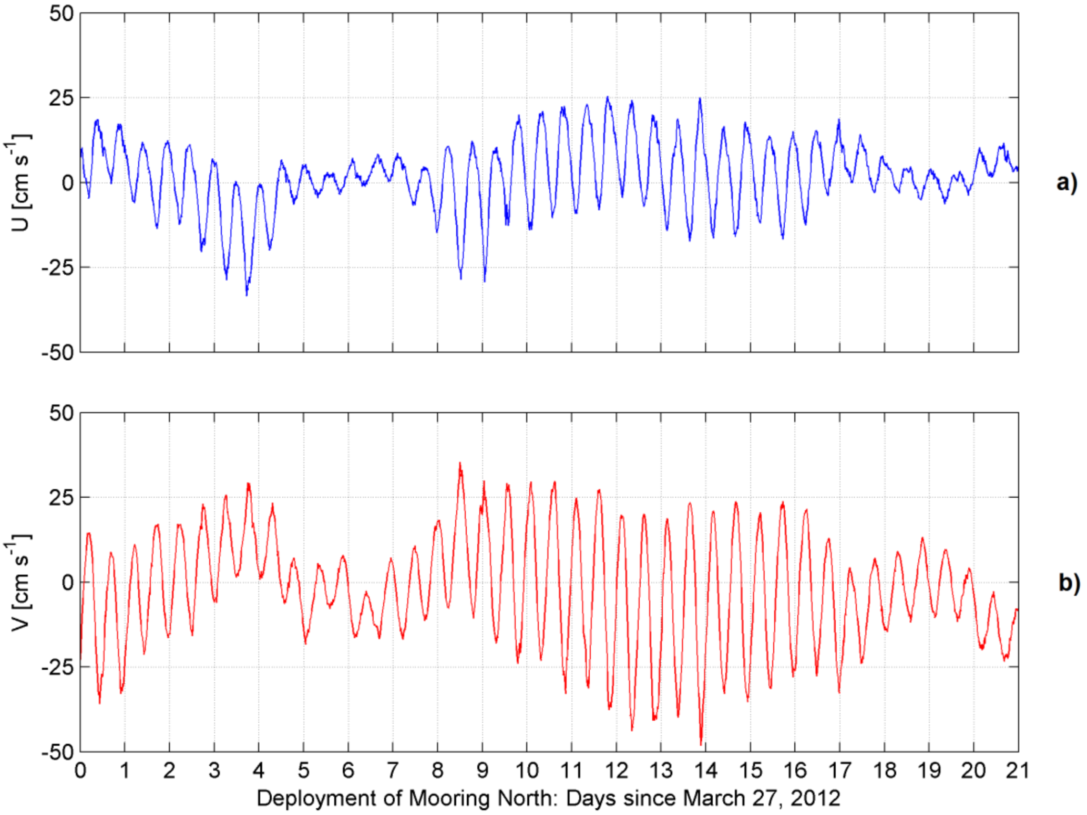

Fig. 24: Time series of depth-averaged zonal (a, blue line) and meridional (b, red line) current velocities obtained at Mooring North between March 27 (day 0) and April 17 (day 21), 2012.

Zonal current velocities vary between ~ -33 cm s^{-1} and 25 cm s^{-1}, and meridional current velocities between ~ -48 cm s^{-1} and 35 cm s^{-1} (see Fig. 24), indicating that oceanic currents at Mooring North, near the landfast ice edge, are significantly stronger than those observed at Mooring Central, at greater distance from the landfast ice edge, for the same time period (see Fig. 16). The dominant characteristic of the record are semidiurnal variations of current velocities and directions (see Fig. 24), supporting the important role of tidal dynamics for the under-ice circulation, as observed at Mooring Central and Mooring LENA (see Fig. 7, 16). Moreover, pronounced variability over time periods of several days is apparent in the record (see Fig. 24), in line with the findings from Mooring Central (see Fig. 16). The principal current ellipse estimated from the depth-averaged current velocity record at Mooring North indicates predominant variability of oceanic currents along its major axis, which is rotated by ~ 149.7°, i.e. in a southeast-northwest direction. The magnitudes of the major and minor axis associated with the principal current ellipse are ~ 18.1 cm s^{-1} and 4.2 cm s^{-1}, respectively. The characteristics of the principal current ellipse also hint at strong influence of tidal currents on the oceanic current regime at Mooring North.

In order to gather information on the vertical structure of current regime at Mooring North, current velocities obtained for individual depth bins are averaged over the entire record length, resulting in a vertical profile of mean current velocities (see Fig. 25).

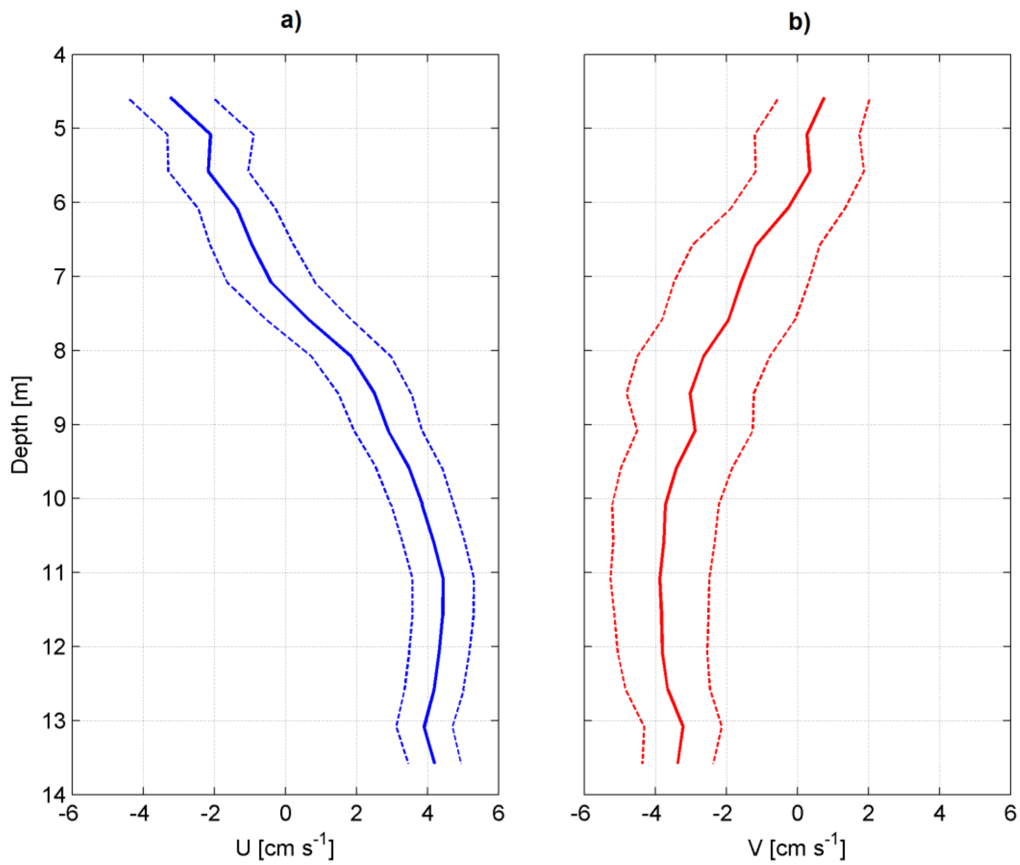

Fig. 25: Vertical profile of time-averaged, zonal (a, blue line) and meridional (b, red line) current velocities obtained at Mooring North for the depth interval from ~ 4.5 m to 13.5 m between March 27 and April 17, 2012. Dashed lines indicate the respective standard error of the mean.

Mean zonal velocities at Mooring North increase from ~ -3.2 cm s^{-1} at 4.5 m depth to ~ 4.4 cm s^{-1} at 11 m depth. Below this depth, the zonal velocity component varies only slightly around 4 cm s^{-1}. Standard errors associated with the mean zonal current velocities vary between ~ ±0.7 cm s^{-1} and ±1.2 cm s^{-1} (see Fig. 25a). The meridional velocity component decreases from ~ 0.8 cm s^{-1} at 4.5 m depth to ~ -3.9 cm s^{-1} at 11 m depth, followed by relatively small variations between ~ -3.4 cm s^{-1} and -3.9 cm s^{-1} in the lower water column. Standard errors associated with the meridional velocity component range from ±1.0 cm s^{-1} to ±1.9 cm s^{-1} (see Fig. 25b). The described vertical structure of mean current velocities indicates a shift from predominantly westward currents near the surface towards southeastward currents at greater water depths. Hence, the observed vertical current profile at Mooring North is very different from the profiles measured at Mooring Central and Mooring LENA, deployed at greater distance to the landfast ice edge, which both indicate predominant northward current directions (see Fig. 8, 17). Furthermore, observed mean current velocities at Mooring North are significantly higher than at the other two locations (see Fig. 8, 17, 25).

To investigate the tidal influence on the oceanic current regime at Mooring North, tidal harmonic analysis is performed using the depth-averaged current velocity record (see Fig. 24) as input. Tidal variability explains 74.6 % of the total variability in the obtained current velocity time series (see Table 8), exceeding the tidal influence estimated for Mooring Central by a difference of 10 %. Six significant tidal constituents have been identified in the three-week record obtained at Mooring North. The dominant tidal constituent for the observed time period is the principal lunar semidiurnal component, M2, followed by the principal solar semidiurnal component, S2, and the lunisolar synodic fortnightly component, MSF. These tidal constituents also play an important role for the tidal dynamics at Mooring Central and Mooring LENA (see Table 6, 7). The tidal current ellipses indicate a strong predominance of tidal variability along the respective major axis. The M2 tidal current ellipse is characterized by a magnitude of 20.6 cm s^{-1} (±2.4 cm s^{-1}) and an orientation of 118.1° (±6.9°). The S2 and MSF tidal current ellipses exhibit major axes with magnitudes of 11.0 cm s^{-1} (±2.3 cm s^{-1}) and 4.5 cm s^{-1} (±3.2 cm s^{-1}), and orientations of 119.4° (±14.5°) and 141.3° (±58.7°), respectively. The lunar diurnal component, K1, which is also identified in the current velocity record at Mooring Central (see Table 7), together with the higher harmonic tidal constituents M4, referring to the shallow water overtides of the principal lunar component, and MS4, the shallow water quarter-diurnal lunisolar diurnal component, account for a considerably smaller part of the tidal variability in the record (see Table 8; see Godin (1972) for further information on tidal constituents).

Table 8: Results of tidal harmonic analysis based on depth-averaged current velocity record obtained at Mooring North between March 27 and April 17, 2012. Information on frequency, major and minor axes of the tidal ellipse, ellipse orientation, constituent phase, and signal-to-noise ratio for all identified significant tidal constituents with a signal-to-noise ratio of over 2. For the major and minor axes, ellipse orientation, and constituent phase, the respective 95 % confidence intervals are provided.

Tidal constituent	**Frequency [cycles h^{-1}]**	**Major axis [cm s^{-1}]**	**Minor axis [cm s^{-1}]**	**Ellipse orientation [°]**	**Constituent phase [° relative to Greenwich]**	**Signal-to-noise ratio**
M2	0.0805114	20.6 ± 2.4	-1.7 ± 2.4	118.1 ± 6.9	37.8 ± 6.8	73
S2	0.0833333	11.0 ± 2.3	-0.5 ± 2.6	119.4 ± 14.5	92.4 ± 13.3	24
MS4	0.1638447	1.1 ± 0.4	-0.7 ± 0.4	162.5 ± 42.9	179.2 ± 50.6	6.9
M4	0.1610228	1.1 ± 0.5	-0.7 ± 0.3	174.8 ± 38.7	115.3 ± 42.7	5.8
K1	0.0417807	1.3 ± 0.9	-0.3 ± 0.8	110.2 ± 38.7	7.0 ± 42.5	2.2
MSF	0.0028219	4.5 ± 3.2	-2.0 ± 3.0	141.3 ± 58.7	243.8 ± 50.9	2
Total variability explained by tidal signal: 74.6 %						

Based on the results of the tidal harmonic analysis, the time series of predicted depth-averaged tidal current velocities at Mooring North is computed, taking into account the magnitude, phase, and orientation of all identified significant tidal constituents (see Fig. 26). Inferred zonal and meridional current velocities range from ~ -13 cm s^{-1} to 18 cm s^{-1} and from ~ -31 cm s^{-1} to 26 cm s^{-1}, respectively. Strongly alternating northwestward and southeastward currents clearly demonstrate the semidiurnal tidal variability in the record. Diurnal and fortnightly variations, which modulate the tidal signal, are also evident in the time series (see Fig. 26). The timescales of temporal variability as well as the directions of the interred tidal currents correspond to the findings from Mooring Central and Mooring LENA (see Fig. 11, 18). However, significantly higher tidal current velocities are predicted for Mooring North, especially with respect to the meridional component. Maximum variations of meridional current velocities at Mooring North are estimated to be 3 to 4 times larger than at Mooring Central during the same time period (see Fig. 18) and 4 to 5 times larger than at Mooring LENA (see Fig. 11).

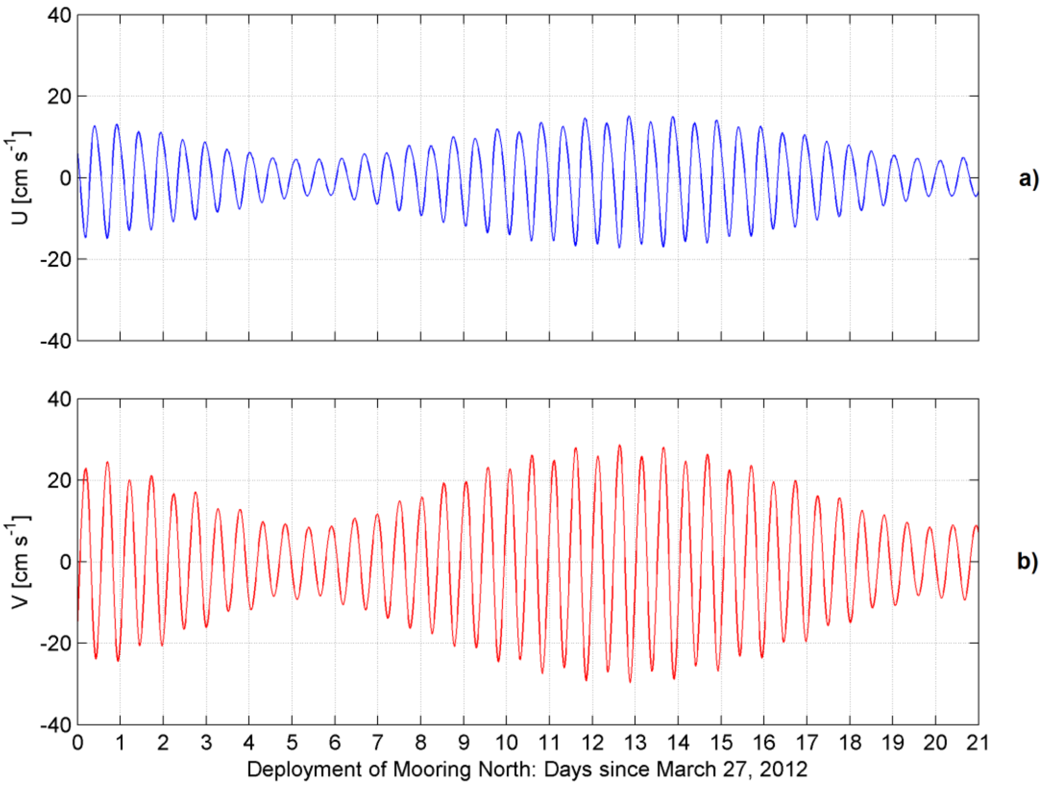

Fig. 26: Time series of inferred zonal (a, blue line) and meridional (b, red line) tidal current velocities based on the results of the tidal harmonic analysis of the depth-averaged current record from Mooring North (see Fig. 24) for the time period from March 27 (day 0) to April 17 (day 21), 2012.

In order to examine the vertical structure of the tidal influence at Mooring North, tidal harmonic analysis is performed for current velocity data obtained from individual depth bins (see Fig. 27). Figure 27 a) depicts the percentage of the total variability that is explained by tidal variability as a function of water depth. The influence of tides on observed current velocities at Mooring North ranges from ~ 58 % to 72 % throughout the water column. The ratio of tidal variability to total variability increases from ~ 58 % at 4.5 m water depth to its maximum of ~ 72 % at 6.5 m water depth. Between ~ 6.5 m and 9 m water depth the tidal influence varies only slightly around 70 %, followed by a decrease to ~ 60 % in the lower water column (see Fig. 27 a). The observed vertical structure of the ratio of tidal variability to total variability at Mooring North indicates pronounced variability with depth, in line with the findings from Mooring Central and Mooring LENA (see Fig. 12a, 19a). In comparison with Mooring Central, the tidal influence is also overall ~ 10 % higher. Furthermore, the maximum of the tidal influence is located at a shallower water depth of ~ 7 m, compared to ~ 10 m at Mooring Central (see Fig. 19 a). Tidal current velocities associated with the major axis of the M2 tidal constituent show a similar vertical structure as the magnitude of the tidal influence.

M2 velocities increase from ~ 18.5 cm s^{-1} at 4.5 m depth to the maximum of ~ 26 cm s^{-1} at ~7-8 m depth, followed by a decrease to ~ 13.3 cm s^{-1} at 13.5 m depth. In general, M2 velocities are significantly higher than at Mooring Central and Mooring LENA. The peak M2 velocity is approximately twice as high as identified at Mooring Central and eight times as high as identified at Mooring LENA, respectively. Moreover, the maximum M2 velocity occurs at a shallower water depth (~ 7 m) compared to the findings from Mooring Central and Mooring LENA (see Fig. 12 b, 19 b). However, M2 velocity maxima generally correspond to the respective maxima in the tidal influence (see Fig. 12, 19, 27).

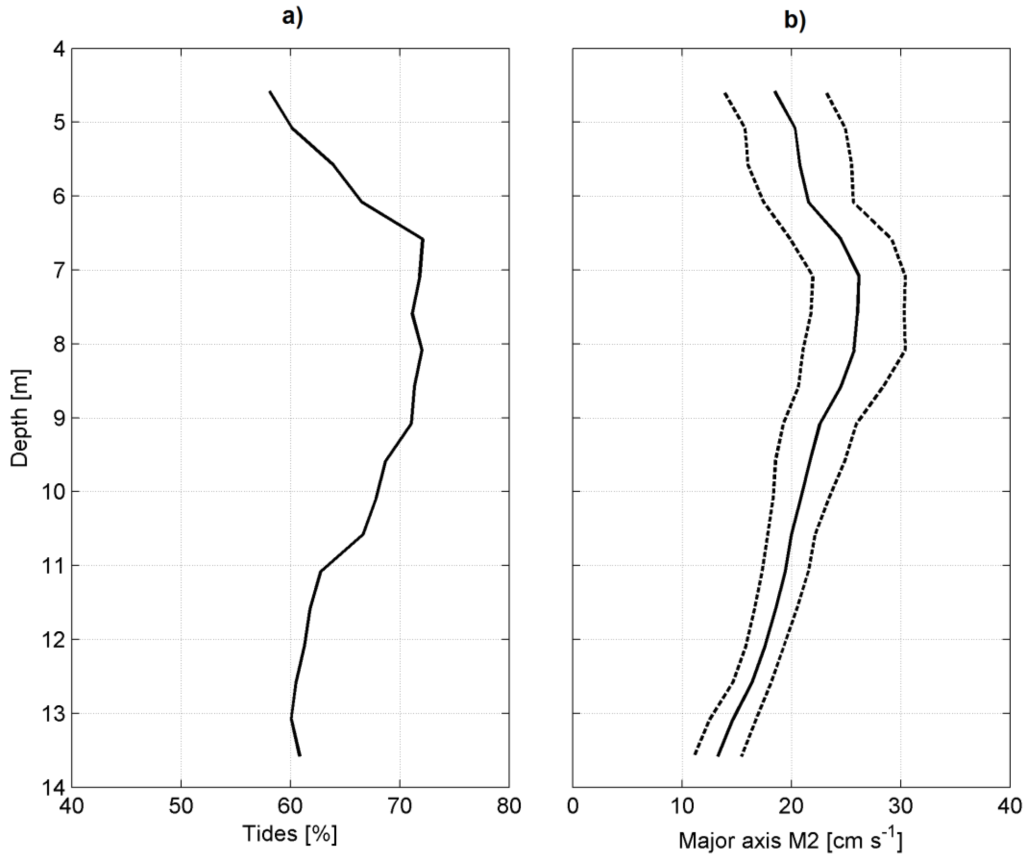

Fig. 27: Results of tidal harmonic analysis for the current velocity record obtained at Mooring North for the depth interval from ~ 4.5 m to 13.5 m between March 27 and April 17, 2012. a) Ratio of tidal variability to total variability of the current velocity record. b) Magnitude of the major axis of the tidal current ellipse associated with the dominant tidal constituent M2. Dashed lines indicate the respective 95 % confidence intervals.

To investigate possible sources of variability of current velocities other than tides in the time series obtained at Mooring North, residual currents are calculated as the difference between the original depth-averaged time series (see Fig. 24) and the predicted tidal signal (see Fig. 26). The resulting time series exhibits still variability on ~ 12-hour cycles, indicating that the influence of tides at Mooring North is not completely removed by the tidal harmonic analysis (see Fig. 28). The short length of the current velocity record likely contributes to this finding. However, it is still possible to identify important features of the residual current regime. Residual current velocities vary significantly from ~ -25 cm s^{-1} to 16 cm s^{-1} for the zonal component, and from ~ -23 cm s^{-1} to 18 cm s^{-1} for the meridional component. Residual currents are predominantly directed towards the southeast. Extremely strong southeastward residual currents, exceeding magnitudes of 20 cm s^{-1}, occur around April 2 (day 6) and April 16, 2012 (day 20). The most prominent features of the record are two phases of strong northwestward residual currents, which can be observed around March 30 (day 3) and April 4, 2012 (day 8) (see Fig. 28). The occurrence of these strong northwestward residual currents at Mooring North corresponds to the findings from Mooring Central (see Fig. 20), indicating that the physical processes associated with the generation of these currents influence the large-scale circulation under the landfast ice on the inner Laptev Sea shelf. Polynya activity associated with persistent, large-scale, northward wind fields may influence the residual current regime at Mooring North (see Fig. 21, 22).

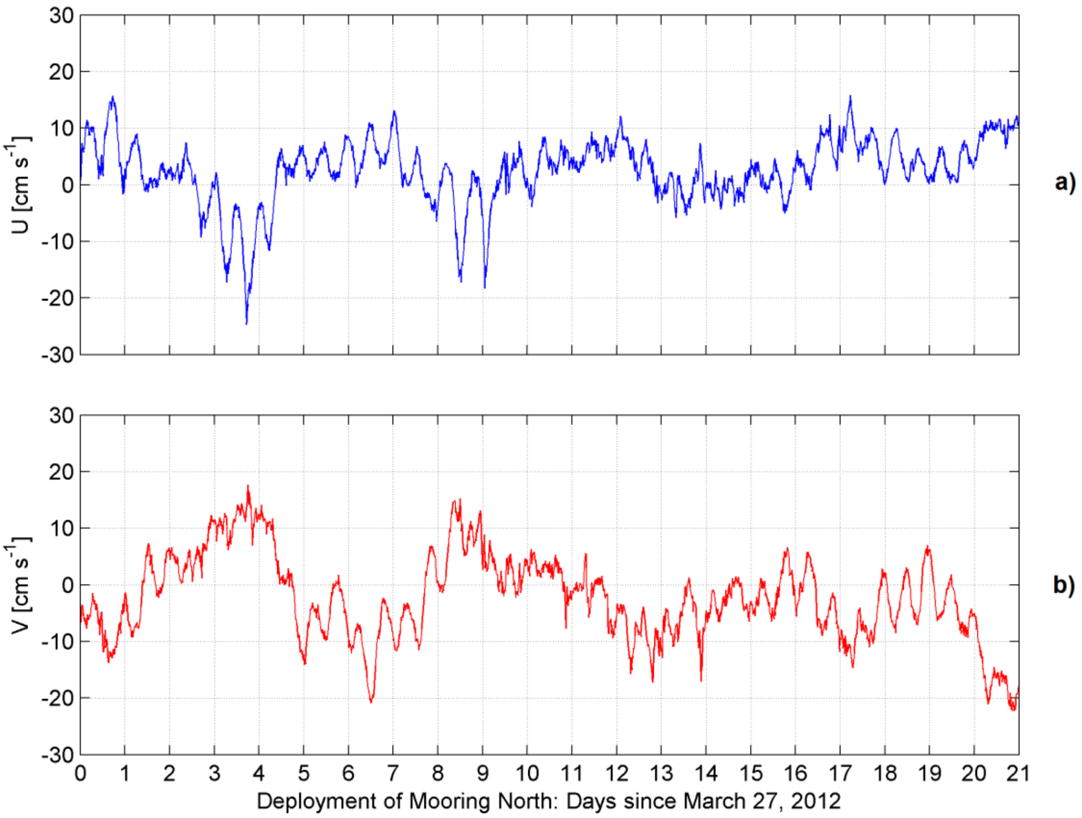

Fig. 28: Time series of the depth-averaged residual zonal (a, blue line) and meridional (b, red line) current velocities at Mooring North for the time period from March 27 (day 0) to April 17 (day 21), 2012 calculated as the difference of the depth-averaged current velocities (see Fig. 24) and the inferred tidal current velocities (see Fig. 26).

The influence of near-surface winds on the oceanic current regime at Mooring North is examined in greater detail with the help of zonal and meridional components of the wind, 10 m above sea level, for the geographic position 74°20’N, 128°20’E, near the landfast ice edge, and the depth-averaged, low-pass-filtered residual current velocities at Mooring North for the period from March 27 to April 17, 2012 (see Fig. 29).

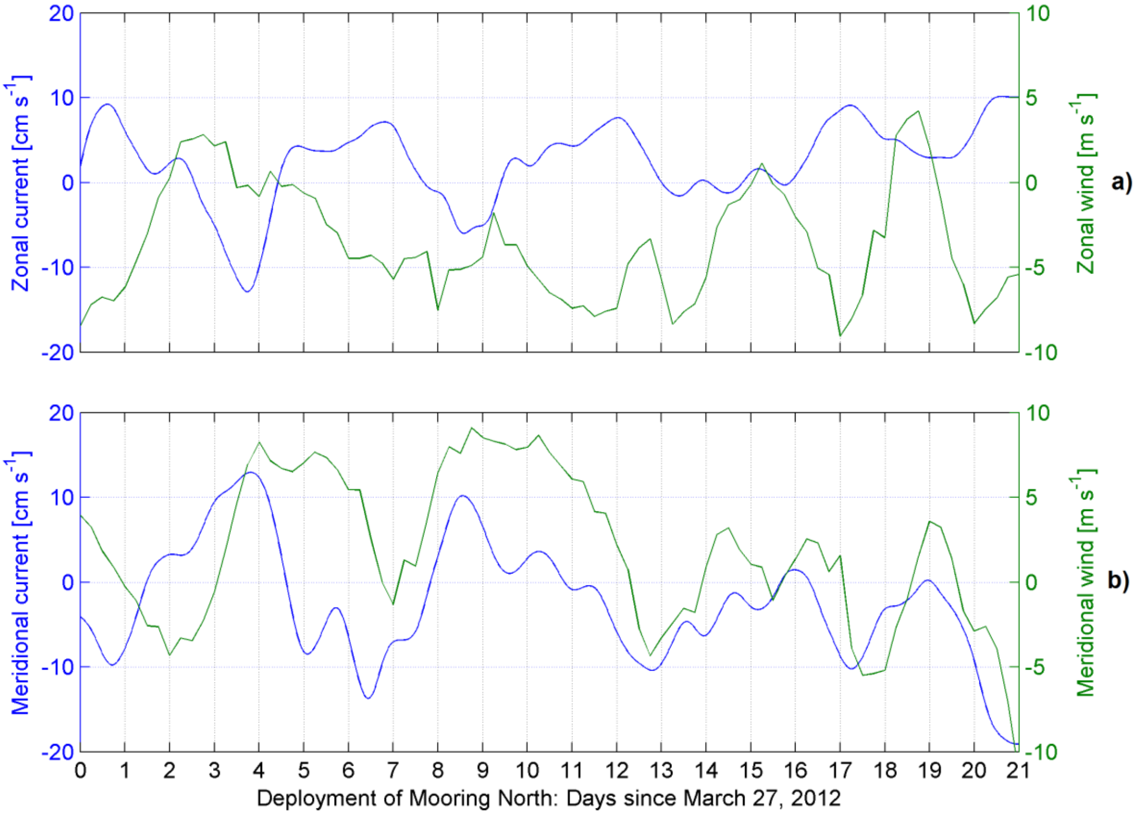

Fig. 29: Time series of depth-averaged, 24-hour low-pass Butterworth filtered residual zonal (a) and meridional (b) current velocities (blue line) at Mooring North for the time period from March 27 to April 17, 2012 compared to the time series of zonal (a) and meridional (b) 10 m wind velocities (green line) derived from the ECMWF ERA-Interim reanalysis dataset at the geographic position 74°20’N, 128°20’E, near the landfast ice edge (Dee et al. 2011, Berrisford et al. 2011).

Wind velocities generally range from ~ -9 m s^{-1} to 4 m s^{-1} for the zonal component and from ~ -10 m s^{-1} to 9 m s^{-1} for the meridional component. The predominant wind direction throughout the observation period is to the northwest (see Fig. 29). While the zonal component of the residual current velocities seems to be largely uncorrelated with the 10 m wind velocities, the meridional component shows reasonable alignment with the 10 m wind velocities after April 3 (day 7), indicating that current velocities at Mooring North might be influenced by wind forcing (see Fig. 29). The effect of near-surface winds on the oceanic current regime seems to be stronger at Mooring North than at Mooring Central and Mooring LENA, which are located at greater distance to the landfast ice edge (see Fig. 14, 23, 29). Consequently, the influence of different physical processes, which determine the current regime under the landfast ice on the southeastern Laptev Sea shelf, likely varies spatially with distance to the landfast ice edge.

In summary, the findings from Mooring Central and Mooring North support the role of tides as the main driver of oceanic currents under the landfast ice on the southeastern Laptev Sea shelf, as identified at Mooring LENA (see Table 6, 7, 8). Wind forcing and other physical processes (e.g. salinity differences) play a significantly smaller role for the under-ice current regime. The detailed investigation of the current records from Mooring Central and Mooring North indicates pronounced spatial differences of the under-ice circulation, which are possibly connected to the different distance of the moorings to the landfast ice edge. Mean current directions at the two locations are completely different from each other (see Fig. 17, 25), indicating the spatially varying influence of different drivers of the under-ice circulation. Observed current velocities at Mooring North are significantly higher than at Mooring Central (see Fig. 16, 24). The results of the tidal harmonic analysis (see Table 7, 8) and the comparison of the residual current signal to near-surface wind forcing (see Fig. 23, 29) indicate that the higher current velocities at Mooring North are likely caused by stronger influence of tidal dynamics and wind forcing at this location. Moreover, polynya activity has been identified to significantly modify the influence of the different physical processes on the oceanic current regime (see Fig. 21, 23, 29). Overall, the circulation under the landfast ice on the southeastern Laptev Sea shelf seems to be dominated by the complex interplay between different physical processes, including tidal dynamics, wind forcing, polynya activity, and possibly large-scale salinity differences.

3.2.2 Current regime in winter 2008 and 2009

During the winter expeditions TRANSDRIFT XIII and XV in 2008 and 2009, respectively, short-term moorings were deployed at seven oceanographic stations (TI0801, TI0802, TI0804, TI0805, TI0808, TI0901, and TI0908) in the vicinity of the landfast ice edge (see Fig. 2). Current velocity records obtained at these stations have already been partly analyzed by earlier studies by Dmitrenko et al. (2010a), Dmitrenko et al. (2010c), and Dmitrenko et al. (2012). The main findings of these studies with respect to the general features of the oceanic current regime along the landfast ice edge are briefly outlined in this section to provide an overview of the datasets before further analysis and to put the findings from Mooring North into a wider context. Furthermore, information on predominant current magnitudes and directions along the landfast ice edge is derived from the current velocity records obtained during TRANSDRIFT XIII and XV, providing some indication of the large-scale circulation pattern under the landfast ice on the inner Laptev Sea shelf during the ice-covered season.

In line with the findings from Mooring North, studies by Dmitrenko et al. (2010a), Dmitrenko et al. (2010c), and Dmitrenko et al. (2012) have also identified tidal dynamics as an important driver of the under-ice oceanic current regime on the inner Laptev Sea shelf at moorings M08-1 (station TI0801), M08-2 (station TI0802), and POLYNYA III (station TI0908) near the landfast ice edge in winter 2008 and 2009, respectively (see Fig. 2). Pronounced semidiurnal variability has been observed in the current records, with M2 being the dominant tidal constituent. Tidal flow velocities have been found to be modulated by the spring-neap tidal cycle and to vary considerably with depth (Dmitrenko et al. 2010c, Dmitrenko et al. 2012). Moreover, the close relationship between wind forcing and oceanic current response observed at Mooring North is supported by the current velocity data from winter 2008, which indicates a largely consistent under-ice flow at mooring M08-2 with the mean wind-forcing (Dmitrenko et al. 2010a). The important role of polynya activity for the oceanic current regime along the landfast ice edge on the inner Laptev Sea shelf observed at Mooring North is also supported by the current velocity records obtained under the landfast ice in winter 2008 and 2009. Polynya events, from April 28 to May 3, 2008, as well as from April 15 to April 23, 2009, have been identified to considerably influence the oceanic current regime at moorings M08-1, M08-2, and POLYNYA III (Dmitrenko et al. 2010a, Dmitrenko et al. 2010c, Dmitrenko et al. 2012). Therefore, the results from earlier studies also indicate tidal dynamics, wind forcing, and polynya activity as important forcing mechanism of the under-ice current regime on the southeastern Laptev Sea shelf during the ice-covered season.

The comparison of the under-ice current regime at Mooring Central and Mooring North indicates significant spatial differences with respect to current directions and magnitudes, as well as the influences of different physical drivers of oceanic currents under the landfast ice on the inner Laptev Sea shelf. These differences may be related to the varying distance from the landfast ice edge. In order to investigate whether spatial differences of the oceanic current regime also exist along the landfast ice edge, current velocity data obtained from short-term oceanographic moorings deployed near the landfast ice edge in winter 2008 and 2009, respectively (see Fig. 2), is analyzed with respect to mean current magnitudes and directions along the landfast ice edge. Figures 30 and 31 depict the vertical profiles of mean current velocities observed at seven different oceanographic stations located along the landfast ice edge during their respective deployment periods in winter 2008 (from southwest to northeast: TI0802, TI0801, TI0808, TI0804, TI0805) and winter 2009 (from southwest to northeast: TI0901, TI0908) (see Fig. 2). Mean zonal and meridional current velocities along the landfast ice edge are generally low with absolute magnitudes below 5 cm s^{-1} (see Fig. 30, 31), respectively, in line with the findings from Mooring Central and Mooring North (see Fig. 17, 25). Standard errors associated with the time-averaged velocity components are up to ~ ±1 cm s^{-1} for measurements from 2008 (see Fig. 30), and up to ~ ±3 cm s^{-1} for measurements from 2009 (see Fig. 31). In general, the vertical profiles of mean current velocities indicate significant spatial differences of current magnitudes and directions along the landfast ice edge (see Fig. 30). The vertical structure of the current velocities at the most southwesterly mooring M08-2 (station TI0802) obtained during TRANSDRIFT XIII in winter 2008 is similar to the pattern observed at Mooring North. It is characterized by a relatively strong northwestward current of ~ 5.6 cm s^{-1} near the surface, changing towards a weaker eastward current below ~ 11 m depth, which reaches a magnitude of ~ 2.5 cm s^{-1} near the bottom (see Fig. 30 a). The mean current velocity profiles obtained further northeast at moorings M08-1 (station TI0801) and M08-5 (station TI0808) show considerably weaker currents, in combination with different directions (see Fig. 30 b, c). At M08-1, the under-ice current regime changes from a northwestward current near the surface associated with a magnitude of ~ 1 cm s^{-1} to a southwestward current near the bottom associated with a magnitude of up to ~ 1.6 cm s^{-1} (see Fig. 30 b). At M08-5, a very weak southward current (~ 0.3 cm s^{-1}) can be observed at the surface, shifting towards a southeastward current with a higher magnitude of ~ 1 cm s^{-1} throughout the water column, and finally returning to a southward current near the bottom with a speed of up to ~ 2.5 cm s^{-1} (see Fig. 30 c). The mean current velocity profile at mooring M08-3 (station TI0804) indicates very weak southwestward currents throughout the water column. Magnitudes of the observed current magnitudes are less than 0.2 cm s^{-1} near the surface and ~ 1 cm s^{-1} in the lower water column (see Fig. 30 d). The current velocity profile obtained at the most northeasterly mooring, M08-4 (station TI0805), reveals similarities with the profile measured at Mooring Central in 2012. A relatively strong northwestward current (~ 3 cm s^{-1}) can be observed near the surface, which changes to a weaker westward current (~ 2 cm s^{-1}) near the bottom (see Fig. 30 e). Since the oceanographic moorings were deployed over similar time intervals, the current regime observed along the landfast ice edge in the southeastern Laptev Sea in April and May 2008 exhibits pronounced spatial variability of current directions and magnitudes.

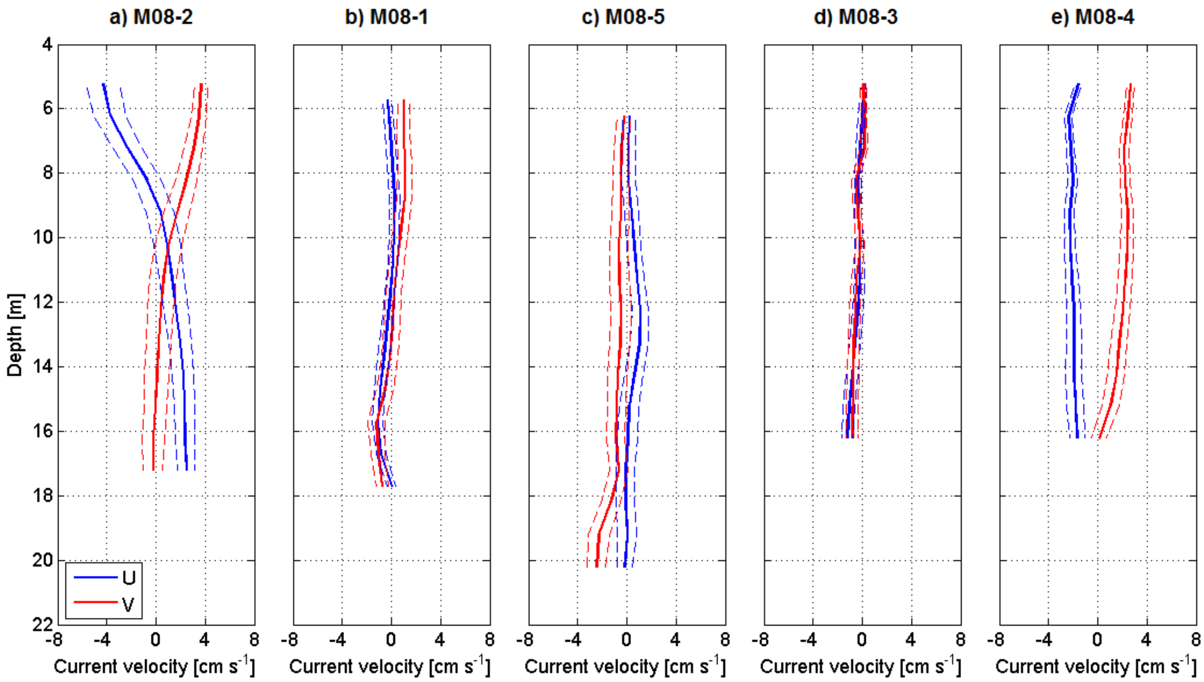

Fig. 30: Vertical profiles of time-averaged, zonal (blue line) and meridional (red line) current velocities obtained at different moorings during TRANSDRIFT XIII in winter 2008. Dashed lines indicate the respective standard error of the mean. a) M08-2 (station TI0802); b) M08-1 (station TI0801); c) M08-5 (station TI0808); d) M08-3 (station TI0804); e) M08-4 (station TI0805).

The mean current velocity profiles obtained from the short-term moorings POLYNYA I and POLYNYA III, deployed along the landfast ice edge, in the vicinity of the locations of moorings M08-1 and M08-8, within the framework of the winter expedition TRANSDRIFT XV in 2009, indicate a significantly different pattern of the under-ice oceanic current regime than observed in 2008. At POLYNYA I, a change from a southwestward current with a magnitude of ~ 2.5 cm s^{-1} near the surface towards a stronger southward current (~ 3-4 cm s^{-1}) in the lower water column can be identified (see Fig. 31 a). At POLYNYA III, a shift from a southwestward current with a magnitude of ~2.2 cm s^{-1} near the surface to a strong northwestward current (~ 4-5 cm s^{-1}) at ~ 9 m depth, which decreases throughout the water column and vanishes near the bottom, can be observed (see Fig. 31 b). Since the moorings were deployed less than 20 km apart from each other (see Fig. 2), the results indicate high variability of current directions and magnitudes along the landfast ice edge, in line with the findings from winter 2008. However, the moorings deployed during TRANSDRIFT XV in winter 2009 measured current velocities during different time intervals. Therefore, the observed differences in the current regime may be significantly influenced by temporal variability of the current regime. In summary, the findings from TRANSDRIFT XIII and XV indicate that the circulation under the landfast ice on the inner Laptev Sea shelf is highly complex.

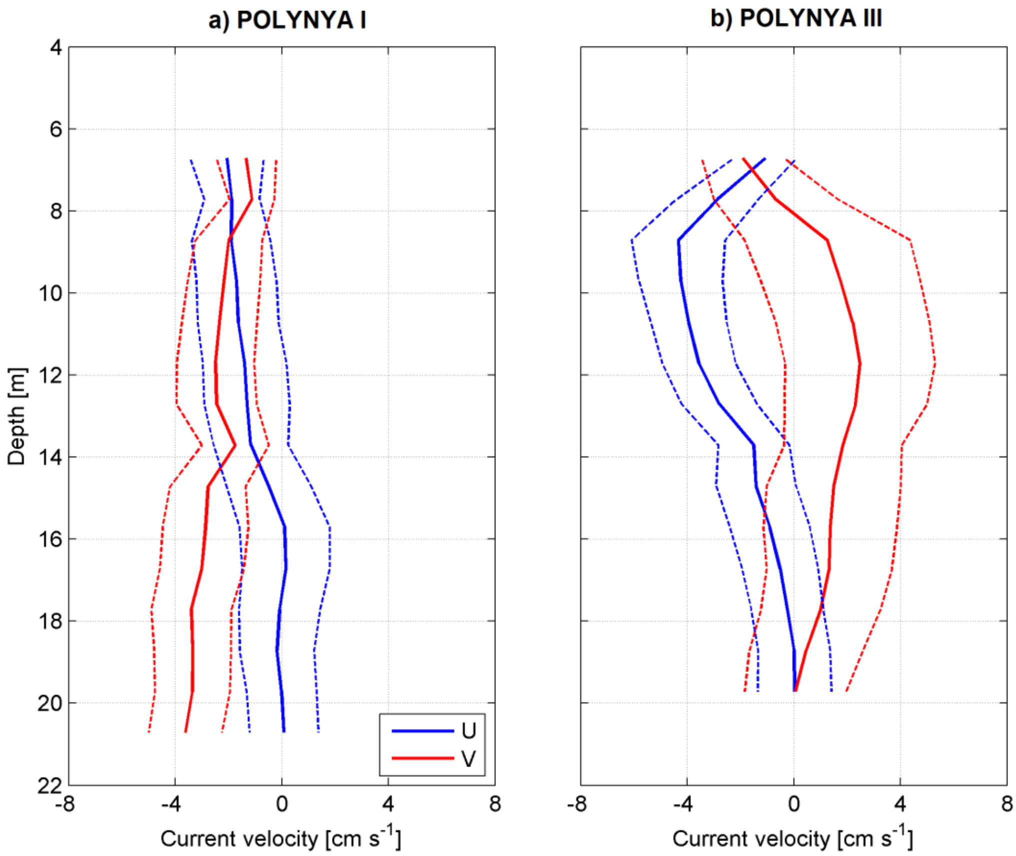

Fig. 31: Vertical profiles of time-averaged, zonal (blue line) and meridional (red line) current velocities obtained at the moorings POLYNYA I (a) and POLYNYA III (b) during TRANSDRIFT XV in winter 2009. Dashed lines indicate the respective standard error of the mean.

To provide a better overview of the complex structure of the under-ice current regime, a map showing the mean current velocity vectors at the different mooring locations in winter 2008 and 2009, complemented by the findings from Mooring LENA, Mooring Central, and Mooring North, is presented in this study (see Fig. 32). The mean current velocity vectors are based on averaging the respective current velocity records over time and depth. It can be inferred that the oceanographic datasets from the different mooring locations do not show a consistent large-scale pattern of the current regime in the southeastern Laptev Sea during the ice-covered season. However, some alignment of mean current directions with the local bathymetry can be observed (e.g. at Mooring Central), indicating that local influences might play an important role for the under-ice current regime on the inner Laptev Sea shelf.

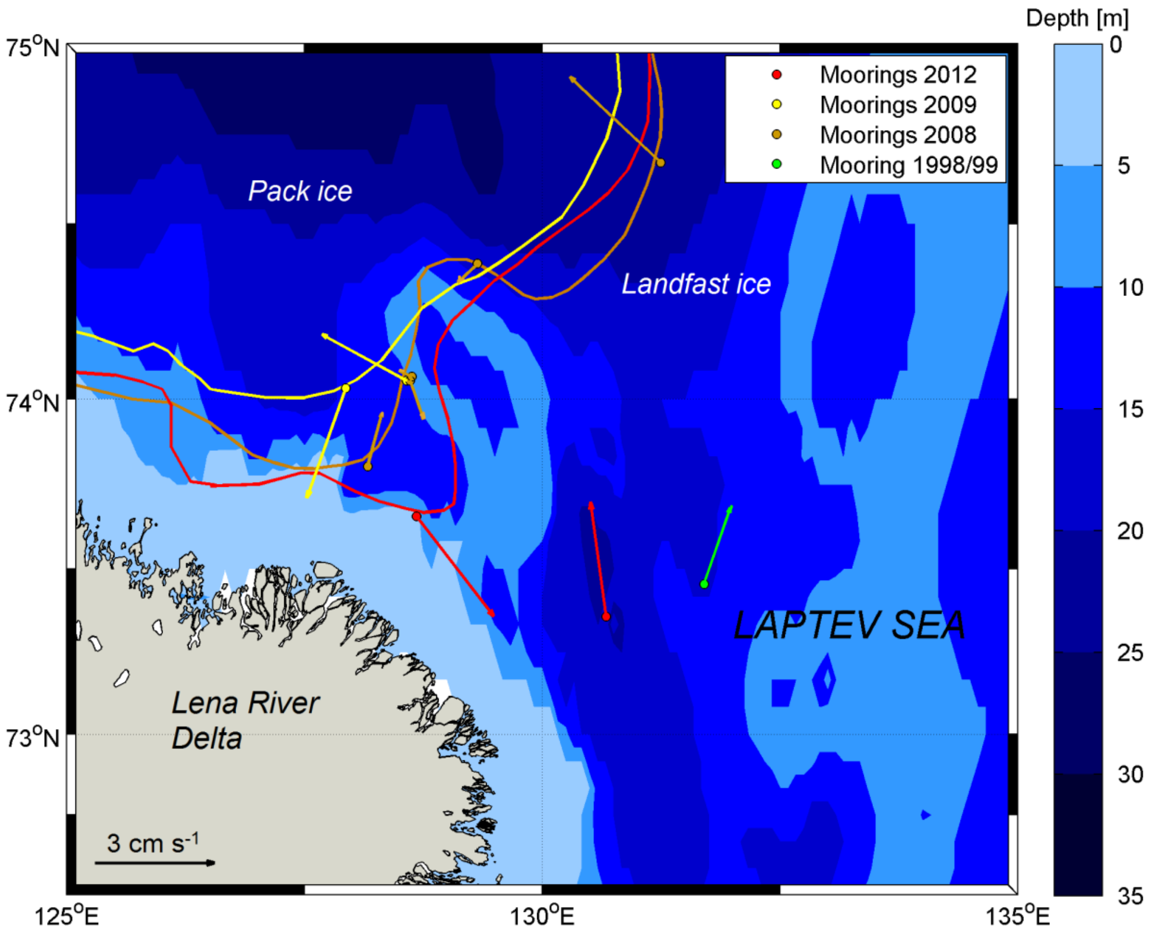

Fig. 32: Map of the study region, showing mean current vectors derived from averaging the current velocity records from the different moorings, deployed under the landfast ice in winter 1998/99 (green), 2008 (brown), 2009 (yellow), and 2012 (red), over time and depth. The black arrow in the left hand corner indicates a current vector with a magnitude of 3 cm s^{-1}, which can be used as a scale. The bathymetry is based on the International Bathymetric Chart of the Arctic Ocean (IBCAO) (Jakobsson et al. 2008). The brown, yellow, and red lines indicate the position of the landfast ice edge, based on operational sea ice charts provided by the Arctic and Antarctic Research Institute (AARI) (Mahoney et al. 2008, Selyuzhenok et al. 2015) for the first week of April in 2008, 2009, and 2012, respectively.

3.3 Hydrographic conditions under the landfast ice

This section provides an overview of the general characteristics of the hydrographic conditions under the landfast ice on the inner Laptev Sea shelf using CTD profiles obtained from three different locations during the winter expedition TRANSDRIFT XX in 2012. Furthermore, CTD profiles from the winter expeditions TRANSDRIFT XIII and XV in 2008 and 2009, respectively, are analyzed to put the results from winter 2012 into a larger spatial and temporal context and to investigate the variability of hydrographic conditions near the landfast ice edge in greater detail.

3.3.1 Hydrographic conditions in winter 2012

During the winter expedition TRANSDRIFT XX in March and April 2012, CTD profiles were measured at three different locations on the inner Laptev Sea shelf, namely Camp North (stations TI1201, TI1206, TI1209), Camp Central (stations TI1202, TI1207), and Camp South (stations TI1205, TI1210), positioned at varying distances to the landfast ice edge (see Fig. 2). Salinity and temperature data obtained from these locations is analyzed to identify the general characteristics of the hydrographic conditions during the ice-covered season as well as spatial differences in a north-south direction under the landfast ice.

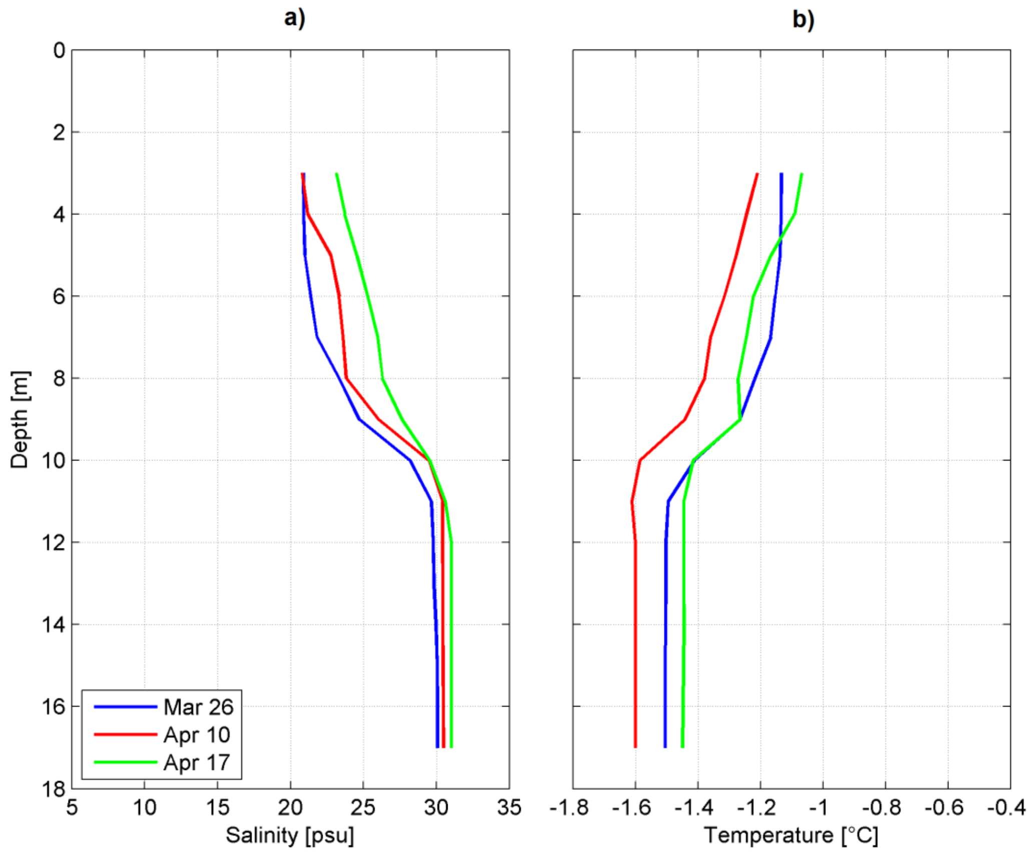

Fig. 33: Vertical salinity (a) and temperature (b) profiles measured at Camp North on the inner Laptev Sea shelf on March 26 (station TI1201, blue line), April 10 (station TI1206, green line), and April 17, 2012 (station TI1209, red line). Data is presented in 1 m depth-averaged intervals.

The vertical temperature and salinity profiles obtained at Camp North on March 26 (TI1201), April 10 (TI1206), and April 17, 2012 (TI1209) reveal a three-layer structure of the water column, characterized by a fresh surface layer, which is separated from a more saline and colder well-mixed bottom layer by a layer of strong density gradients, known as the pycnocline (see Fig. 33). Surface salinity varies between ~ 21 psu and 23 psu, while surface temperatures range from ~ -1.2 °C to -1.1 °C. The observations from March 26 clearly indicate the presence of a well-mixed surface layer, separated from the bottom layer by strong salinity and temperature gradients, which occur between ~ 7 m and 10 m depth. In contrast, the measurements obtained on April 10 and April 17 show a salinity increase and temperature decrease throughout the upper water column. However, in all three profiles, the strongest temperature and salinity gradients occur between ~ 7 m and 10 m depth. The bottom layer is located below ~ 10 m to 11 m water depth. The layer is generally well-mixed and shows only small salinity and temperature variations of ~ 30 psu to 31 psu and ~ -1.6 °C to -1.45 °C, respectively. In general, observed temperature profiles closely correspond to the salinity profiles. Overall, an increase in salinity over time can be observed in the water column (see Fig. 33).

The salinity profiles measured at Camp Central at stations TI1202 and TI1207 on March 27 and April 12, 2012, respectively, indicate a similar three-layer structure of the water column as the observations from Camp North (see Fig. 33, 34). Surface salinity varies between ~ 15-18 psu and increases throughout the water column to ~ 29-30 psu in the bottom layer (see Fig. 34). The strongest salinity increase can be observed in the pycnocline, covering the depth interval from ~ 10-11 m to ~ 15-16 m, which separates the surface waters from the subjacent bottom layer. In general, the salinity profiles indicate an increase in salinity as well as an extension of the thickness of the surface layer between March 27 and April 12, 2012. The vertical temperature distribution exhibits much greater complexity than the salinity distribution. Surface temperatures range from ~ -0.85 °C to -1.0 °C. For the depth interval from ~ 1 m to 9 m, the vertical temperature profile measured on March 27 indicates a slight decrease of the temperature, while temperatures remain nearly constant for the profile from April 12. Both stations exhibit a temperature inversion of ~ 0.15 °C in the depth range from ~ 9 m to 11.5-12.5 m, followed by a strong temperature decrease in the pycnocline to ~ 1.2 °C. Moreover, the temperature profile obtained on March 27 indicates another pronounced temperature inversion of ~ 0.3 °C in the bottom layer. In contrast, bottom temperatures remain nearly constant for the profile measured on April 12 (see Fig. 34).

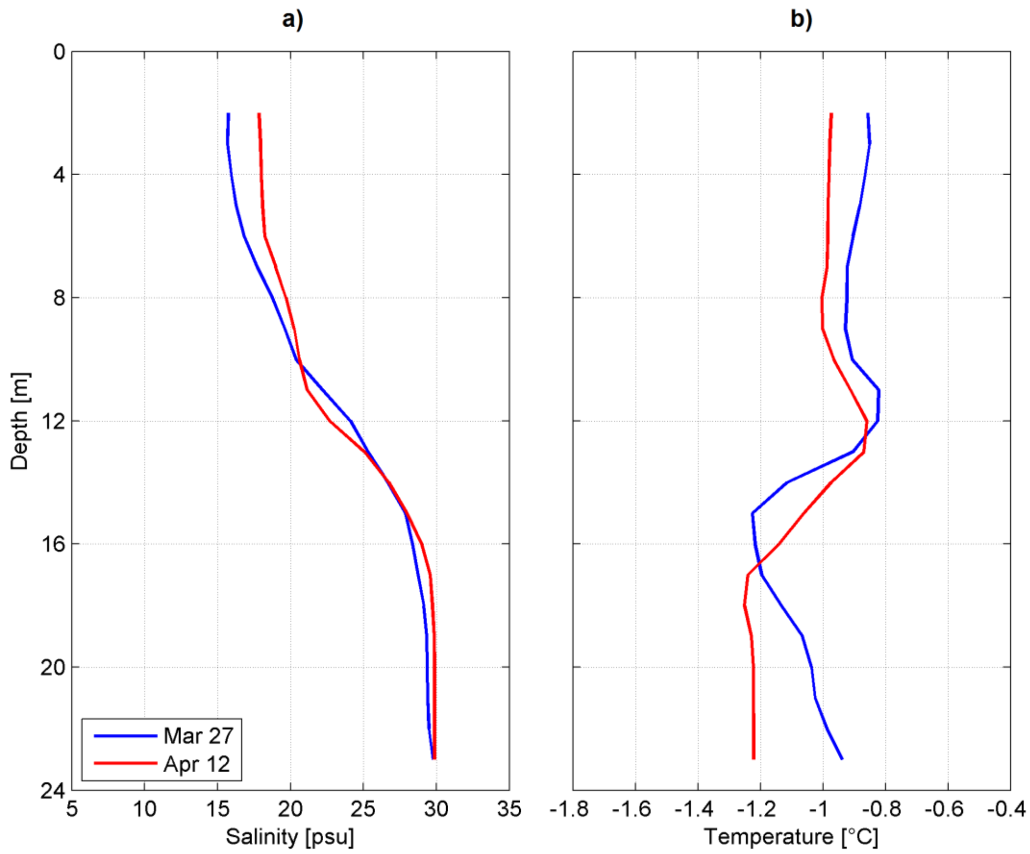

Fig. 34: Vertical salinity (a) and temperature (b) profiles measured at Camp Central on the inner Laptev Sea shelf on March 27 (station TI1202, blue line) and April 12, 2012 (station TI1207, red line). Data is presented in 1 m depth-averaged intervals.

The salinity profile obtained at Camp South at station TI1210 on April 19, 2012 shows an increase of salinity with depth (see Fig. 35). Observations indicate a surface salinity of ~ 9 psu, which increases to ~ 23 psu at ~ 9 m depth. The salinity gradient appears to become smaller with increasing depth. Below ~ 9 m water depth, the salinity retains a nearly constant value. The measured temperature profile shows a decrease of the water temperature from ~ -0.5 °C to -0.9 °C in the depth interval from ~ 2 m to 5 m, followed by a pronounced temperature inversion of ~ 0.2 °C in the lower water column (see Fig. 35).

The comparison of the salinity and temperature profiles obtained at the three different ice camps suggests a three-layer water column structure under the landfast ice on the inner Laptev Sea shelf, characterized by a fresh surface layer and a more saline, colder, well-mixed bottom layer separated by a sharp pycnocline layer. The observations indicate an increase of salinity and a decrease of temperature with decreasing distance to the landfast ice edge (i.e. towards the north, see Fig. 2). In general, salinity profiles at Camp North and Camp Central display an increase of salinity in the water column over time. Temperature seems to be closely associated with salinity in the surface layer and coincide with the freezing temperature at the respective salinity. However, bottom temperatures do not necessarily exhibit this relationship. For example, stations TI1202 and TI1210 indicate temperature inversions in the bottom layer, which are ~ 0.2-0.3 °C above the freezing point.

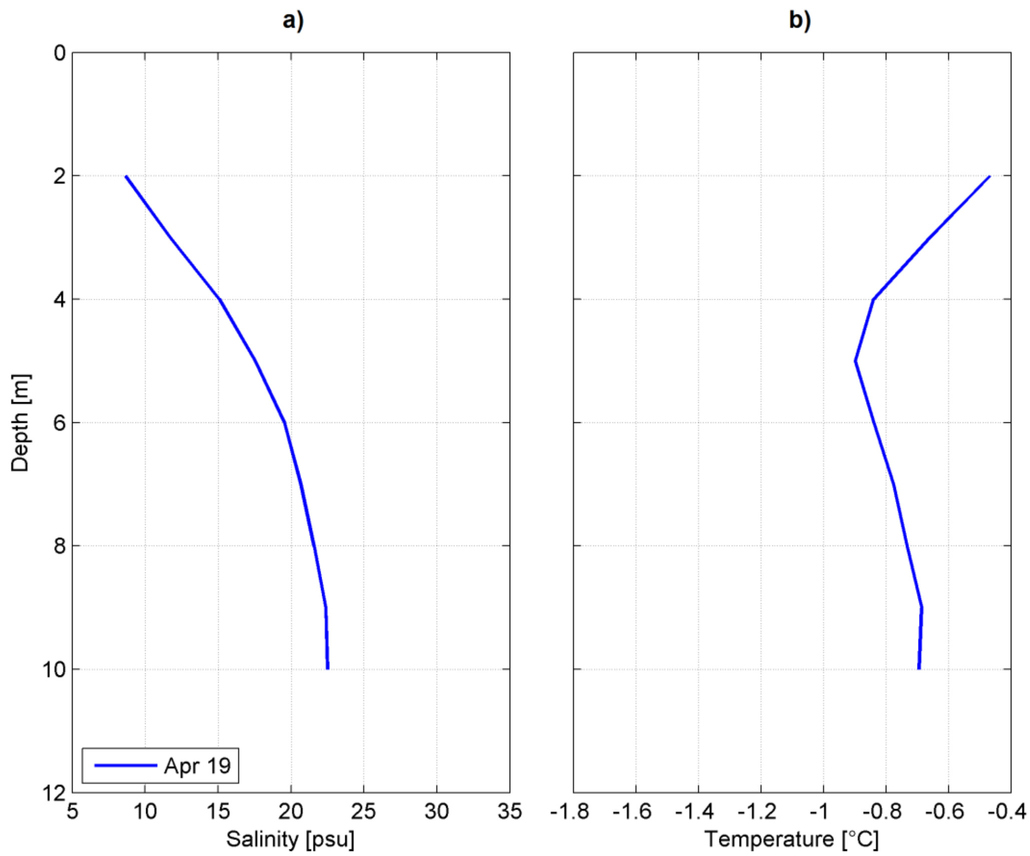

Fig. 35: Vertical salinity (a) and temperature (b) profiles measured at Camp South on the inner Laptev Sea shelf on April 19, 2012 (station TI1210). Data is presented in 1 m depth-averaged intervals.

3.3.2 Hydrographic condtions in winter 2008 and 2009

In order to put the hydrographic conditions observed on the inner Laptev Sea shelf during winter 2012 into a wider spatial and temporal context, the aforementioned results are compared to CTD data obtained as part of earlier winter expeditions in the Laptev Sea in 2008 and 2009. During TRANSDRIFT XIII and XV, temperature and salinity profiles were measured at several different locations beyond the landfast ice edge (in close vicinity to the landfast ice zone), along the landfast ice edge, as well as at one location under the landfast ice, at greater distance to the landfast ice edge (see Fig. 2). Therefore, the oceanographic dataset is suitable to investigate spatial variability of water properties on the southeastern

Laptev Sea shelf in greater detail, particularly in the vicinity of the landfast ice edge. Moreover, it provides the opportunity to examine interannual changes of hydrographic conditions on the inner Laptev Sea shelf.

In order to investigate water properties beyond the landfast ice edge, salinity and temperature measurements acquired at five different locations beyond the landfast ice edge during winter 2008 and 2009 (see Fig. 2) are analyzed with respect to spatial and temporal differences. Figure 36 depicts the salinity and temperature profiles obtained within the framework of TRANSDRIFT XIII at stations TI0811, TI0814, and TI0816 on April 19, April 21, and April 24, 2008, respectively.

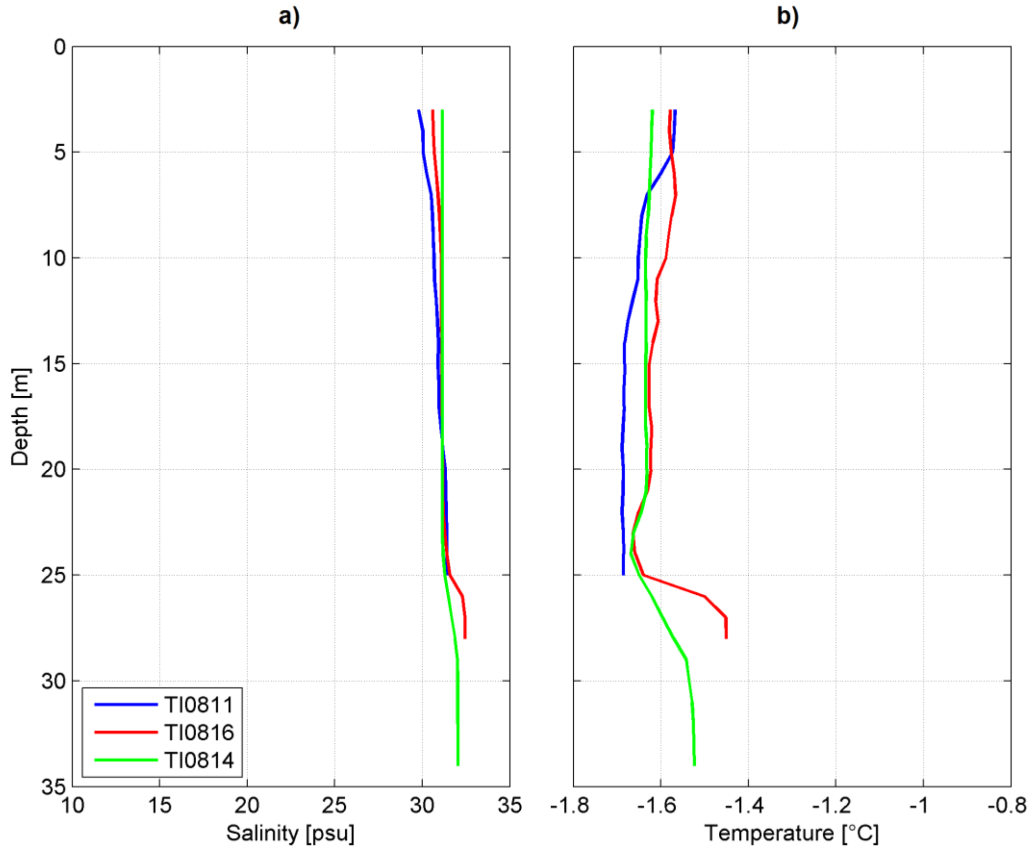

Fig. 36: Vertical salinity (a) and temperature (b) profiles measured beyond the landfast ice edge, in close vicinity to the landfast ice zone, on the Laptev Sea shelf at stations TI0811 (April 19, blue line), TI0816 (April 24, red line), and TI0814 (April 21, green line) in winter 2008. Data is presented in 1 m depth-averaged intervals.

The salinity profiles indicate only small variations of salinity between ~ 30 psu and 32 psu throughout the water column. In general, an increase of salinity by ~ 1-2 psu from the surface to the bottom can be observed (see Fig. 36 a). Measured temperatures generally vary around ~ -1.6 °C near the surface and between ~ -1.7 °C and -1.45 °C near the bottom (see Fig. 36 b).

While the profiles obtained at stations TI0814 and TI0816 clearly reveal the presence of a warm and saline, well-mixed bottom layer, separated from the fresher surface layer by sharp gradients of water properties in the depth interval from ~ 25 m to 28 m, the profile measured at station TI0811 does not indicate the presence of sharp gradients or a temperature inversion near the bottom. Instead, a parabolic decrease of temperature and increase of salinity with depth can be observed at this station (see Fig. 36). Figure 37 shows the salinity and temperature profiles measured at stations TI0902 and TI0911 beyond the landfast ice edge (see Fig. 2) on March 26 and April 15 within the framework of the winter expedition TRANSDRIFT XV in 2009. The observations indicate a three-layer water column structure, characterized by a fresher and warmer surface layer separated from a more saline and cooler, well-mixed bottom layer by a pycnocline between ~ 12 m and 22 m depth. Surface salinities range vary around ~ 25 psu and increase to ~ 32 psu in the bottom layer (see Fig. 37 a). The observed temperature distribution corresponds closely to the observed vertical salinity profiles. Temperatures range from ~ -1.4 °C to -1.3 °C near the surface and decrease to ~ -1.6 °C in the bottom layer (see Fig. 37 b).

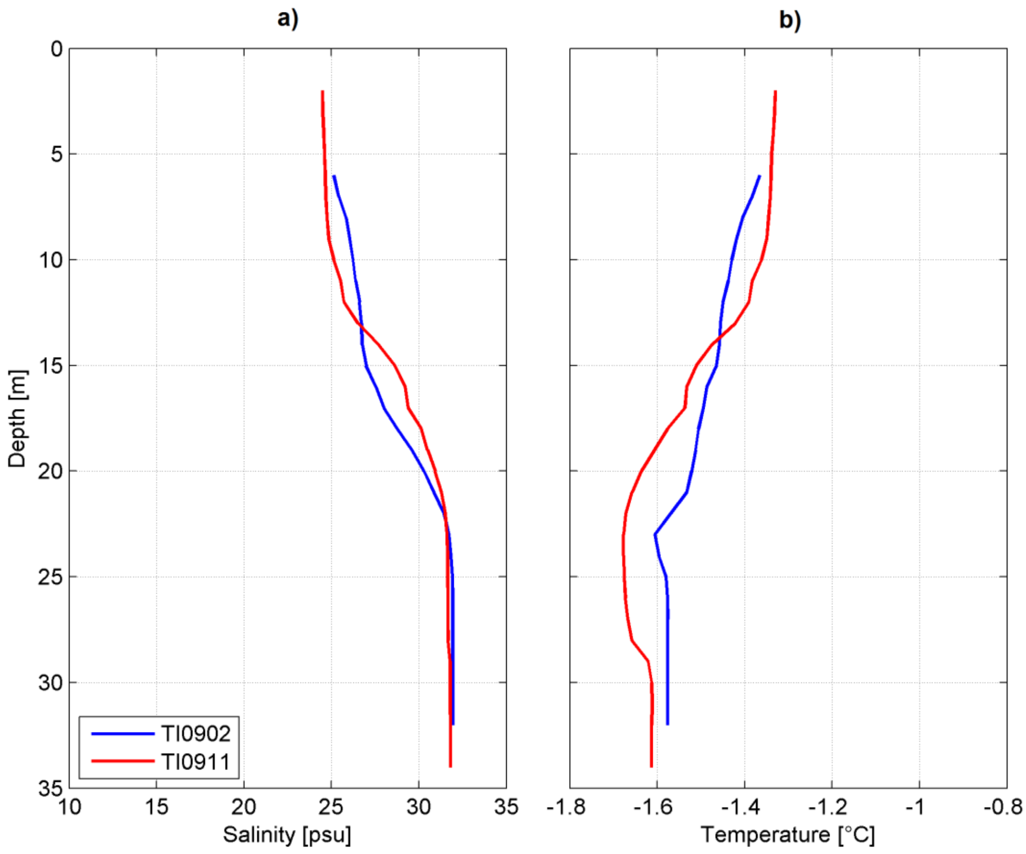

Fig. 37: Vertical salinity (a) and temperature (b) profiles measured beyond the landfast ice edge, in close vicinity to the landfast ice zone, on the Laptev Sea shelf at stations TI0902 (March 26, blue line) and TI0911 (April 15, red line) in winter 2009. Data is presented in 1 m depth-averaged intervals.

In summary, the temperature and salinity profiles obtained beyond the landfast ice edge during winter 2008 and 2009 indicate considerable interannual differences of hydrographic conditions. Observations from 2009 indicate a three-layer water column structure, characterized by a fresher and warmer surface layer and a more saline and colder, well-mixed bottom layer separated from each other by a pycnocline in the depth interval from ~ 12 m to 22 m (see Fig. 37). In contrast, measurements from 2008 reveal variations in the water column structure at different locations. In the vicinity of the Lena River Delta, a parabolic decrease of temperature and increase of salinity with depth can be observed, while at greater distance to the Lena River Delta a three-layer water column structure can be observed, characterized by a colder and fresher surface layer and a warmer and saltier bottom layer separated by strong gradients in the depth interval from ~ 25 m to 28 m (see Fig. 36). In general, observed surface salinities in winter 2008 are ~ 4-7 psu higher and observed surface temperatures ~ 0.2-0.3 °C lower than in winter 2009, while hydrographic conditions in the bottom layer are similar (see Fig. 36, 37).

In total, nine different locations along the landfast ice edge in the southeastern Laptev Sea (see Fig. 2) are analyzed with respect to their vertical temperature and salinity distribution (see Fig. 38, 39, 40, 41). Observations are used to evaluate the results from Camp North in 2012 within a larger spatial and temporal context. In particular, the development of hydrographic conditions along the landfast ice edge with increasing distance to the Lena River Delta is investigated in detail. Figure 38 displays the vertical salinity profiles obtained at four different locations along the landfast ice edge from southwest to northeast in winter 2008 (see Fig. 2). The vertical salinity distributions measured at the most southwesterly stations TI0802, TI0807, TI0810, TI0815, and TI0825 (see Fig. 2) on April 11, April 14, April 19, April 24, and May 4, 2008, respectively, indicate the presence of a three-layer structure of the water column between April 11 and April 24 (see Fig. 38 a), in line with the findings from Camp North in 2012 (see Fig. 33). However, the pycnocline is not as distinct as at Camp North and the salinity differences between the surface layer and the bottom layer are significantly smaller (~ 3-4 psu, compared to ~ 8-10 psu at Camp North) due to higher surface salinities (~ 26-28 psu). Bottom salinities range from ~ 30 psu to 32 psu, comparable to the findings at Camp North. In general, differences between surface and bottom salinities tend to increase between April 11 and May 4. Moreover, the salinity profile obtained on May 4 shows a parabolic increase of salinity with depth in the upper water column, as opposed to the three-layer structure observed in the other profiles (see Fig. 38 a). Figure 38 b) depicts the vertical salinity profiles obtained at the stations TI0801, TI0808, and TI0819/TI0820 (see Fig. 2) on April 10, April 16, and April 28, 2008, respectively. In contrast to the profiles from Camp North and from the most southwesterly measurement location, the profiles indicate the presence of a well-mixed water column up to ~ 18 to 20 m depth, followed by a sharp pycnocline and a well-mixed bottom layer with salinities between ~ 31 psu and 33 psu. In general, salinity differences between upper and lower water column increase at this location between April 10 and April 28 (see Fig. 38 b). The salinity profiles obtained at the two most northeasterly locations, based on observations from stations TI0804 (April 12) and TI0823 (April 24) and from stations TI0805 (April 14), TI0813 (April 21), and TI0822 (April 29) (see Fig. 2), respectively, indicate the presence of an entirely well-mixed water column (see Fig. 38 c, d). Observed salinities at stations TI0804 and TI0823 generally vary by less than 1 psu around ~ 31 psu throughout the water column. Slight salinity increases can only be observed in the lower water column between ~ 15 m to 18 m depth.

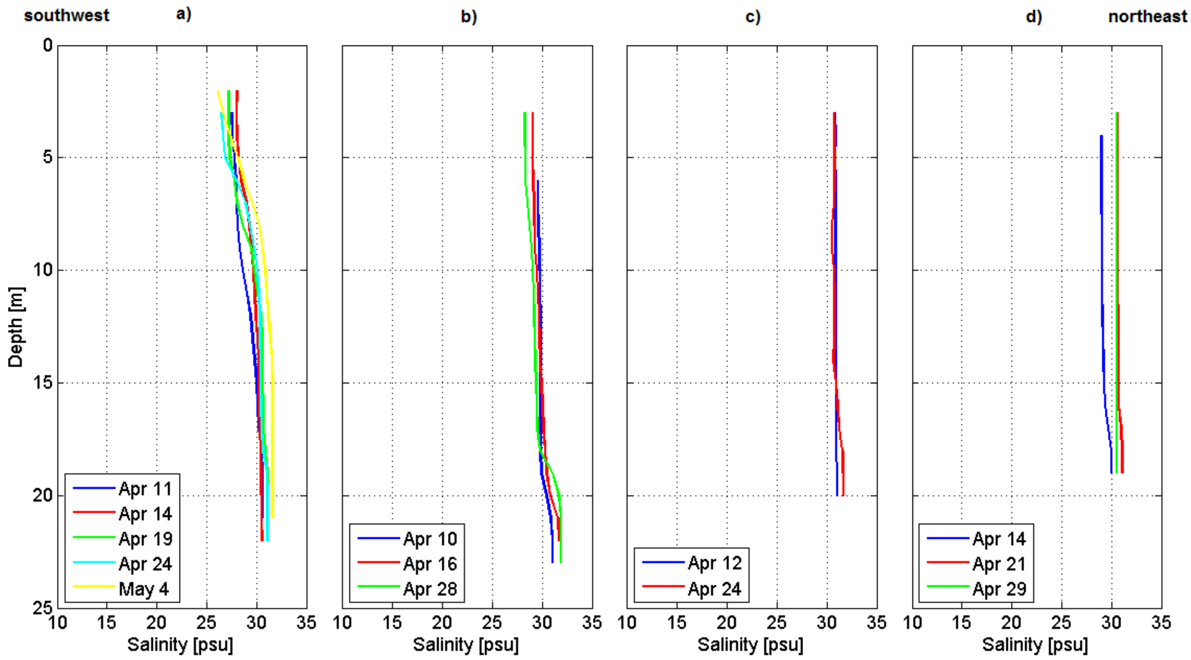

Fig. 38: Vertical salinity profiles measured at four different locations (a-d) along the landfast ice edge (from southwest to northeast) on the Laptev Sea shelf in winter 2008. a) stations TI0802 (April 11, blue line), TI0807 (April 14, red line), TI0810 (April 19, green line), TI0815 (April 24, cyan line), TI0825 (May 4, yellow line); b) stations TI0801 (April 10, blue line), TI0808 (April 10, red line), TI0819/20 (averaged together since very similar and both obtained on April 28, green line); c) stations TI0804 (April 12, blue line), TI0823 (April 24, red line); d) stations TI0805 (April 14, blue line), TI0813 (April 21, blue line), TI0822 (April 29, green line). Data is presented in 1 m depth-averaged intervals.

Figure 39 displays the vertical temperature profiles obtained at the four different measurement locations along the landfast ice edge (from southwest to northeast) during the winter expedition TRANSDRIFT XIII in 2008 (see Fig. 2). The results of the temperature measurements at the most southwesterly stations TI0802, TI0807, TI0810, TI0815, and TI0825 (see Fig. 2) obtained on April 11, April 14, April 19, April 24, and May 4, 2008, respectively, indicate that the three-layer water column structure identified in the corresponding salinity profiles is also apparent in the temperature distribution (see Fig. 39 a). Surface temperatures generally vary between ~ -1.5 °C and -1.4 °C, while bottom temperatures range from ~ -1.7 °C to -1.6 °C. Therefore, observed temperatures show a similar distribution as at Camp North in 2012 but are ~ 0.2 °C to 0.3 °C lower (see Fig. 33, 39a). The profile obtained at station TI0825 on May 4 represents a pronounced example of a temperature inversion, indicating the occurrence of relatively warm bottom layer temperatures (see Fig. 39 a).

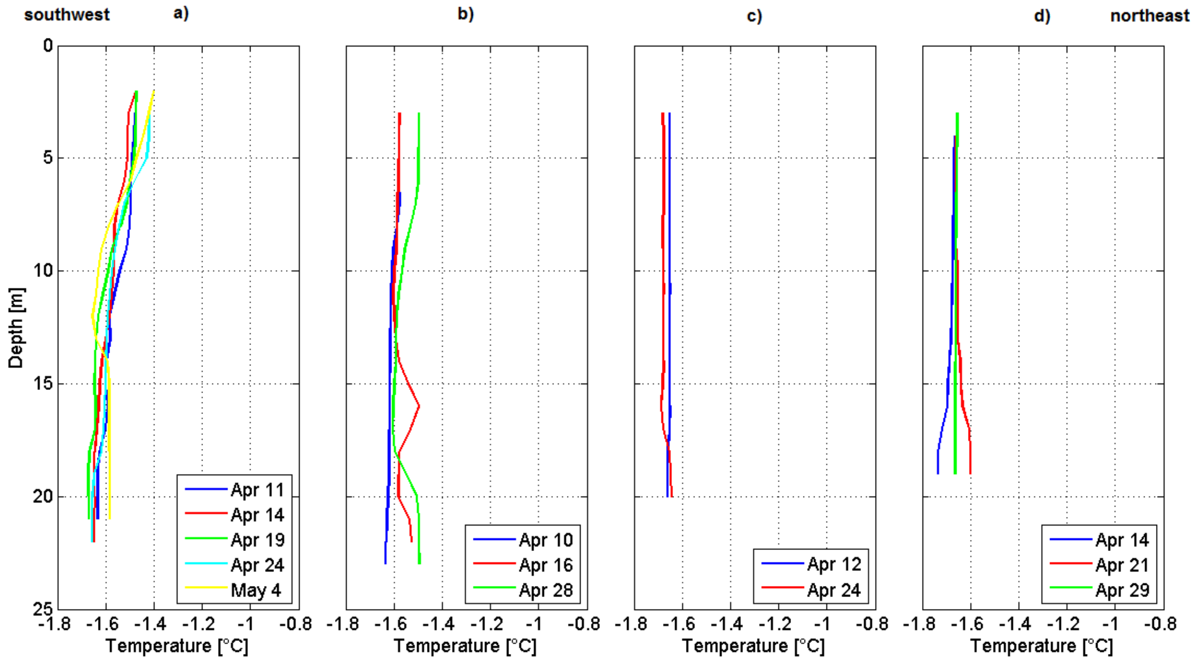

Fig. 39: Vertical temperature profiles measured at different locations (a-d) along the landfast ice edge (from southwest to northeast) on the Laptev Sea shelf in winter 2008. a) stations TI0802 (April 11, blue line), TI0807 (April 14, red line), TI0810 (April 19, green line), TI0815 (April 24, cyan line), TI0825 (May 4, yellow line); b) stations TI0801 (April 10, blue line), TI0808 (April 10, red line), TI0819/20 (averaged together since very similar and both obtained on April 28, green line); c) stations TI0804 (April 12, blue line), TI0823 (April 24, red line); d) stations TI0805 (April 14, blue line), TI0813 (April 21, blue line), TI0822 (April 29, green line). Data is presented in 1 m depth-averaged intervals.

Temperature profiles obtained at stations TI0801, TI0808, and TI0819/TI0820 (see Fig. 2) on April 10, April 16, and April 28, 2008, respectively, show varying vertical temperature distributions with values ranging from ~ -1.6 °C to -1.5 °C (see Fig. 39 b). All three profiles indicate the presence of a well-mixed surface layer up to ~ 6 m depth, followed by a temperature decrease in the underlying water column. However, pronounced temperature inversions in the lower water column can be observed at ~ 14-16 m depth and below ~ 20 m depth on April 16, and below ~ 19 m depth on April 28 (see Fig. 39 b). The vertical temperature profiles measured at the two most northeasterly locations associated with stations TI0804 (April 12), and TI0823 (April 24) and at stations TI0805 (April 14), TI0813 (April 21) and TI0822 (April 29) (see Fig. 2), respectively, support the finding of the occurrence of a well-mixed water column at the two most northeasterly measurement locations (see 39 c, d), as apparent in the respective salinity profiles (see Fig. 38 c, d). Generally, temperatures range from ~ -1.75 °C to -1.6 °C. The temperature profiles obtained on April 21 (station TI0813) and April 24 (station TI0823) indicate slight temperature inversions near the bottom at ~ 16 m to 18 m water depth (see Fig. 39 c, d).

Figure 40 and 41 show the vertical salinity and temperature profiles measured at five different locations along the landfast ice edge (from southwest to northeast) during TRANSDRIFT XV in March and April 2009 (see Fig. 2). All obtained profiles indicate a similar salinity and temperature distribution throughout the water column, characterized by a salinity increase and temperature decrease throughout the upper water column and a well-mixed bottom layer below ~ 18 m to 23 m depth (see Fig. 40, 41). In general, surface salinities range from ~ 15 psu to 22 psu and increase to ~ 30 psu to 32 psu near the bottom (see Fig. 40). The salinity profile obtained at station TI0915 on April 23 is the only measurement which indicates the occurrence of a well-mixed surface layer up to ~ 5 m depth (see Fig. 40 d). Observed temperature profiles correspond closely to the respective salinity profiles, in line with the findings from Camp North in 2012 (see Fig. 33). In general, temperatures exhibit a decrease throughout the upper water column from ~ -1.1 °C to -0.8 °C near the surface to ~ -1.5 °C in the well-mixed bottom layer (see Fig. 41). Generally, the observed salinity and temperature distributions correspond well to the observations at Camp North in 2012, which exhibit similar measurement values near the surface as well as near the bottom (see Fig. 33). However, the salinity and temperature measurements from winter 2009 do not show such a distinct pycnocline as observed at Camp North in winter 2012 (see Fig. 33, 40, 41).

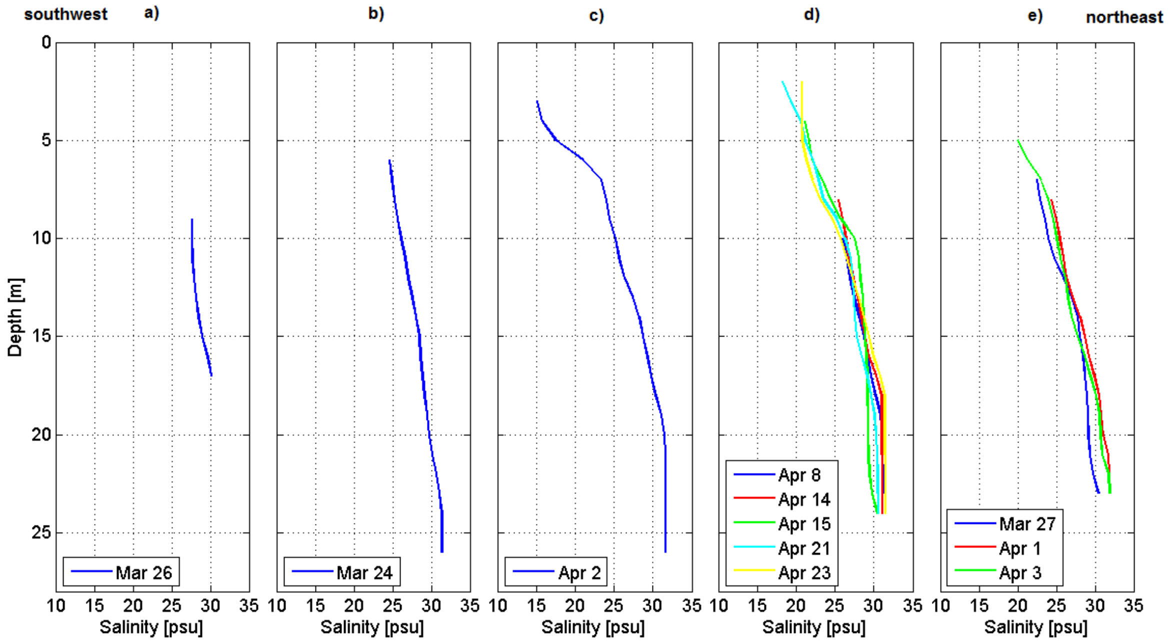

Fig. 40: Vertical salinity profiles measured at different locations (a-e) along the landfast ice edge (from southwest to northeast) on the Laptev Sea shelf in winter 2009. a) station TI0903 (March 26); b) station TI0901 (March 24); c) station TI0906 (April 19); d) stations TI0908 (April 8, blue line), TI0910 (April 14, red line), TI0912 (April 15, green line), TI0913 (April 21, cyan line), TI0915 (April 23, yellow line); e) stations TI0904 (March 27, blue line), TI0905 (April 1, red line), TI0907 (April 3, green line). Data is presented in 1 m depth-averaged intervals.

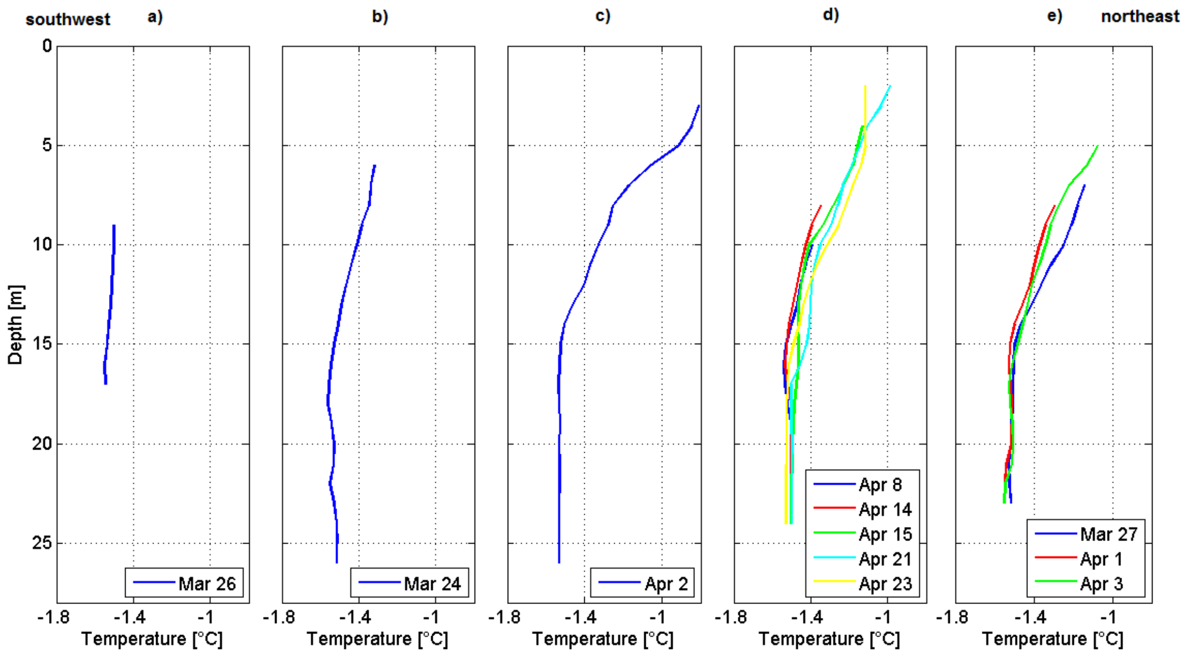

Fig. 41: Vertical temperature profiles measured at different locations (a-e) along the landfast ice edge (from southwest to northeast) on the Laptev Sea shelf in winter 2009. a) station TI0903 (March 26); b) station TI0901 (March 24); c) station TI0906 (April 19); d) stations TI0908 (April 8, blue line), TI0910 (April 14, red line), TI0912 (April 15, green line), TI0913 (April 21, cyan line), TI0915 (April 23, yellow line); e) stations TI0904 (March 27, blue line), TI0905 (April 1, red line), TI0907 (April 3, green line). Data is presented in 1 m depth-averaged intervals.

In summary, temperature and salinity profiles obtained along the landfast ice edge in winter 2008 and 2009 provide mixed evidence with respect to spatial variability of hydrographic conditions on the southeastern Laptev Sea shelf. The observations from 2008 show a shift from a three-layer water column structure at the most southwesterly location, characterized by a warmer and fresher surface layer and a colder, more saline bottom layer separated from each other by a pycnocline, towards an entirely well-mixed water column with increasing distance to the Lena River Delta. Hydrographic conditions near the bottom are similar at all four measurement locations. In contrast, surface salinities along the landfast ice edge increase at greater distance to the Lena River Delta, while surface temperatures exhibit a decrease. In general, surface temperatures are close to or slightly above the respective freezing temperatures, while bottom temperatures do not necessarily exhibit this relationship. For example, pronounced temperature inversions of up to ~ 0.1 °C occur near the bottom at several stations (see Fig. 39). At the two most southwesterly locations, differences between surface and bottom salinities increase over time. Moreover, a significant increase of salinity at the most northeasterly location occurs between April 14 and April 21, indicating considerable variability of hydrographic conditions on short timescales of days to weeks. In contrast to the strong lateral variability observed along the landfast ice edge in 2008, the comparison of the temperature and salinity distribution measured at the landfast ice edge to observations from beyond the landfast ice edge shows that water properties show relatively small changes across the landfast ice edge in 2008. The observations of water properties along the landfast ice edge in winter 2009 show high consistency in themselves. The salinity and temperature measurements indicate a similar structure of the water column at all five locations along the landfast ice edge, characterized by a salinity increase and a temperature decrease throughout the upper water column (up to ~ 15-18 m depth) and a well-mixed lower water column. Measurement values of salinity and temperature are comparable at all five locations along the landfast ice, exhibiting only small variations. Moreover, temporal changes of water properties on timescales of days to weeks are relatively small. However, observations from winter 2009 indicate considerable lateral variability across the landfast ice edge associated with higher surface salinities and lower surface temperatures beyond the landfast ice edge, resulting in a less pronounced pycnocline. Comparing the large-scale salinity and temperature distribution observed in winter 2008, 2009, and 2012 to each other, indicates considerable interannual variability. While the observations from 2009 show similar magnitudes of temperature and salinity measurements near the surface and near the bottom as observed at Mooring North in 2012, measurements obtained in winter 2008 exhibit ~ 4-8 psu higher salinity values and ~

0.3-0.6 °C lower temperature values near the surface, suggesting pronounced interannual variability of the physical processes influencing the under-ice hydrography near the landfast ice edge on the southeastern Laptev Sea shelf.

Within the framework of the winter expedition TRANSDRIFT XV in 2009, salinity and temperature profiles were measured at one location under the landfast ice situated at considerable distance to the landfast ice edge (see Fig 2). These observations can be used to put the results from Camp Central in 2012 into a wider context.

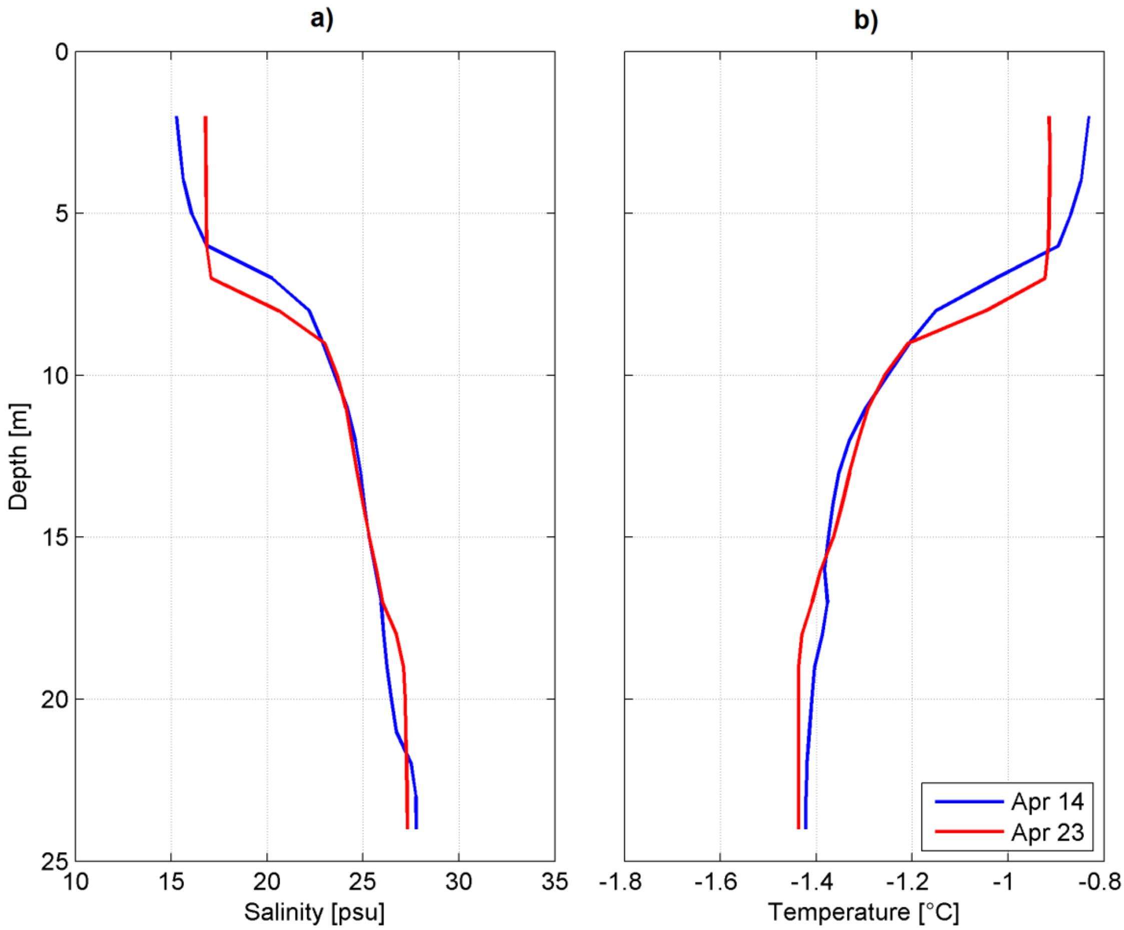

Fig. 42: Vertical salinity (a) and temperature (b) profiles measured under the landfast ice on the Laptev Sea shelf at stations TI0909 (April 14, blue line), and TI0916 (April 23, red line) in winter 2009. Data is presented in 1 m depth-averaged intervals.

Figure 42 displays the vertical salinity and temperature distributions obtained at stations TI0909 and TI0916 on April 14 and April 23, 2009, respectively. Observed salinity and temperature profiles indicate the presence of a fresh surface layer, separated from a colder and more saline well-mixed bottom layer by a sharp pycnocline (see Fig. 42), similar to the observations from Camp Central in 2012 (see Fig. 34). Surface salinities and surface temperatures are in the range of ~ 15 psu to 17 psu and -0.9 °C to -0.8 °C, respectively. Salinities and temperatures near the bottom vary around ~ 27-28 psu and ~ -1.4 °C, respectively (see Fig. 42). Hence, the magnitudes of observed hydrographic conditions under the landfast ice at considerable distance to the landfast ice edge in winter 2009 are similar to the findings from 2012 (see Fig. 34, 42).

Overall, the under-ice hydrography on the southeastern Laptev Sea shelf is characterized by great spatial variability. Generally, a decrease of salinity and an increase of temperature with increasing distance to the landfast ice edge can be observed. Furthermore, significant lateral differences in salinity and temperature distributions can be observed on relatively small spatial scales in the vicinity of the landfast ice edge, both along the landfast ice edge and across the landfast ice edge. Moreover, hydrographic conditions on the inner Laptev Sea shelf during the ice-covered season exhibit pronounced temporal variability, both locally on short timescales of several days to weeks as well as larger-scale interannual variations.

3.4 Relationship of salinity, temperature, and currents under the landfast ice

The results of the previous sections indicate pronounced variability of oceanic currents and water properties on the southeastern Laptev Sea shelf during the ice-covered season, especially in the vicinity of the landfast ice edge. In order to closely investigate the relationship between hydrographic conditions and physical processes under the landfast ice, particularly detailed salinity and temperature time series measured at Mooring North near the landfast ice edge in 2012 are compared to the respective current velocity record at this location. Moreover, salinity, temperature, and current velocity records from Mooring Central are analyzed to put the findings from Mooring North into a larger spatial context.

Figure 43 presents the time-series of current velocities, temperature, and salinity recorded at Mooring North (see Fig. 2) over a time period of three weeks in March and April 2012. The salinity and temperature records, measured at ~ 3 m, 8 m, 9.5 m, 11 m, 12.5 m, and 15.5 m water depth, reflect the vertical three-layer water column structure derived from the CTD profiles at Camp North (see Fig. 33). The observations indicate pronounced salinity and temperature variability in the pycnocline between ~ 7 m and 10 m depth and, to a lesser extent, also in the surface layer. In general, observed surface salinities and surface temperatures range from ~ 14 psu to 25 psu and from ~ -1.7 °C to -1.3 °C over the measurement period, while the CTD sensor mounted at 8 m water depth indicates salinity and temperature variations of ~ 16 psu to 30 psu and ~ -0.85 °C to -1.5 °C in the pycnocline (see Fig. 43).

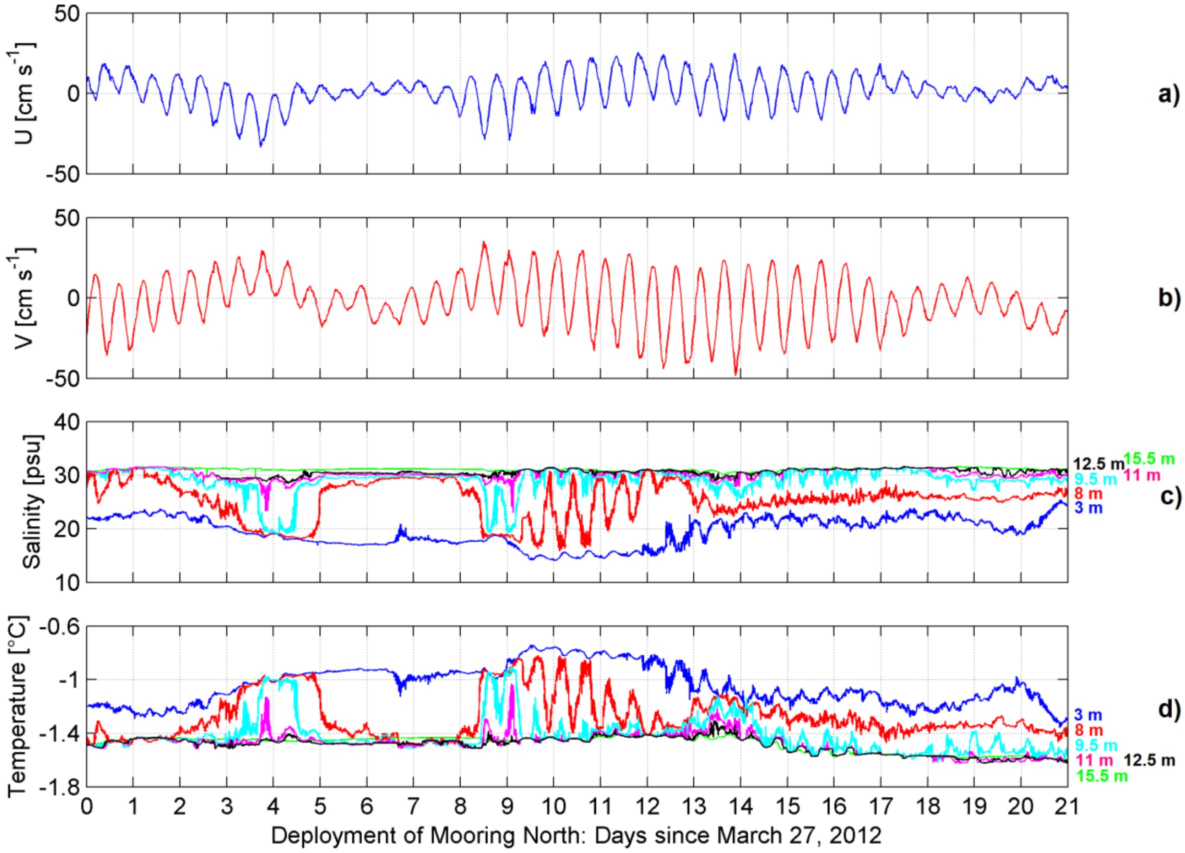

Fig. 43: Time series of depth-averaged zonal (a) and meridional (b) current velocities, salinity (c), and temperature (d) obtained at Mooring North for the time period from March 27 (day 0) to April 17 (day 21) 2012. CTD sensors were fixed at ~ 3 m (blue line), 8 m (red line), 9.5 m (cyan line), 11 m (magenta line), 12.5 m (black line), and 15.5 m (green line).

Extreme fluctuations of salinity and temperature in the pycnocline occur from March 28 (day 1) to April 1 (day 5) and from April 4 (day 9) to April 8 (day 12). The fluctuations coincide with the onset of strong currents of alternating direction with magnitudes of up to 50 cm s^{-1}. These currents are strongly influenced by semidiurnal tidal dynamics (see Fig. 26). Changes in hydrographic conditions lag changes in tidal dynamics by ~ 3 h, indicating advection of water masses from the close-by landfast ice edge, at ~ 3 km distance. Within a semidiurnal tidal cycle, salinity and temperature measurements in the pycnocline show variations with amplitudes of up to 15 psu and up to 0.5 °C, respectively. Rapid decreases of salinity and increases of temperature are associated with advection of water masses by tidal currents from the southeast. In contrast, southeastward tidal currents result in rapid increases in salinity and decreases in temperature. The second occurrence of rapid fluctuations of salinity and temperature in the pycnocline coincides with the opening of a flaw polynya along the landfast ice edge (see Fig. 21). Although strong semidiurnal currents are sustained beyond April 8, the extreme temperature and salinity fluctuations in the pycnocline layer decay. In contrast, the surface layer, which only shows a slight increase in temperature and decrease in salinity over the course of the polynya event, starts to show greater variability after the closure of the flaw polynya. Differences in temperature and salinity between the surface and bottom layer seem to decline after the fluctuations in the pycnocline have vanished. Observations indicate a significant decrease of temperature in the surface layer by ~ 0.3 °C to 0.4 °C as well as a pronounced increase in salinity of ~ 7-8 psu, while temperature and salinity of the bottom layer only slightly decrease and increase, respectively. In general, the bottom layer exhibits relatively small temperature and salinity variations throughout the entire record, ranging from ~ -1.6 °C to -1.4 °C and from ~ 30 psu to 31 psu, respectively (see Fig. 43).

To obtain detailed information on the temporal development of the vertical structure of the water column at Mooring North, salinity and temperature observations from the individual sensors at ~ 3 m, 8 m, 9.5 m, 11 m, 12.5 m, and 15.5 m water depth are vertically interpolated (see Fig. 44 a, b). The resulting salinity and temperature sections indicate great variability of the water column structure over the three-week long measurement period. The most striking features of the 2D interpolated records are the pronounced low salinities (below 22 psu) and high temperatures (above -1.1 °C) in the surface layer, which occur between March 30 (day 3) and April 10 (day 14). During the time intervals from March 30 (day 3) to April 1 (day 5) and April 4 (day 8) to April 8 (day 12), the low salinity and high temperature layer extends down to ~ 8-10 m depth, while it is confined to the upper ~ 4-5 m of the water column at other times. Another pronounced characteristic of the 2D interpolated salinity and temperature time series are the semidiurnal fluctuations of the hydrographic conditions, which result in changes of the water depth that is associated with a specific salinity and temperature level. These fluctuations are especially noticeable during the time period of the polynya event from April 4 (day 8) to April 8 (day 12) and lead to alterations of the pynocline depth (see Fig. 44). Furthermore, the distinct decrease in water temperature which occurs in the lower water column below ~ 10 m depth during the time interval from April 11 (day 15) to April 17 (day 21) (see Fig. 44) should be noted since it has not been as clearly visible in Figure 43.

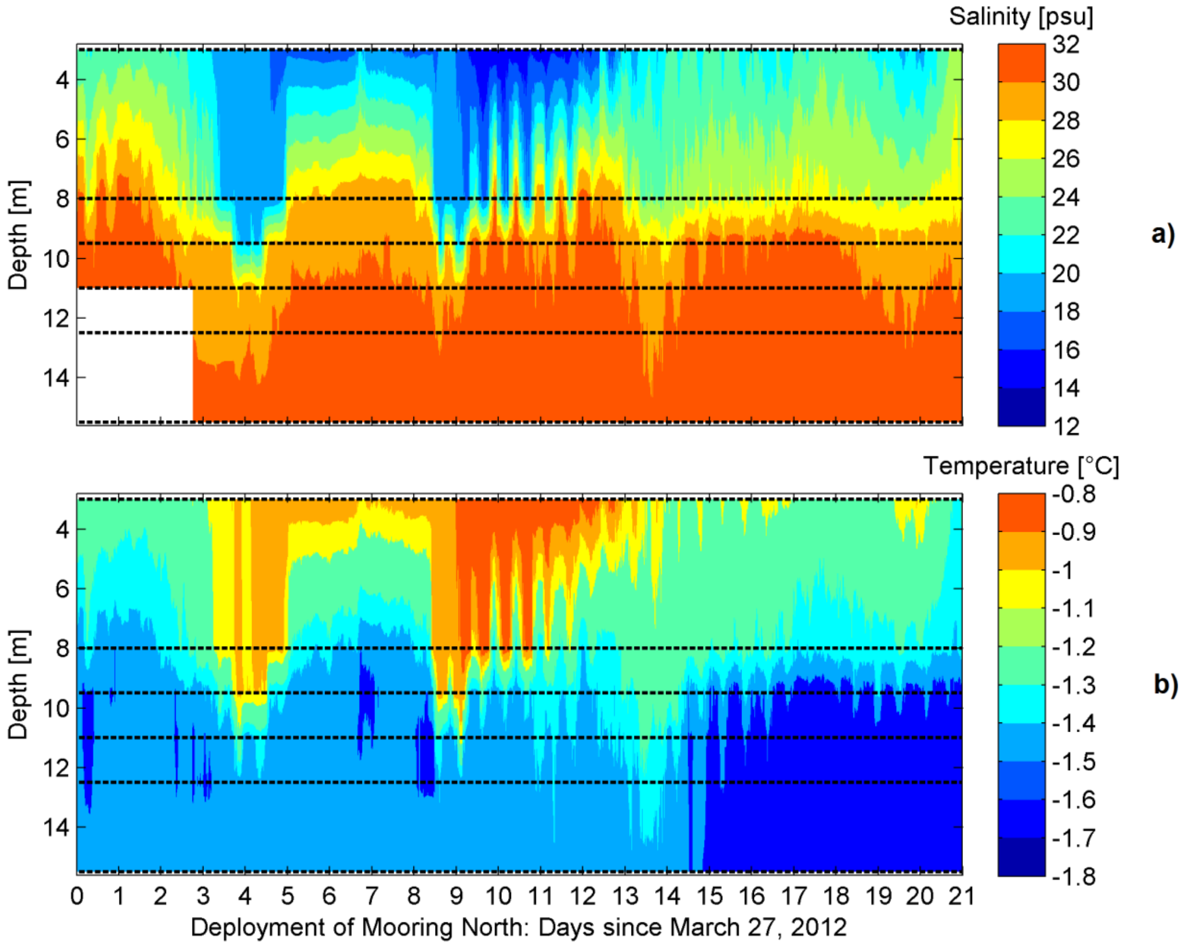

Fig. 44: Time series of the vertical distribution of salinity (a) and temperature (b) at Mooring North over the time period from March 27 (day 0) to April 17 (day 21), 2012 obtained from 2D linear interpolation between measurements at different CTD sensors. Dashed black lines indicate the depth of in-situ CTD measurements (~ 3 m, 8 m, 9.5 m, 11 m, 12.5 m, and 15.5 m).

In order to obtain a measure of the stability of the water column, the salinity and temperature time series obtained from the individual CTD sensors at Mooring North are used to compute the Brunt-Väisälä frequency squared (N^2) at the respective mid-depths (see Fig. 45). The obtained results are linearly interpolated to visualize the stratification of the water column. The results indicate the occurrence of particularly high values of N^2 in the pycnocline throughout the measurement period from March 27 to April 17, 2012. Especially in the time intervals from March 29 (day 2) to March 31 (day 4) and from April 4 (day 8) to April 8 (day 12), distinct maxima of N^2 can be observed, indicating pronounced stratification of the water column. These time intervals correspond to the occurrences of the particularly fresh and warm surface layer identified in Figures 43 and 44. Moreover, the time series of the vertically interpolated N^2 exhibits significant semidiurnal variations, in particular during the time period from April 4 (day 8) to April 8 (day 12). This phase coincides with the identified polynya event (see Fig. 21), indicating the strong influence of lateral gradients of water properties and tides on the water column structure at Mooring North over the course of the polynya event. After the closure of the flaw polynya, the water column shows significantly weaker vertical stratification (see Fig. 45), suggesting that mixing processes may alter the hydrography at Mooring North in response to the polynya event.

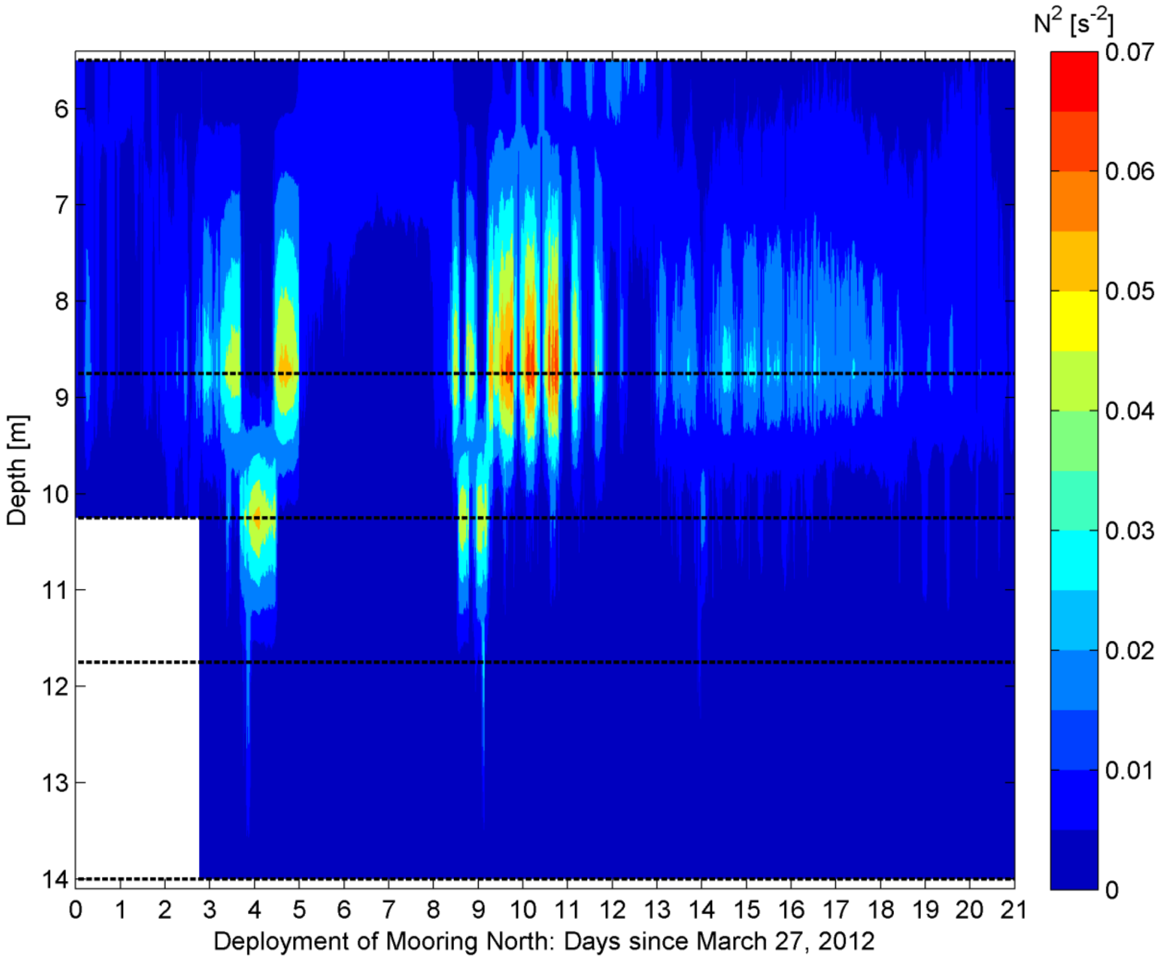

Fig. 45: Time series of the stratification of the water column as indicated by the Brunt-Väisälä frequency squared (*N^2*) at Mooring North over the time period from March 27 (day 0) to April 17 (day 21), 2012. *N^2* is calculated from the salinity and temperature measurements from individual CTD sensors at the respective mid-depths. Results are vertically interpolated (linear interpolation). Dashed black lines indicate the position of the respective mid-depths between the individual CTD measurements.

Since the opening of the flaw polynya from April 3 to April 8, 2012 coincides with prominent changes of the water properties at Mooring North, the vertical pattern of the current regime during this time period is examined in detail. Figure 46 shows the vertical profile of mean current velocities for the respective time period, indicating the occurrence of a strong surface flow towards the northwest and an eastward current at depth. Zonal current velocities increase significantly from ~ -3.3 cm s^{-1} near the surface to ~ 4.3 cm s^{-1} at 8.5 m water depth and exhibit only small variations of ~ 4.3 cm s^{-1} to 5.7 cm s^{-1} in the lower water column.

Meridional current velocities show a considerable decrease from ~ 8.5 cm s^{-1} near the surface to ~ -0.8 cm s^{-1} at 10 m water depth, followed by small variations between ~ -0.8 cm s^{-1} and -1.3 cm s^{-1} in depth interval from 10 m to 14 m. Standard errors associated with the mean zonal and meridional velocity components are in the range of ~ 2-3 cm s^{-1} (see Fig. 46). Hence, the described vertical profile of mean current velocities indicates advection of water masses from different directions in the upper and lower water column, in line with the differing behavior of surface and bottom water properties during the polynya event in April 2012 (see Fig. 43, 44).

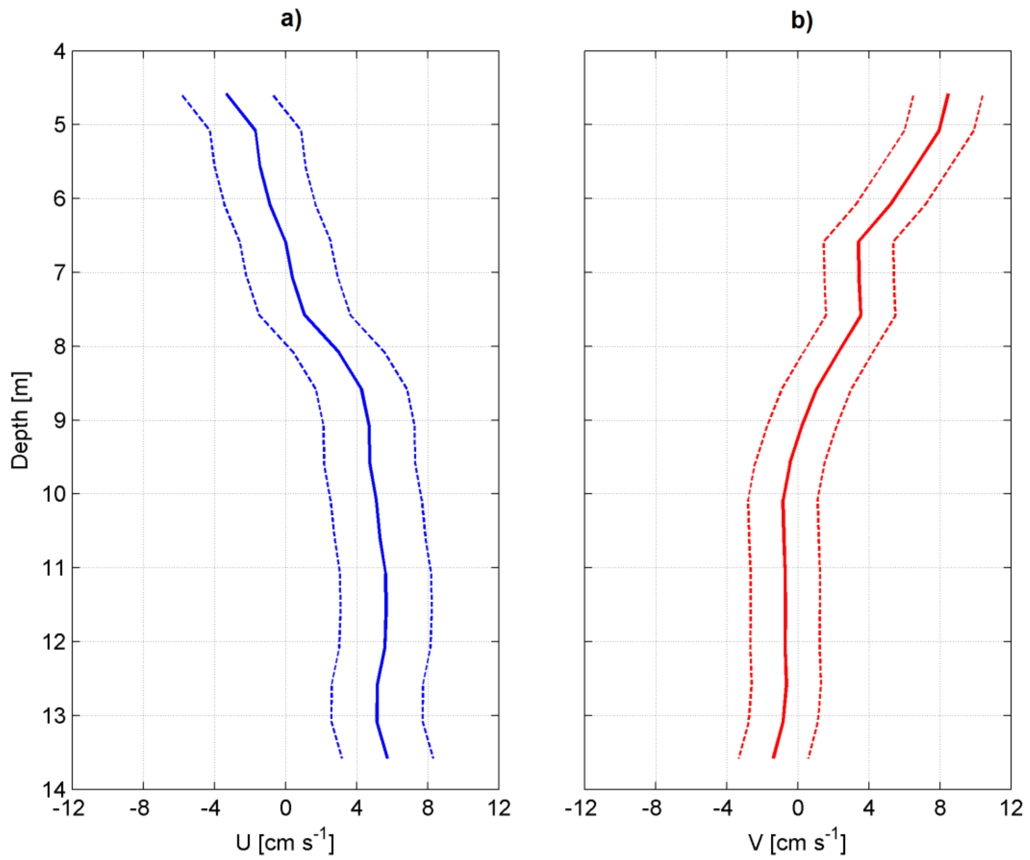

Fig. 46: Vertical profile of time-averaged zonal (a, blue line) and meridional (b, red line) current velocities at Mooring North for the depth interval from ~ 4.5 m to 13.5 m over the course of the polynya event (see Fig. 21) from April 3 to April 8, 2012. Dashed lines indicate the respective standard errors of the mean.

In order to put the results of the described relationship between observed water properties and current regime at Mooring North into a larger spatial context, the time series of salinity, temperature, and current velocities at Mooring Central obtained at greater distance to the landfast ice edge are investigated with respect to similarities and differences to the findings from Mooring North (see Fig. 43, 47).

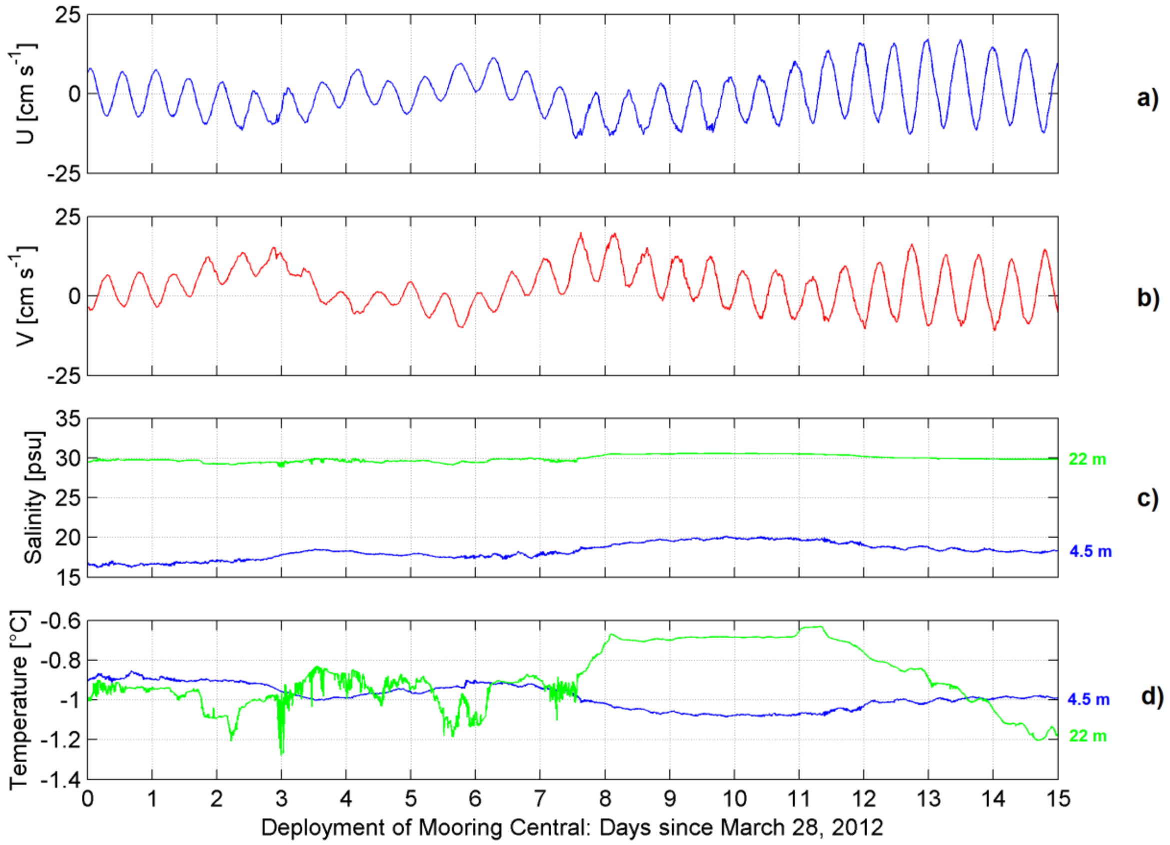

Fig. 47: Time series of depth-averaged zonal (a) and meridional (b) current velocities, salinity (c), and temperature (d) obtained at Mooring Central for the time period from March 27 (day 0) to April 17 (day 21), 2012. CTD sensors were fixed at ~ 3 m (blue line), 8 m (red line), 9.5 m (cyan line), 11 m (magenta line), 12.5 m (black line), and 15.5 m (green line).

Salinity and temperature measurements at Mooring Central were obtained at water depths of ~ 4.5 m and 22 m, respectively, over the time period from March 28 (day 0) to April 12 (day 15), 2012 (see Fig. 47 c, d). To facilitate the comparison with the respective current regime, depth-averaged zonal and meridional current velocities at Mooring Central for the same time period are shown. The time series of salinity and temperature correspond to the results from the respective CTD profiles acquired at Camp Central (see Fig. 34). In general, surface salinities and temperatures show only slight variations between ~ 16 psu and 20 psu and between ~ -1.1 °C and -0.9 °C, respectively. Bottom salinities are also characterized by very small variations over the measurement period. Associated values vary between ~ 29 psu and 31 psu. In contrast, bottom temperatures exhibit pronounced changes with magnitudes ranging from ~ -1.3 °C to -0.6 °C. In line with the observations from Mooring North, the polynya event at the beginning of April coincides with the period of the greatest changes in the water properties at Mooring Central. From April 4 (day 7) to April 8 (day 11), bottom temperatures increase significantly by ~ 0.3 °C, corresponding to the occurrence of comparatively strong northwestward currents (see Fig. 47). While the direction of the oceanic current regime is similar to Mooring North, the pronounced increase of bottom temperatures is not observed at Mooring North (see Fig. 42). Furthermore, the surface layer at Mooring Central exhibits a slight increase of salinity and decrease of temperature over the course of the polynya event, contrasting with the findings from Mooring North which indicate a pronounced contrary development. Unfortunately, it is not possible to examine temporal changes of water properties in the pycnocline at Mooring Central due to the lack of reliable measurements in the respective depth interval, preventing a comparison to the strong fluctuations observed at Mooring North. Bottom temperatures decrease considerably after the closure of the polynya, coinciding with predominantly southward currents, in line with the results from Mooring North. Associated changes in temperature are in the range of ~ 0.5 °C, which significantly exceed the changes observed at Mooring North. Overall, the location of Mooring Central is more sensitive to changes in bottom water properties over the measurement interval than the location of Mooring North, which, in contrast, shows great variability in the surface layer and particularly the pycnocline (see Fig. 43, 47).

In summary, the time series of salinity, temperature, and current velocities obtained at Mooring North and Mooring Central in March and April 2012 correspond to the CTD profiles observed at the respective locations. Both locations exhibit pronounced changes of water properties associated with changes in major current directions over the respective measurement intervals. In particular, the opening of a flaw polynya along the landfast ice edge on the southeastern Laptev Sea shelf from April 3 to April 8, 2012 considerably influences water properties at the two moorings. However, the effect of the polynya event on salinity and temperature distributions at the two locations is very different. Mooring North exhibits a strong increase of temperature and decrease of salinity in the pycnocline at the onset of the polynya event. This development is followed by rapid fluctuations of water properties with magnitudes of up to 15 psu and up to 0.5 °C, associated with considerable changes in the vertical position of the pycnocline. These fluctuations vanish over the course over the polynya event and a less stratified, cooler, and saltier water mass can be observed at Mooring North after polynya closure. In contrast, the response of water properties to the polynya event at Mooring Central is characterized by a strong increase in bottom temperatures, indicating that the change of hydrographic conditions due to polynya events varies spatially under the landfast ice.

5. Discussion of results

In order to interpret the findings of this study in the wider context of enhancing the understanding of the circulation and water properties under the landfast ice on the southeastern Laptev Sea shelf during the ice-covered season, this section aims to relate the individual results described in the previous section to each other as well as to the results of earlier studies conducted in the Laptev Sea.

5.1 Circulation under the landfast ice

The results obtained from the yearlong current velocity measurements at Mooring LENA indicate significant variations of the oceanic current regime over the annual freeze-thaw cycle on the southeastern Laptev Sea shelf (see Fig. 7). Based on daily sea ice concentration data derived from satellite observations, three different periods have been identified, namely the ice-covered, the break-up, and the ice-free season (see Fig. 7, 8, 9, 10). This division is in line with earlier investigations of the seasonal cycle of the oceanic current regime in the southeastern Laptev Sea by Dmitrenko et al. (2002), which also indicate significant variations of the oceanic current regime between the three phases. During the ice-covered season from early October to early June, predominantly northward to northeastward currents are observed east of the Lena River Delta (see Fig. 8). This finding supports the dominance of an offshore directed winter circulation regime as suggested by the modeling results of Pavlov and Pavlov (1999), which are based on the large-scale surface salinity distribution in the Laptev Sea. However, the under-ice oceanic current regime on the southeastern Laptev Sea shelf is also characterized by high temporal variability throughout the ice-covered season (see Fig. 7). This finding is supported by the detailed investigation of short-term current velocity records at Mooring Central and Mooring North in winter 2012 (see Fig. 16, 24) as well as by the results of earlier studies by Dmitrenko et al. (2010a), Dmitrenko et al. (2010c) and Dmitrenko et al. (2012), which analyzed temporal variability of short-term current velocity records obtained in winter 2008 and 2009. The results of the tidal harmonic analyses performed in this study indicate that the oceanic current regime under the landfast ice on the inner Laptev Sea shelf is strongly influenced by tidal dynamics (see Tables 6, 7, 8; Fig. 11, 18, 26). The tidal signal is dominated by M2, the principal lunar semidiurnal component, followed by S2, the principal solar semidiurnal component (see Tables 6, 7, 8), in line with the findings of earlier studies conducted in the Laptev Sea (Dmitrenko et al. 2010c, Lenn et al. 2011, Dmitrenko et al. 2012, Janout and Lenn 2014). However, the semidiurnal tidal signal is significantly modulated by various lower-frequency components (see Table 6). Especially, fortnightly variations of current velocities associated with the spring-neap tidal cycle also play an important role for the oceanic current regime (see Fig. 11, 18, 26). This finding supports the results of Dmitrenko et al. (2002) and Dmitrenko et al. (2012), which indicate strong modulation of the semidiurnal tidal flow near the landfast ice edge on the Laptev Sea shelf. The major axes of the tidal current ellipses associated with the dominant semidiurnal tidal constituents, M2 and S2, are aligned in a northwest-southeast direction (see Tables 6, 7, 8), resulting in predominant current variability towards and away from the landfast ice edge (see Fig. 2, 7, 11, 16, 18, 24, 26). The observed direction of the tidal flow under the landfast ice corresponds well to earlier observations by Dmitrenko et al. (2012) near the landfast ice edge and is likely influenced by the bottom topography of the inner Laptev Sea shelf (see Fig. 2). The southeastern Laptev Sea shelf is incised by relic submarine river valleys (Naidina 2005), which have been found to exert a strong influence on the local current regime (Dmitrenko et al. 2012, Janout et al. 2013, Janout and Lenn 2014, Fofonova et al. 2014).

The results of the tidal harmonic analysis show an amplification of M2 tides under the landfast ice, which seems to contribute to the strengthening of the tidal influence during the ice-covered season compared to the ice-free season (see Fig. 12). Amplification of M2 tides due to the presence of an ice cover has been previously observed on the Laptev Sea shelf by Dmitrenko et al. (2002), Lenn et al. (2011), Dmitrenko et al. (2012), and Janout and Lenn (2014). However, the physical processes which lead to the increased magnitude of M2 tides under the landfast ice cover of the southeastern Laptev Sea have not been fully understood yet. Petrusevich et al. (2016) have described strong semidiurnal tides related to resonant generation of internal tides due to interaction of M2 tides with the rough bottom topography in a highly stratified water column under the landfast ice in the southeastern Hudson Bay. Hence, the interaction of M2 tides with bottom topography, water column stratification, and landfast ice cover may play an important role in the amplification of M2 tides during the ice-covered season. The inner Laptev Sea shelf exhibits rough bottom topography (Naidina 2005), which would allow for the generation of internal tides. However, further investigations are needed to support this hypothesis. In contrast, the S2 tide maximum occurs in the time period from September to mid October, coinciding with the ice-free season and the beginning of the freeze-up phase (see Fig. 7, 12). This observation corresponds to earlier findings of Janout and Lenn (2014), which indicate increased S2 magnitudes during the ice-free season. However, Janout and Lenn (2014) also observed semiannual oscillations of S2 on the outer

Laptev Sea shelf, which have been linked to the superposition of S2 with the K2 constituent (Janout and Lenn 2014). Since the K2 constituent only exhibits a minor role for the tidal current regime at Mooring LENA, semiannual oscillations of S2 are not observed in this study (see Fig. 12). The seasonal magnitude variations of S2 tides may represent an indication of a damping effect due to the presence of an ice cover. However, this hypothesis needs to be tested in future studies.

The results of this study indicate considerable vertical variability of the tidal influence on the under-ice current regime throughout the water column (see Fig. 12, 19, 27). The ratio of tidal variability to total variability at Mooring LENA is highest in the depth interval from ~ 14 m to 20 m depth, while the tidal influences at Mooring Central and Mooring North peak at water depths of ~ 10 m and ~ 7 m, respectively (see Fig. 12, 19, 27). The observed maxima in the tidal influence correspond to the maxima in the magnitude of the dominant tidal constituent M2 (see Fig. 12, 19, 27), indicating the strong influence of M2 tides on the vertical structure of the oceanic current regime. Depth-dependency of tidal currents under the landfast ice on the inner Laptev Sea shelf has been identified in previous studies by Dmitrenko et al. (2002) and Dmitrenko et al. (2012). According to Dmitrenko et al. (2012), depth-dependent tidal currents are generated by the interaction of the tidal flow with the rough bottom topography of the inner shelf, generating internal waves of similar frequency, known as baroclinic tides, and with the seasonal ice cover, representing an additional source of friction. The potential of both influences to modify the vertical structure of tidal dynamic has been discussed extensively in the literature (e.g. Prinsenberg and Bennet 1989, Prinsenberg and Ingram 1991, Dovgaya and Cherkesov 2001, St-Laurent et al. 2008, Pradhan et al. 2015). Moreover, interaction of tidal currents with the local stratification has been discussed as an important physical process influencing the vertical structure of tidal currents on the Laptev Sea shelf (Lenn et al. 2011, Dmitrenko et al. 2012, Janout and Lenn 2014). The relationship between stratification and the vertical tidal structure has been shown in numerous studies (e.g. Visser et al. 1994, Danielson and Kowalik 2005, Makinson et al. 2006). The results of this study indicate that the maximum of the tidal influence at Mooring Central and Mooring North coincides with the depth of the respective pycnocline (see Fig. 19, 27, 33, 34), supporting the findings of earlier studies. In the case of Mooring North, the maximum of the tidal influence has also been shown to correspond to the vertical maximum of the Brunt-Väisälä frequency (see Fig. 45), indicating the important role of stratification on the vertical structure of tides under the vast landfast ice cover of the southeastern Laptev Sea shelf. Therefore, the observed depth-dependency of the tidal influence under the landfast ice in the southeastern Laptev Sea is likely the result of complex interactions of the tidal flow with stratification, bottom topography, and the seasonal ice cover. Dmitrenko et al. (2012) and Janout and Lenn (2014) have suggested that baroclinic tides may promote shear instabilities and diapycnical mixing of seawater properties on the Laptev Sea shelf. Hence, tidal dynamics may have an important influence on the hydrography on the inner Laptev Sea shelf during the ice-covered season.

The results of this study have shown that the influence of tides on the oceanic current regime increases throughout the ice-covered season (see Fig. 12), despite the occurrence of nearly 100 % ice cover on the inner Laptev Sea shelf by mid October (see Fig. 7). Janout and Lenn (2014) have made a similar observation for the region north of the landfast ice edge, which is seasonally covered with pack ice. They have related their findings to the development of the sea ice cover over the ice-covered season. While the ice cover is thinner and more mobile in early winter, the ice becomes thicker and less mobile over the course of the ice-covered season, likely reducing the transfer of stress at the ice-ocean interface (Janout et al. 2013). Although sea ice has been found to dampen wind-generated inertial oscillations (Rainville and Woodgate 2009), the oscillations are known to penetrate loose pack ice (Padman and Kottmeier 2000, Kwok et al. 2003). Since the development of landfast ice occurs over the time period from October to January, the ice cover on the southeastern Laptev Sea shelf is still mobile during early winter (Selyuzhenok et al. 2015), which may lead to the transfer of wind stress at the ice-ocean interface to the underyling water column and may explain the lower influence of tides on the oceanic current regime during early winter. The comparison of residual currents to surface wind forcing at Mooring LENA provides some indications which support this hypothesis (see Fig. 15). Generally, the wind influence on the oceanic current regime at Mooring LENA is very low during the ice-covered season. However, while there is some evidence that winds may induce changes in the under-ice oceanic current regime during freeze-up and early winter, the wind influence becomes negligible as the landfast ice cover develops (see Fig. 15). This finding is in line with earlier observations of reduced wind influence during the ice-covered season by Dmitrenko et al. (2002) and supports the proposed decoupling of the oceanic current regime from the atmosphere by the immobile landfast ice cover, as stated by Itkin et al. (2015). An exception to this pattern represents the oceanic current regime in the vicinity of the landfast ice edge, which exhibits significantly higher current velocities compared to locations at greater distance fromthe landfast ice edge (see Fig. 7, 16, 24), which are likely influenced by considerable wind forcing (see Fig. 29). This finding is supported by earlier observations of the under-ice flow near the landfast ice edge showing consistency with the mean wind forcing during the ice-covered season (Dmitrenko et al. 2010a). Therefore, the under-ice current regime is likely influenced by considerable lateral variations of the wind influence, which tends to decrease under the landfast ice with increasing distance to the landfast ice edge, i.e. towards south. Consequently, other physical processes, such as salinity differences (Pavlov and Pavlov 1999), likely exert a stronger influence on the under-ice oceanic current regime at greater distance to the landfast ice edge. This hypothesis is supported by the occurrence of strong residual currents of non-tidal origin at the locations of Mooring Central and Mooring LENA (see Fig. 13, 20), which have been discussed to be largely shielded from direct wind forcing. The greater role of wind forcing for the under-ice current regime near the landfast ice edge is likely connected to the response of oceanic currents to the large-scale wind forcing beyond the landfast ice edge. Janout et al. (2013) have identified a complex relationship between wind forcing, ice drift, and current response under the adjacent pack ice, which might also induce a current response under the landfast ice. Hence, response flows to wind-induced currents might play an important role for mixing and transport processes under the landfast ice and, thereby, might significantly impact hydrographic conditions on the inner Laptev Sea shelf, especially in the vicinity of the landfast ice edge. Consequently, the scarcely investigated relationship of wind forcing and under-ice current response in the Laptev Sea, in particular in the vast southeastern region which is dominated by landfast ice, needs to be examined with greater detail in future studies.

Similar to the wind forcing, tidal dynamics have also been identified to exhibit considerable lateral variations under the landfast ice cover on the southeastern Laptev Sea shelf. The magnitude of the major axis of the tidal ellipse associated with the dominant M2 tidal component is approximately twice as high at Mooring North as at Mooring Central (see Tables 7, 8), despite the analyzed current velocity records covering very similar measurement periods. This finding suggests that the M2 tide is amplified in the vicinity of the landfast ice edge (see Fig. 2). However, it should be noted that the inertial frequency f, defined as twice the rotation rate of the Earth multiplied by the sine of the latitude, is close to the frequency of the dominant semidiurnal tidal constituent M2 over the Laptev Sea shelf (Dmitrenko et al. 2012, Janout and Lenn 2014). Hence, the obtained current velocity records at Mooring Central and Mooring North are too short to distinguish between inertial motion with a period of 12.51 h to 12.33 h for the Laptev Sea shelf (73° N to 76° N) and semidiurnal tides (12.42 h for M2 and 12.00 h for S2). As a result, inertial oscillations may be included in tidal signal.

While the current velocity time series recorded at Mooring North shows some correspondence to the near-surface wind as discussed above, the location of Mooring Central is shielded from atmospheric wind forcing, which is mainly responsible for the generation of inertial currents (Rainville and Woodgate 2009). Hence, inertial current generation at Mooring North cannot be ruled out to explain the observed differences of the M2 tidal current magnitudes between the two locations. However, spatial differences in the interaction of M2 tides with local bottom topography, sea ice cover and stratification, as discussed above, could also be the reason for the observed differences in M2 tidal current magnitudes.

As aforementioned, tidal dynamics, wind forcing, and salinity differences have been identified as potential drivers of the circulation under the landfast ice on the southeastern Laptev Sea shelf. The results of this study show that the influence of different drivers on the under-ice oceanic current regime is significantly modified by the opening of flaw polynyas along the landfast ice edge in the southeastern Laptev Sea. From April 3 to April 8, 2012, a flaw polynya opened along the landfast ice edge of the southeastern Laptev Sea (see Fig. 21), driven by large-scale northwestward winds (see Fig. 22). The opening of the polynya coincides with a period of strong depth-averaged northwestward residual currents at Mooring North and Mooring Central (see Fig. 20, 28), directed towards the open water (see Fig. 2). The vertical structure of the mean current regime at Mooring North for this time period indicates a two-layer structure, with strong northwestward currents near the surface and eastward currents at depth (see Fig. 44). The strong offshore directed surface currents might be influenced by enhanced wind forcing on the under-ice oceanic current regime during the polynya event (see Fig. 23, 29). Increased wind influence on the under-ice current regime during the opening of the polynya may result from the formation of an extensive open water surface along the landfast ice edge, which can transmit wind stress to the underlying water column more effectively than pack ice (Rainville and Woodgate 2009). Moreover, flaw polynyas have been identified as regions of vigorous sea ice production, resulting in a local salinity increase in the upper water column due to brine rejection and consequently impacting hydrographic conditions and physical processes under the adjacent landfast ice cover (Ivanov and Golovin 2007, Dmitrenko et al. 2010a, Krumpen et al. 2011, Dmitrenko et al. 2012). Sub-ice surface currents directed towards open water have been observed repeatedly in flaw polynyas and leads, which are transient linear-like areas of open water, on the Arctic shelves in winter (e.g. Smith et al. 1990, Morison et al. 1992, Smith and Morison 1993). These currents have been linked to the development of circulation cells induced by polynya-generated salinity fields, consisting of an off-ice flow of the upper water layers and a compensatory current developing below (Smith 1973, Smith and Morison 1993). Geostrophic adjustment to the polynya-generated density fields has been discussed to exert a considerable influence on the oceanic current regime on the inner Laptev Sea shelf (Dmitrenko et al. 2005, Dmitrenko et al. 2010a, Dmitrenko et al. 2010c, Kirillov et al. 2013). According to Dmitrenko et al. (2010a), local thermohaline forcing during polynya events may be more important for the oceanic current regime under the landfast ice in the southeastern Laptev Sea than regional wind forcing. Hence, polynya-generated density differences likely contribute significantly to the observed under-ice circulation during the opening of the flaw polynya event in April 2012.

As discussed above, the results of this study suggest that the circulation under the landfast ice in the southeastern Laptev Sea is the product of the complex interplay of tidal dynamics, wind forcing, and thermohaline forcing. Additionally, these factors are modified by polynya activity, resulting in a highly variable under-ice oceanic current regime during the ice-covered season. The attempt to detect a general large-scale pattern of the oceanic current regime under the landfast ice with the help of vertical profiles of mean current velocities obtained from the yearlong mooring LENA as well as various short-term moorings deployed under the landfast ice in 2008, 2009, and 2012, respectively, has yielded only limited success (see Fig. 8, 17, 25, 30, 31, 32). This result may be owed to the scarce availability of current velocity measurements under the landfast ice. Due to the high temporal variability of the under-ice current regime, especially over the course of polynya events, short-term current velocity records obtained during different time intervals are limited in their explanatory power with respect to the general pattern of the under-ice circulation on the southeastern Laptev Sea shelf in winter. Therefore, more long-term measurements of the current regime under the landfast ice edge are desirable to adequately answer the question of large-scale circulation patterns on the inner Laptev Sea shelf during the ice-covered season. Nevertheless, the vertical profiles of mean current velocities have indicated some important characteristics of the oceanic current regime under the landfast ice. The high variability of the current regime observed in this study is typical of shallow Arctic shelves, where bathymetric features, sea ice dynamics, and river freshwater input strongly influence the local current regime (e.g. Pavlov and Pavlov 1999, Janout et al. 2017). Observed mean current directions have been identified to clearly follow the local bathymetry at some measurement locations (e.g. Mooring Central, see Fig. 32), indicating that bathymetric features may have a significant influence on the main circulation pathways under the landfast ice on the southeastern Laptev Sea shelf. However, this hypothesis needs to be investigated further as part of a future study aimed at identifying large-scale circulation patterns on the southeastern Laptev Sea shelf.

In contrast to the ice-covered season, tidal dynamics on the southeastern Laptev Sea shelf lose importance during the break-up season and explain less than 10 % of the variability of current velocities during the ice-free season (see Fig. 12). Furthermore, the relative importance of the tidal influence and the magnitude of the dominant semidiurnal tides are more evenly distributed with depth during these seasons (see Fig. 12), in line with earlier findings of Dmitrenko et al. (2002). While wind-driven advection is largely prevented by the landfast ice cover during the ice-covered season (see Fig. 15), wind forcing is of great importance during the ice-free season (see Fig. 14), resulting in significantly higher magnitudes and increased variability of current velocities than during the ice-covered season (see Fig. 7). These findings are in line with earlier observations of enhanced wind influence and reduced tidal influence on the current regime on the inner Laptev Sea shelf during the ice-free season (Dmitrenko et al. 2002, Janout and Lenn 2014). Janout and Lenn (2014) have inferred that reductions in the seasonal ice cover will induce changes in the tidal dynamics as well as the vertical water column structure on the inner Laptev Sea shelf. Moreover, they proposed that the predictability of the oceanic current regime will decrease due to a decreasing importance of tides (Janout and Lenn 2014). The results of this study support the proposed effects associated with a decreasing ice cover by Janout and Lenn (2014). Furthermore, they indicate that a reduction of the landfast ice cover in a changing climate (Yu et al. 2014) will have a particularly strong effect on the circulation and hydrography on the inner Laptev Sea shelf since seasonal differences in this area are even more pronounced compared to the pack ice region due to the decoupling of the ocean from the atmosphere (Itkin et al. 2015). The observed prominent seasonal variability of the current regime due to the varying importance of different drivers of the oceanic current regime on the southeastern Laptev Sea is in line with the findings of earlier in-situ investigations and modeling studies of the annual cycle in circulation on other Arctic shelves with a seasonal landfast ice cover (Wang et al. 2014, Weingartner et al. 2017). Therefore, reductions in the landfast ice cover would likely also have an extensive effect on the coastal circulation of other Arctic shelves.

5.2 Water properties under the landfast ice

The vertical salinity and temperature distributions observed at the three different ice camps in March and April 2012 indicate the presence of a highly stratified water column under the landfast ice on the southeastern Laptev Sea shelf despite the shallow water depth (see Fig. 2, 33, 34, 35). The water column exhibits a typical three-layer structure (see Bauch et al. 2009), which is characterized by a fresh surface layer and a colder, more saline, well-mixed bottom layer separated by a sharp pycnocline layer. These findings are supported by the majority of the salinity and temperature profiles measured during winter 2008 and 2009, respectively, which reveal a similar vertical water column structure under the landfast ice (see Fig. 38, 39, 40, 41, 42), corresponding to the results of earlier studies by Bauch et al. (2009) and Dmitrenko et al. (2012). However, the measurements also indicate significant lateral differences of water properties, especially in the vicinity of the landfast ice edge, as well as pronounced temporal variations on a variety of different timescales, in line with the observed complexity of the oceanic current regime under the landfast ice. Hydrographic conditions on the Laptev Sea shelf have been discussed to be the result of complex interactions of different physical processes related to the Lena River freshwater discharge, sea ice formation, tides, wind-induced mixing, and episodic advection (Bauch et al. 2009, Dmitrenko et al. 2010a, Dmitrenko et al. 2010c, Dmitrenko et al. 2012, Kirillov et al. 2013, Janout and Lenn 2014, Janout et al. 2016).

The freshwater input from the Lena River has been identified as the main contribution to the formation of a highly stratified water column (Bauch et al. 2009). The observed stratification on the inner Laptev Sea shelf in winter is likely maintained due to the landfast ice cover, which effectively decouples the atmosphere from the ocean and prevents wind-induced mixing of water masses (Itkin et al. 2015). This finding is in line with the weak current velocities observed at Mooring LENA during the ice-covered season (see Fig. 7) as well as the weak correlation of wind forcing and oceanic current regime at Mooring LENA and Mooring Central (see Fig. 15, 22), as discussed above. The lack of evidence for a well-mixed surface layer in the majority of the salinity and temperature profiles obtained in winter 2008, 2009, and 2012 is another indicator that wind-induced mixing is prevented by the landfast ice cover. An exception to this pattern can be observed in the vicinity of the landfast ice edge. Multiple salinity and temperature profiles obtained near the landfast ice edge reveal the occurrence of mixing of water properties throughout the water column (see Fig. 33, 38, 39, 40, 41). In some cases, mixing processes only lead to the formation of a well-mixed surface layer (e.g. at Mooring North, see Fig. 33), while in other cases an entirely well-mixed water column can be observed (see Fig. 38 c, d; 39 c, d). The observed homogenous surface water layers are likely the result of advection of water masses from locations beyond the landfast ice edge, where a mobile pack ice cover and episodic opening of flaw polynyas allow for wind-induced mixing (Janout et al. 2013). Moreover, enhanced convective mixing has been observed to occur beyond the landfast ice edge as a result of changes in salinity due to brine rejection during thermodynamic ice formation associated with polynya events (Krumpen et al. 2011, Kirillov et al. 2013). Unfortunately, supporting evidence for the advection of well-mixed water masses under the landfast ice edge is not presented in this study as the respective CTD profile which demonstrates the presence of a well-mixed surface layer at Camp North was obtained before the deployment of Mooring North. However, the results of Kirillov et al. (2013) based on oceanographic data from winter 2008 have shown the advection of water masses across the landfast ice edge. While observations indicate that turbulent, wind-induced mixing is prevented under the landfast ice cover, the inner Laptev Sea shelf has been identified to be very sensitive to tidally-induced mixing due to its shallow character and topographic features (Krumpen et al. 2011, Dmitrenko et al. 2012, Kirillov et al. 2013, Janout and Lenn 2014, Fofonova et al. 2014, Fofonova et al. 2015). The results of the tidal harmonic analysis presented in this study support the dominant role of tides for the current regime under the landfast ice as described in previous studies. Therefore, tidally-induced mixing is interpreted as the main cause of the observed well-mixed bottom layer under the landfast ice cover. The presence of an entirely well-mixed water column at the two most northeasterly measurement locations in winter 2008 (see Fig. 38 c, d; 39 c, d) indicates the occurrence of vigorous mixing processes in the vicinity of the landfast ice edge, likely representing a combination of wind, tidal and thermodynamic influences. Due to the greater distance from the Lena River Delta (see Fig. 2), the influence of Lena River freshwater on the hydrography at these locations is likely reduced, increasing the likelihood of degradation of the stratified water column. This hypothesis is supported by the increase in surface salinity along the landfast ice edge with increasing distance from the Lena River Delta (Dmitrenko et al. 2005).

In general, surface temperature under the landfast ice is closely associated with salinity and corresponds to or slightly exceeds the respective freezing temperature (see Fig. 33, 34, 35, 38, 39, 40, 41, 42). In contrast, several pronounced positive temperature anomalies are observed in the interior water column at different locations under the landfast ice cover, which are independent of the observed salinity (see Fig. 34, 35, 39). Dmitrenko et al. (2010c) have discussed advection of warm Atlantic-derived waters as the likely heat source to the interior water column based on the CTD profiles obtained in winter 2008. This interpretation is not supported by the observed salinity distribution under the landfast ice on the southeastern

Laptev Sea shelf in winter 2012 because Atlantic-derived water masses are characterized by higher salinities, which are not evident in the observations from this study. The comparison of bottom temperatures with the oceanic current regime at Mooring Central indicates the advection of particularly warm water masses during the time period from April 4 to April 9, 2012, coinciding with predominantly northwestward depth-averaged currents (see Fig. 47). Unfortunately, current velocity measurements obtained in the lower water column are fragmentary during this time period, preventing in-depth analysis of the location of the heat source to the lower water column. Based on the findings of the depth-averaged current velocity record, an inshore heat source would be assumed. Hölemann et al. (2011) have discussed the occurrence of positive near-bottom temperature anomalies on the mid-shelf due to vertical mixing of warm surface water masses, heated by solar radiation and warm river water discharge in summer. These temperature anomalies may persist throughout the ice-covered season, trapped in the interior water column by salinity stratification. The results of Janout et al. (2016) support the role of the upper ocean as the heat source for episodic temperature anomalies in the bottom layer on the Laptev Sea shelf in winter. Therefore, temperature inversions observed under the landfast ice during winter 2012 may result from overwintered heat accumulated in the water column during the previous summer. While Hölemann et al. (2011) and Janout et al. (2016) focus on temperature anomalies in the bottom layer, the findings of this study also suggest the occurrence of considerable temperature inversions in the surface layer just above the pycnocline (see Fig. 34). These temperature anomalies might have been maintained on the inner Laptev Sea shelf due to the presence of the landfast ice cover, which prevents wind-induced mixing of the surface layer.

Observations of salinity and temperature distributions under the landfast ice indicate significant lateral variability of water properties in a north-south direction over the ice-covered inner Laptev Sea shelf (see Fig. 33, 34, 35). The observed increase of salinity and decrease of temperature with decreasing distance to the landfast ice edge likely result from the diminishing influence of Lena River freshwater and increasing importance of cooler and more saline water masses on hydrographic conditions on the inner Laptev Sea shelf. This finding is in line with earlier observations of the large-scale salinity fields in the Laptev Sea by Dmitrenko et al. (2005), which indicate a northward increase of salinity from the Lena River Delta towards the outer shelf. Lateral variability of water properties seems to play a particularly important role in the vicinity of the landfast ice edge, where strong salinity and temperature gradients, as well as changes in the water column structure have been observed on relatively small spatial scales, both along the landfast ice edge and across the landfast ice edge. As discussed above, the salinity and temperature profiles obtained along the landfast ice edge in winter 2008 indicate a shift from a three-layer water column structure at the most southwesterly location towards an entirely well-mixed water column at the two most northeasterly locations. This change coincides with the occurrence of lower surface salinities with increasing distance to the Lena River Delta and likely reflects the decreasing influence of Lena River freshwater, which may weaken the stratification and may facilitate mixing of water properties. In contrast, the salinity and temperature distributions measured along the landfast ice edge in 2009 exhibit a similar structure of the water column associated with comparable measurement values of water properties at all measurement locations (see Fig. 40, 41). It should be noted that the majority of the CTD profiles were obtained at different measurement locations in 2008 and 2009 (see Fig. 2). The observations from the two most northeasterly stations in 2008 were acquired at considerably greater distances to the landfast ice edge than all measurements obtained in 2009. While these differences in the measurement setup may influence the investigation of lateral gradients along the landfast ice edge, the observed changes in the water properties between the different years likely also have a physical cause because the CTD profiles obtained at similar locations in 2008 and 2009 indicate significant differences in water column structure (see Fig. 38 b, 39 b, 40 d, 41 d). Besides, CTD measurements obtained in winter 2008 generally exhibit significantly higher salinity values and lower temperature values near the surface than observations from winter 2009 (see Fig. 38, 39, 40, 41), suggesting pronounced interannual variability of the physical processes influencing the under-ice hydrography near the landfast ice edge on the southeastern Laptev Sea shelf. Dmitrenko et al. (2012) have linked these differences in water properties over the consecutive winter seasons of 2007/08 and 2008/09 to preconditioning of the inner Laptev Sea shelf from differences in summer wind-driven diversion of river runoff (Dmitrenko et al. 2010b). As in the case of the discussed temperature inversions in the interior water column, hydrographic conditions and physical processes on the southeastern Laptev Sea shelf in summer seem to exert a strong influence on the under-ice hydrography in the following winter. Temperature and salinity profiles measured near the landfast ice edge in winter 2009 exhibit significant lateral variability across the landfast ice edge. Observations indicate higher surface salinities and lower surface temperatures beyond the landfast ice edge than compared to locations under the landfast ice, resulting in a less pronounced pycnocline (see Fig. 37, 40, 41). The differences in the water properties across the landfast ice edge are likely a result of polynya activity. From April 15 to April 23, 2009, a considerable opening of a flaw polynya along the landfast ice edge occurred on the southeastern Laptev Sea shelf (Dmitrenko et al. 2012). Extremely low air temperatures and associated surface heat loss within flaw polynyas have been identified to significantly impact the energy budget of the underlying water column (Gutjahr et al. 2016). Moreover, thermodynamic ice formation in flaw polynyas in the Laptev Sea has been found to result in a local salinity increase in the upper water column due to brine rejection (Dmitrenko et al. 2010a, Krumpen et al. 2011, Dmitrenko et al. 2012). Hence, polynya activity is capable of inducing significant lateral gradients of salinity and temperature across the landfast ice edge. The observed salinity and temperature profiles obtained near the landfast ice edge in 2008 do not exhibit strong lateral gradients across the landfast ice edge despite the opening of a flaw polynya along the landfast ice edge. However, the CTD measurements at stations beyond the landfast ice edge were obtained before the prominent polynya event from April 28 to May 3, 2008, indicating that polynya activity before this event may have been too weak to induce significant lateral gradients across the landfast ice edge. Polynya activity can also be interpreted as the likely driver of temporal changes in water properties over short time periods of several days to weeks, which have been identified by comparing CTD profiles obtained at the same location before and after a polynya event as well as by analyzing the salinity and temperature time series at Mooring North and Mooring Central. Observations from Camp North and Camp Central in winter 2012 (see Fig. 33, 34, 43, 47) show an increase of salinity and a decrease of temperature after the polynya event, which occurred from April 3 to April 8, 2012, in line with the discussed effects of surface heat loss and brine rejection due to polynya activity. Similar observations have been made at several stations along the landfast ice edge in response to polynya events in winter 2008 and 2009 (see Fig. 38, 39, 40, 41). Hence, polynya events seem to have the ability to significantly alter water properties and water column structure under the landfast ice on the southeastern Laptev Sea shelf. This interpretation is in line with the findings of earlier studies by Krumpen et al. (2011), Dmitrenko et al. (2010a), and Dmitrenko et al. (2012), which indicate pronounced changes in the local hydrography near the landfast ice edge in the southeastern Laptev Sea as a result of polynya activity. However, the alteration of water properties at Camp Central presented in this study (see Fig. 47) indicates that polynya events may have a considerable effect on the hydrographic conditions under the landfast ice at larger spatial scales than previously identified.

The combined analysis of salinity, temperature, and current velocity records from Mooring North performed in this study provides some indication on the physical processes which alter water properties and circulation patterns under the landfast ice in response to polynya activity. The salinity and temperature time series obtained at Mooring North in March and April 2012 support the finding of pronounced lateral gradients of water properties in the vicinity of the landfast ice edge (see Fig. 43). Semidiurnal tidal variability has been identified to dominate the direction and strength of oceanic currents at Mooring North (see Table 8), resulting in advection of warmer and fresher water masses from the inner shelf and cooler and saltier water masses from beyond the landfast ice edge (see Fig 43). Due to the short distance between Mooring North and the landfast ice edge (see Fig. 2), semidiurnal tidal currents can transport water masses from beyond the landfast ice edge to the mooring location in one tidal cycle, explaining the high sensitivity of hydrographic conditions to tidal variability. This finding is in line with earlier observations by Dmitrenko et al. (2010a), which indicate consistency of salinity and temperature changes near the landfast ice edge with the advection of water masses from regions beyond the landfast ice edge and from regions inshore by tidal currents. From March 28 to April 1, 2012 and from April, 4 to April 8, 2012, vigorous semidiurnal salinity and temperature fluctuations can be identified in the pycnocline at Mooring North, leading to significant alteration of pycnoline depths (see Fig. 43, 44). Extremely rapid and strong salinity and temperature fluctuations under the landfast ice such as these, with amplitudes of up to 15 psu and 0.5°C recorded at ~ 8 m water depth, have not been previously observed on the inner Laptev Sea shelf. However, Kirillov et al. (2013) have identified rapid changes in salinity and temperature of significantly smaller magnitudes at the landfast ice edge, which have been related to horizontal advection of water masses induced by strong lateral gradients due to the alteration of pycnocline depths across a flaw polynya in winter 2008. The results of this study indicate that a similar process may have played an important role for the observed fluctuations of water properties at Mooring North. The recorded salinity and temperature fluctuations are closely linked to the occurrence of strong semidiurnal currents associated with tidal dynamics (see Fig. 26, 43) as well as the presence of pronounced vertical and lateral gradients of salinity and temperature, as discussed above. The most pronounced fluctuations from April 4 to April 8, 2012 correspond to the opening of a flaw polynya along the landfast ice edge on the inner Laptev Sea shelf (see Fig. 21), which has been identified to enhance lateral gradients of water properties due to the discussed effects of surface heat loss and brine rejection. Current velocity measurements at Mooring North indicate relatively strong northwestward residual currents (see Fig. 28), which coincide with the onset of the extreme salinity and temperature fluctuations in the pycnocline (see Fig. 43). The analysis of the vertical structure of the current regime observed for the most pronounced event, from April 4 to April 8, 2012, reveals a two-layer flow in the water column, characterized by a strong northward flow in the upper water column and a countercurrent at depth (see Fig. 46). Although wind forcing seems to have a considerable effect on the under-ice oceanic current regime near the landfast ice edge (see Fig. 29), polynya-generated enhanced density gradients across the landfast ice edge may significantly contribute to the offshore directed surface currents and may lead to the formation of circulation cells under the landfast ice (see discussion in section 4.1). The advection of surface water masses from the southeast over the course of the polynya event likely leads to the intermittent increase of temperature and decrease of salinity in the upper water column at Mooring North, initially enhancing the lateral gradients of surface water properties at the landfast ice edge. However, the increased vertical and lateral gradients of salinity and temperature observed at the onset of the polynya opening have been identified to diminish over the course of the polynya event (see Fig. 43, 44), indicating the occurrence of pronounced mixing processes initiated by oceanic currents. As a result, the vertical stratification of the water column at Mooring North is significantly weakened after the closure of the polynya (see Fig. 44, 45). This observation is linked to a pronounced increase of salinity in the surface layer compared to relatively constant bottom salinity. Moreover, temperatures have been found to decrease after the closure of the polynya (see Fig. 43, 44). Both findings are in line with a shift of the current regime towards a predominantly southward direction over the course of the polynya event, in line with the surface wind forcing (see Fig. 29), resulting in advection of water masses from beyond the landfast ice edge, which have been subject to the discussed effects of surface heat loss and brine rejection due to polynya activity. Hence, the observations from Mooring North provide detailed insights into the complex interplay between wind forcing, thermohaline forcing due to sea ice formation, and tidal dynamics over the course of a polynya event, which has been identified to significantly alter the hydrography and physical processes under the landfast ice on the southeastern Laptev Sea shelf.

5. Conclusion

Since the winter circulation under the landfast ice on the vast and shallow southeastern Laptev Sea shelf had been scarcely investigated in previous studies, the aim of this study has been to contribute the characterization of the under-ice current regime and hydrography of this remote and hard-to-access region. Overall, the results of this study have indicated that the circulation and water properties under the landfast ice in the southeastern Laptev Sea are determined by the complex interplay of immobile landfast ice, Lena River freshwater discharge, tidal dynamics, wind forcing, and thermohaline forcing, additionally modified by polynya activity along the landfast ice edge.

As expected, oceanographic conditions on the southeastern Laptev Sea shelf are subject to pronounced seasonal variability caused by the annual freeze-thaw cycle. Three different periods have been identified, namely the ice-covered, the break-up, and the ice-free season, which are characterized by differing influences of various physical processes on the oceanic current regime. During the ice-covered season from early October to early June, tidal dynamics play an important role for the under-ice circulation. The tidal influence under the landfast ice is mainly dominated by the principal lunar semidiurnal constituent, M2, followed by the principal solar semidiurnal constituent, S2. Tidal currents flow mainly in a northwest-southeast direction and are highly depth-dependent. Maxima of tidal currents have been identified to correspond to the depth of the pycnocline. The observed vertical structure of tidal currents is likely the result of the complex interplay of the tidal flow with stratification, bottom topography, and landfast ice and may promote shear instabilities and diapycnical mixing on the inner Laptev Sea shelf. Furthermore, the aforementioned interactions might also cause the observed alteration of the magnitudes of M2 and S2 tides under the landfast ice during the ice-covered season. While under-ice amplification of M2 tides had been previously detected on the southeastern Laptev Sea shelf, the results of this study have also identified the damping of S2 tides under the landfast ice, which should be investigated in future studies. The influence of tides on the oceanic current regime on the inner Laptev Sea shelf has been found to increase throughout the ice-covered season, despite a nearly 100 % ice cover early in the season. This development may be related to the reduced mobility of sea ice as it becomes attached to the coast over the time period from October to January, preventing transfer of wind stress to the water column. However, the relationship between wind influence and tidal dynamics over the course of the ice-covered season should be investigated in future studies as the results of this study can only provide a first indication for this linkage. In general, the landfast ice cover has been found to largely decouple the inner Laptev Sea shelf from atmospheric forcing during the ice-covered season. Beside tidal dynamics, thermohaline forcing has been discussed to influence the under-ice current regime on the southeastern Laptev Sea shelf. Lateral salinity differences are a possible driver of the observed residual background circulation. In contrast to the ice-covered season, tidal dynamics lose importance over the break-up season and explain only a small fraction of the variability of the current regime during the ice-free season (less than 10 % based on the results from Mooring LENA). The influence of wind forcing on the oceanic current regime increases significantly as the landfast ice cover vanishes, resulting in significantly greater magnitudes and higher variability of current velocities in summer. In summary, the results of this study have shown that the pronounced seasonality of oceanographic conditions on the southeastern Laptev Sea shelf is largely caused by the development of the landfast ice cover in winter, which decouples the water column from atmospheric forcing and provides an additional boundary layer to the water column that likely interacts with tidal dynamics. Consequently, future reductions of the seasonal landfast ice cover in a changing climate may significantly alter the winter circulation on the southeastern Laptev Sea and may considerably reduce its predictability as the tidal influence is likely to decrease in response to a reduction of the landfast ice cover.

The investigation of the spatial differences of oceanographic conditions on the inner Laptev Seas shelf in winter has supported the hypothesis that Lena River freshwater discharge and the relative distance to the landfast ice edge influence the local current regime and water properties under the landfast ice. Strong lateral salinity and temperature gradients occur on the southeastern Laptev Sea shelf, indicating a decreasing influence of Lena River freshwater and an increasing importance of cooler and more saline water masses on hydrographic conditions with decreasing distance to the landfast ice edge. Moreover, the water column structure under the landfast ice has been observed to exhibit pronounced spatial differences, which depend on the distance to the landfast ice edge and to the Lena River Delta. In general, the prevention of wind-induced mixing due to the immobile landfast ice allows for the formation of a highly stratified water column under the landfast ice, characterized by a fresh surface layer separated from a colder and saltier, well-mixed bottom layer by a sharp pycnocline. While surface temperatures under the landfast ice are generally close to or slightly above the freezing point, the strong under-ice stratification has presumably helped to maintain pronounced positive temperature anomalies in the bottom layer as well as in the surface layer just above the pycnocline. The observed temperature anomalies may have been caused by the accumulation of heat in the water column during the previous summer. In contrast, observed temperature anomalies in the bottom layer near the landfast ice edge coincide with high salinities and have been discussed in previous studies to result from episodic advection of warm Atlantic-derived water masses. Wind forcing seems to exert a considerable influence on the under-ice circulation near the landfast ice edge compared to regions at greater distance to the landfast ice edge. Strong residual currents of non-tidal origin may represent the indirect response of the under-ice current regime to the large-scale wind forcing and may advect well-mixed water masses from beyond the landfast ice edge, where mobile pack ice and episodic polynya opening allow for wind-induced mixing of water properties and consequent weakening or degradation of the stratification. Locations at greater distance to the Lena River Delta are generally more susceptible to mixing due to the diminishing influence of Lena River freshwater discharge. The diversion of the Lena River freshwater plume during the previous summer plays a great role in determining lateral gradients of water properties on the southeastern Laptev Sea in the following winter. Additionally, brine rejection due to thermodynamic ice formation and surface heat loss associated with polynya openings have been found to enhance lateral gradients in water properties across the landfast ice edge. Overall, the results of this study have indicated pronounced spatial differences of oceanographic conditions under the landfast ice on the southeastern Laptev Sea shelf, which are influenced by the presence of immobile landfast ice, polynya openings, and preconditioning of the inner Laptev Sea shelf during the previous summer by the variable extent of the Lena River freshwater plume and possible heat accumulation in the interior water column. However, the complex interactions between these influences need further investigation. In particular, enhancing the understanding about the processes which influence heat storage in the interior water column under the landfast ice is highly desirable as overwintered heat may potentially contribute to ice melting.

As expected, the winter circulation and water properties under the landfast ice on the southeastern Laptev Sea are characterized by high temporal variability. The analysis of detailed short-term time series of salinity, temperature, and current velocities obtained under the landfast ice in winter 2012 has provided some insights into the complex interactions between different forcing mechanisms of the under-ice current regime on the inner Laptev Sea shelf, which induce changes in water properties on short timescales during the ice-covered season. Particularly strong changes of the circulation and hydrographic conditions near the landfast ice edge have been linked to the opening of a flaw polynya in the southeastern Laptev Sea in response to prolonged northwestward winds over the Laptev Sea in April 2012. The event has been observed to significantly enhance lateral salinity and temperature gradients across the landfast ice edge due to surface heat loss and brine rejection associated with sea ice formation. Convective mixing in the polynya in combination with strong northwestward winds likely induced an offshore directed surface current and a counter current at depth, possibly leading to the development of a circulation cell under the landfast ice. Advection of fresher and warmer water masses from inshore regions additionally enhanced lateral gradients of water properties near the landfast ice edge. Pronounced semidiurnal fluctuations of salinity and temperature in the pycnocline near the landfast ice edge with amplitudes of up to 15 psu and 0.5 °C have been interpreted to reflect the episodic advection of cooler and more saline water masses from beyond the landfast ice edge by tides, superimposed on the described polynya-generated circulation cell. The enhanced vertical and lateral salinity and temperature gradients observed at the onset of the polynya opening have been identified to diminish over the course of the polynya event, indicating the occurrence of pronounced mixing processes initiated by oceanic currents. As a result, the vertical stratification of the water column near the landfast ice edge is significantly weakened after the closure of the polynya. Moreover, an increase in salinity and a decrease in temperature have been observed near the landfast ice edge after the closure of the polynya, which are likely the result of advection of cooler and more saline water masses from beyond the landfast ice edge in response to southward wind-driven residual currents. Additionally, pronounced changes of bottom temperatures at greater distance to the landfast ice edge over the course of the polynya event have indicated that polynya activity may have a considerable effect on the hydrographic conditions under the landfast ice at larger spatial scales than previously identified. However, the linkages between the current regime and hydrography at different locations under the landfast ice are not fully understood yet and need further investigation. As the circulation under the landfast ice exhibits pronounced temporal variability and is highly complex due to the interplay between tidal dynamics, wind forcing, and thermohaline forcing, additionally modified polynya activity, detailed long-term measurements of current velocities and water properties are desirable to investigate large-scale circulation patterns as well as their temporal variability under the landfast ice on the southeastern Laptev Sea shelf in future studies.

6. References

Alexandrov, V. Y., Martin, T., Kolatschek, J., Eicken, H., Kreyscher, M., Makshtas, A. P. (2000): Sea ice circulation in the Laptev Sea and ice export to the Arctic Ocean: Results from satellite remote sensing and numerical modeling. Journal of Geophysical Research, 105(C7), 17143-17159, doi: 10.1029/2000JC900029.

Bareiss, J., Eicken, H., Helbig, A., Martin, T. (1999): Impact of river discharge and regional climatology on the decay of sea ice in the Laptev Sea during spring and early summer. Arctic, Antarctic, and Alpine Research, 31(3), 214-229, doi: 10.2307/1552250.

Bareiss, J., Görgen, K. (2005): Spatial and temporal variability of sea ice in the Laptev Sea: Analyses and review of satellite passive-microwave data and model results, 1979 to 2002. Global and Planetary Change, 48(1), 28-54, doi: 10.1016/j.gloplacha.2004.12.004.

Bauch, D., Dmitrenko, I., Kirillov, S., Wegner, C., Hölemann, J., Pivovarov, S., Timokhov, L., Kassens, H. (2009): Eurasian Arctic shelf hydrography: Exchange and residence time of southern Laptev Sea waters. Continental Shelf Research, 29(15), 1815-1820, doi: 10.1016/j.csr.2009.06.009.

Berrisford, P., Dee, D. P., Poli, P., Brugge, R., Fielding, K., Fuentes, M., Kållberg, P. W., Kobayashi, S., Uppala, S., Simmons, A. (2011): The ERA-Interim archive Version 2.0. ERA report series, European Centre for Medium Range Weather Forecasts, Reading, UK. http://www.ecmwf.int/sites/default/files/elibrary/2011/8174-era-interim-archive-version-20.pdf, retrieved 16/02/2017.

Bowden, K. F. (1983): Physical Oceanography of Coastal Waters. Ellis Horwood Limited, Chichester.

Brumley, B. H., Cabrera, R. G., Deines, K. L., Terray, E. A. (1991): Performance of a broad-band acoustic Doppler current profiler. IEEE Journal of Oceanic Engineering, 16(4), 402-407, doi: 10.1109/48.90905.

Cavalieri, D. J., Parkinson, C., Gloersen, P., Zwally, H. J. (2008): Sea ice concentrations from Nimbus-7 SMMR and DMSP SSM/I-SSMIS passive microwave data, 1998-2011. NASA DAAC at the Snow and Ice Data Center, Boulder, CO, doi: 10.5067/8GQ8LZQVL0VL.

Chaudhuri, A. H., Ponte, R. M., Nguyen, A. T. (2014): Comparison of atmospheric reanalysis products for the Arctic Ocean and implications for uncertainties in the air-sea fluxes. Journal of Climate, 27(14), 5411-5421, doi: 10.1175/JCLI-D-13-00424.1.

Chen, C., Gao, G., Qi, J., Proshutinsky, A., Beardsley, R. C., Kowalik, Z., Lin, H., Cowles, G. (2009): A new high-resolution unstructured grid finite volume Arctic Ocean model (AO-FVCOM): an application for tidal studies. Journal of Geophysical Research, 114, C08017, doi: 10.1029/2008JC004941.

Dai, A., Trenberth, K. E. (2002): Estimates of freshwater discharge from continents: Latitudinal and seasonal variations. Journal of Hydrometeorology, 3, 660-687.

Danielson, S., Kowalik, Z. (2005): Tidal currents in the St. Lawrence Island region. Journal of Geophysical Research, 110, C1004, doi: 10.1029/2004JC002463.

Dee, D. P., Uppala, S. M., Simons, A. J., Berrisford, P., Poli, P., Kobayashi, S., Andrae, U., Balmaseda, M. A., Balsamo, G., Bauer, P., Bechthold, P., Beljaars, A. C. M., van de Berg, L., Bidlot, J., Bormann, N., Delsol, C., Dragani, R., Fuentes, M., Geer, A. J., Haimberger, L., Healy, S. B., Hersbach, H., Hólm, E. V., Isaken, L., Kållberg, P., Köhler, M., Matricardi, M., McNally, A. P., Monge-Sanz, B. M., Morcrette, J.-J., Park, B.-K., Peubey, C., de Rosnay, P., Tavolato, C., Thépaut, J.-N., Vitart, F. (2011): The ERA-Interim reanalysis: configuration and performance of the data assimilation system. Quarterly Journal of the Royal Meteorological Society, 134(656), 553-597, doi: 10.1002/qj.828.

Dmitrenko, I., Hölemann, J., Kirillov, S., Berezovskaya, S., Ivanova, D., Eicken, H., Kassens, H. (2002): The impact of sea ice on the periodic shallow water dynamics in the Laptev Sea (Siberian Arctic). Paper presented at 16th IAHR International Synopsium on Ice: Ice in the Environment, International Association for Hydro-Environment Engineering and Research, Dunedin.

Dmitrenko, I. A., Tyshko, K. N., Kirillov, S., Eicken, H., Hölemann, J. A., Kassens, H. (2005): Impact of flaw polynyas on the hydrography of the Laptev Sea. Global Planetary Change, 48(13), 9-27, doi: 10.1016/j.gloplacha.2004.12.016.

Dmitrenko, I. A. Kirillov, S. A., Tremblay, L. B. (2008): The long-term and interannual variability of summer fresh water storage over the eastern Siberian shelf: Implication for climatic change. Journal of Geophysical Research, 113, C03007, doi: 10.1029/2007JC004304.

Dmitrenko, I. A., Kirillov, S. A., Tremblay, L. B., Bauch, D., Willmes, S. (2009): Sea-ice production over the Laptev Sea shelf inferred from historical summer-to-winter hydrographic observations of 1960s-1990s. Geophysical Research Letters, 36(13), L13605, doi: 10.1029/2009GL038775.

Dmitrenko, I. A., Wegner, C., Kassens, H., Kirillov, S. A., Krumpen, T., Heinemann, G., Helbig, A., Schröder, D., Hölemann, J. A., Klagge, T., Tyshko, K. P., Busche, T. (2010a): Observations of supercooling and frazil ice formation in the Laptev Sea coastal polynya. Journal of Geophysical Research, 115, C05015, doi: 10.1029/2009JC005798.

Dmitrenko, I. A., Kirillov, S. A., Krumpen, T., Makhotin, M., Povl Abrahamsen, E., Willmes, S., Bloshkina, E., Hölemann, J. A., Kassens, H., Wegner, C. (2010b): Wind-driven diversion of summer river runoff preconditions the Laptev Sea coastal polynya hydrography: Evidence from summer-to-winter hydrographic records of 2007-2009. Continental Shelf Research, 30(15), 1656-1664, doi: 10.1016/j.csr.2010.06.012.

Dmitrenko, I. A., Kirillov, S. A., Tremblay, L. B., Bauch, D., Hölemann, J. A., Krumpen, T., Kassens, H., Wegner, C., Heinemann, G., Schröder, D. (2010c): Impact of Arctic Ocean Atlantic water layer on Siberian shelf hydrography. Journal of Geophysical Research, 115, C08010, doi: 10.1029/2009JC006020.

Dmitrenko, I. A., Kirillov, S. A., Bloshkina, E., Lenn, Y.-D. (2012): Tide-induced vertical mixing in the Laptev Sea coastal polynya. Journal of Geophysical Research, 117, C00G14, doi: 10.1029/2011JC006966.

Dovgaya, S. V., Cherkesov, L. V. (2001): Investigation of transformations of barotropic tides in the coastal zone. Physical Oceanography, 11(4), 323-332, doi: 10.1007/BF02509227.

Emery, W. J., Thomson, R. E. (1998): Data analysis methods in oceanography. Pergamon, New York.

Fofonoff, P., Millard, R. C. (1983): Algorithms for computation of fundamental properties of seawater. UNESCO Technical Papers in Marine Science, 44, 53.

Fofonova, V., Androsov, A., Danilov, S., Janout, M., Sofina, E., Wiltshire, K. H. (2014): Semidiurnal tides in the Laptev Sea Shelf zone in the summer season. Continental Shelf Research, 73, 119-132, doi: 10.1016/j.csr.2013.11.010.

Fofonova, V., Danilov, S., Androsov, A., Janout, M., Bauer, M., Overduin, P., Itkin, P., Wiltshire, K. H. (2015): Impact of wind and tides on the Lena River freshwater plume dynamics in the summer season. Ocean Dynamics, 65, 951-968, doi: 10.1007/s10236-015-0847-5.

Francis, J. A. (2002): Validation of reanalysis upper-level winds in the Arctic with independent rawinsonde data. Geophysical Research Letters, 29(9), 29-1 – 29-4, doi: 10.1029/2001GL014578.

Godin, G. (1972): The analysis of tides. Liverpool University Press, Liverpool.

Greene, C. (2012): SEAWATER_FREEZETEMP. MATLAB tool.
https://de.mathworks.com/matlabcentral/fileexchange/36435-sea-water-freezing-temperature-calculator,
retrieved 10/10/2017.

Gutjahr, O., Heinemann, G., Preußer, A., Willmes, S., Drüe, C. (2016): Quantification of ice production in Laptev Sea polynyas and its sensitivity to thin-ice parameterizations in a regional climate model. The Cryosphere, 10, 2999-3019, doi: 10.5194/tc-10-2999-2016.

Hinzmann, L. D., Bettez, N. D., Bolton, W. R., Chapin, F. S., Dyurgerov, M. B., Fastie, C. L., Griffith, B., Hollister, R. D., Hope, A., Huntington, H. P., Jensen, A. M., Jia, G. J., Jorgenson, T., Kane, D. L., Klein, D. R., Kofinas, G., Lynch, A. H., Lloyd, A. H., McGuire, A. D., Nelson, F. E., Oechel, W. C., Osterkamp, T. E., Racine, C. H., Romanovsky, V. E., Stone, R. S., Stow, D. A., Sturm, M., Tweedie, C. E., Vourlitis, G. L., Walker, M. D., Walker, D. A., Webber, P. J., Welker, J. M., Winker, K. S., Yoshikawa, K. (2005): Evidence and implications of recent climatic change in northern Alaska and other Arctic regions. Climatic Change, 72(3), 251-298, doi: 10.1007/s10584-005-5352-2.

Hölemann, J. A., Kirillov, S., Klagge, T., Novikhin, A., Kassens, H., Timokhov, L. (2011): Near-bottom warming in the Laptev Sea in response to atmospheric and sea ice conditions in 2007. Polar Research, 30, 6425, doi: 10.3402/polar.v30i0.6425.

Holland, M. M., Finnis, J., Serreze, M. C. (2006): Simulated Arctic Ocean freshwater budgets in the twentieth and twenty-first centuries. Journal of Climate, 19, 6621-6642, doi: 10.1175/JCLI3967.1.

Horn, W. (1960): Some recent approaches to tidal problems. International Hydrographic Review, 37(2), 65-88.

Itkin, P., Losch, M., Gerdes, R. (2015): Landfast ice affects the stability of the Arctic halocline: Evidence from a numerical model. Journal of Geophysical Research Oceans, 120, 2622-2635, doi: 10.1002/2014JC010353.

Ivanov, V. V., Golovin, P. N. (2007): Observations and modeling of dense water cascading from the northwestern Laptev Sea shelf. Journal of Geophysical Research, 112, C09003, doi: 10.1029/2006JC003882.

Jakobson, E., Vihma, T., Palo, T., Jakobson, L., Keernik, H., Jaagus, J. (2012): Validation of atmospheric reanalyses over the central Arctic Ocean. Geophysical Research Letters, 39, 10, L10802, doi: 10.1029/2012GL051591.

Jakobsson, M., Macnab, R., Mayer, L., Anderson, R., Edwards, M., Hatzky, J., Schenke, H. W., Johnson, P. (2008): An improved bathymetric portrayal of the Arctic Ocean: Implications for ocean modeling and geological, geophysical and oceanographic analyses. Geophysical Research Letters, 35(7), L07602, doi: 10.1029/2008GL033520.

Janout, M. A., Hölemann, J., Krumpen, T. (2013): Cross-shelf transport of warm and saline water in response to sea ice drift on the Laptev Sea shelf. Journal of Geophysical Research, 118, 563-576, doi: 10.1029/2011JC007731.

Janout, M. A., Lenn, Y.-D. (2014): Semidiurnal tides on the Laptev Sea shelf with implications for shear and vertical mixing. Journal of Physical Oceanography, 44, 202-219, doi: 10.1175/JPO-D-12-0240.1.

Janout, M. A., Hölemann, J., Juhls, B., Krumpen, T., Rabe, B., Bauch, D., Wegner, C., Kassens, H., Timokhov, L. (2016): Episodic warming of near-bottom waters under the Arctic sea ice on the central Laptev Sea shelf. Geophysical Research Letters, 43, doi: 10.1002/2015GL066565.

Janout, M. A., Hölemann, J., Timokhov, L., Gutjahr, O., Heinemann, G. (2017): Circulation in the northwest Laptev Sea in the eastern Arctic Ocean: Crossroads between Siberian river water, Atlantic water and polynya-formed dense water. Journal of Geophysical Research, 122(8), 6630-6647, doi: 10.1002/2017JC013159.

Johnson, M., Polyakov, I. V. (2001): The Laptev Sea as a source for recent Arctic Ocean salinity change. Geophysical Research Letters, 28(10), 2017-2020.

Joseph, A. (2014): Measuring ocean currents. Tools, technologies, and data. Elsevier, San Diego.

Kagan, B. A., Romanenkov, D. A., Sofina, E. V. (2008): Tidal drift and ice-generated changes in the tidal dynamics/energetic on the Siberian continental shelf. Continental Shelf Research, 28(3), 351-368, doi: 10.1016/j.csr.2007.09.004.

Kassens, H., Bauch, H. A., Dmitrenko, I. A., Eicken, H., Hubberten, H.-W., Melles, M., Thiede, J., Timokhov, L. (1999): Land-ocean systems in the Siberian Arctic: Dynamics and history. Springer, New York, 711 pp.

Kern, S., Harms, I., Bakan, S., Chen, Y. (2005): A comprehensive view of Kara Sea polynya dynamics, sea-ice compactness and export model and remote sensing data. Geophysical Research Letters, 32(15), L15501, doi: 10.1029/2005GL023532.

Kirillov, S. A., Dmitrenko, I. A., Hölemann, J. A., Kassens, H., Bloshkina, E. (2013): The penetrative mixing in the Laptev Sea coastal polynya pycnocline layer. Continental Shelf Research, 63, 34-42, doi: 10.1016/j.csr.2013.04.040.

Kowalik, Z., Proshutinsky, A. Y. (1994): The Arctic Ocean tides. In Johannessen, O. M., Muench, R. D., Overland, J. E. (eds.): The Polar Oceans and their role in shaping the global environment (eds). American Geophysical Union, Washington, D. C., pp. 137-158, doi: 10.1029/GM085p0137.

Kwok, R., Cunningham, G. F., Hibler, W. D. (2003): Sub-daily ice motion and deformation from RADARSAT observations. Geophysical Research Letters, 30, 2218, doi: 10.1029/2003GL018723.

Krumpen, T., Hölemann, J. A., Willmes, S., Morales Maqueda, M. A., Busche, T., Dmitrenko, I. A., Gerdes, R., Haas, C., Heinemann, G., Hendricks, S., Kassens, H., Rabenstein, L., Schröder, D. (2011): Sea ice production and water mass modification in the eastern Laptev Sea. Journal of Geophysical Research, 116, C05014, doi: 10.1029/2010JC006545.

Lenn, Y.-D., Rippeth, T. P., Old, C. P., Bacon, S., Polyakov, I., Ivanov, V., Hölemann, J. A. (2011): Intermittent intense turbulent mixing under ice in the Laptev Sea Continental Shelf. Journal of Physical Oceanography, 41(3), 531-547, doi: 10.1175/2010JPO4425.1.

Lindsay, R., Wensnahan, M., Schweiger, A., Zhang, J. (2014): Evaluation of seven different reanalysis products in the Arctic. Journal of Climate, 27, 2588-2605, doi: 10.1175/JCLI-D-13-00014.1.

Mahoney, A. R., Barry, R. G., Smolyanitsky, V., Fetterer, F. (2008): Observed sea ice extent in the Russian Arctic, 1933-2006. Journal of Geophysical Research, 113, C11005, doi: 10.1029/2008JC004830.

Makinson, K., Schröder, M., Østerhuis, S. (2006): Effect of critical latitude and seasonal stratification on tidal current profiles along Ronne Ice Front, Antarctica. Journal of Geophysical Research, 111, C03022, doi: 10.1029/2005JC0030.

Martin, S., Kauffman, P. (1981): A field and laboratory study of wave dumping by grease ice. Journal of Glaciology, 27, 283-313.

Morgan, P., Pender, L. (2003): CSIRO MatLab Seawater Library. MATLAB tool. https://de.mathworks.com/matlabcentral/linkexchange/links/741-seawater-library, retrieved 10/10/2017.

Morison, J. H., McPhee, M. G., Curtin, T. B., Paulson, C. A. (1992): The oceanography of winter leads. Journal of Geophysical Research, 97(C7), 11199-11218, doi: 10.1029/92JC00684.

Mysak, L. A. (2001): Patterns of Arctic circulation. Science, 293(5533), 1269-1270, doi: 10.1126/science.1064217.

Naidina, O. D. (2005): Paleogeography of the Laptev Sea eastern shelf in the first half of the Holocene based on faunal and palynological evidence. Stratigraphy and Geological Correlation, 14(3), 331-340, doi: 10.1134/S0869593806030075.

Naval Postgraduate School (2017): Navy operational ocean circulation and tides. http://www.oc.nps.edu/nom/day1/partc.html, retrieved 03/19/2017.

Padman, L., Kottmeier, C. (2000): High-frequency ice motion and divergence in the Weddell Sea. Journal of Geophysical Research, 105(C2), 3379-3400, doi: 10.1029/1999JC900267.

Pavlov, V. K., Pavlov, P. V. (1999): Features of seasonal and interannual variability of the sea level and water circulation in the Laptev Sea. In Kassens, H., Bauch, H. A., Dmitrenko, I. A., Eicken, H., Hubberten, H.-W., Melles, M., Thiede, J., Timokhov, L. A. (eds.): Land-ocean systems in the Siberian Arctic: Dynamics and history, Springer, New York, pp. 3-16.

Pawlowicz, R., Beardsley, B., Lentz, S. (2002): Classical tidal harmonic analysis including error estimates in MATLAB using T_TIDE. Computers & Geosciences, 28(8), 929-937, doi: 10.1016/S0098-3004(02)00013-4.

Peterson, B. J., Holmes, R. M., McClelland, J. W., Vörösmarty, C. J., Lammers, R. B., Shiklomanov, A. I., Shiklomanov, I. A., Rahmstorf, S. (2002): Increasing river discharge to the Arctic Ocean. Science, 298(5601), 2171-2173, doi: 10.1126/science.1077445.

Petrusevich, V., Dmitrenko, I. A., Kirillov, S. A., Kuzyk, Z. Z., Heath, J., Komarov, A., Eastwood, R., Barber, D. G., Ehn, J. K. (2016): Internal tidal wave propagation under the landfast sea ice in the southeast Hudson Bay. Conference Proceedings, CMOS/CGU 2016, Fredericton, Canada.

Pfirman, S. L., Colony, R., Nürnberg, D., Eicken, H., Rigor, I. G. (1997): Reconstructing the origin and trajectory of drifting Arctic sea ice. Journal of Geophysical Research, 102(C6), 12575-12586, doi: 10.1029/96JC03980.

Pradhan, H. K., Rao, A. D., Mohanty, S. (2015): Generation of internal tides: An interaction of tides with variable topography and coastal geometry. Ocean Science Journal, 50(2), 183-194, doi: 10.1007/s12601-015-0014-4.

Prinsenberg, S. J., Bennett, E. B. (1989): Vertical variations of tidal currents in shallow land fast ice covered regions. Journal of Physical Oceanography, 19(9), 1268-1278, doi: 10.1175/1520-0485(1989)019<1268:VVOTCI>2.0.CO;2.

Prinsenberg, S. J., Ingram, R. G. (1991): Under-ice physical oceanographic processes. Journal of Marine Systems, 2(1-2), 143-152, doi: 10.1016/0924-7963(91)90020-U.

Rainville, L., Woodgate, R. A. (2009): Observations of internal wave generation in the seasonally ice-free Arctic. Geophysical Research Letters, 36, L23604, doi:10.1029/2009GL041291.

Roberts, J., Roberts, T. D. (1978): Use of the Butterworth low-pass filter for oceanographic data. Journal of Geophysical Research Oceans, 83(C11), 5510-5514, doi: 10.1029/JC083iC11p05510.

Rosén, P.-O., Andersson, P. S., Alling, V., Morth, C.-M., Bjork, G., Semiletov, I., Porcelli, D. (2015): Ice exports from the Laptev and East Siberian Sea derived from $\delta^{18}O$ values. Journal of Geophysical Research Oceans, 120, 5997-6007, doi: 10.1002/2015JC010866.

Schwiderski, E. W. (1980): On charting global ocean tides. Reviews of Geophysics and Space Physics, 18(1), 243-269, doi: 10.1029/RG018i001p00243.

Selyuzhenok, V., Krumpen, T., Mahoney, A., Janout, M., Gerdes, R. (2015): Seasonal and interannual variability of fast ice extent in the southeastern Laptev Sea between 1999 and 2013. Journal of Geophysical Research Oceans, 120, 7791-7806, doi: 10.1002/2015JC011135.

Signell, R. (2000): PRINCAX. Principal axis, rotation angle, principal ellipse. MATLAB tool. https://woodshole.er.usgs.gov/operations/sea-mat/RPSstuff-html/princax.html, retrieved 10/10/2017.

Smith, J. D. (1973): Lead driven convection in the Arctic Ocean. EOS Transactions, AGU 54, 1108-1109.

Smith, D. C., Morison, J. H. (1993): A numerical study of haline convection beneath leads in sea ice. Journal of Geophysical Research, 98(C6), 10069-10083, doi: 10.1029/93JC00137.

Smith, S. D., Muench, R. D., Pease, C. H. (1990): Polynyas and leads: An overview of physical processes and environment. Journal of Geophysical Research, 95(C6), 9461-9479, doi: 10.1029/JC095iC06p09461.

Spreen, G., Kaleschke, L., Heygster, G. (2008): Sea ice remote sensing using AMSR-E 89-GHz channels. Journals of Geophysical Research: Oceans, 113(C2), 2156-2202, doi: 10.1029/2005JC003384.

Stedmon, C. A., Amon, R. M. W., Rinehart, A. J., Walker, S. A. (2011): The supply and characteristics of colored dissolved organic matter (CDOM) in the Arctic Ocean: Pan Arctic trends and differences. Marine Chemistry, 124, 108-118, doi: 10.1016/j.marchem.2010.12.007.

St-Laurent, P., Saucier, F. J., Dumais, J.-F. (2008): On the modification of tides in a seasonally ice-covered sea. Journal of Geophysical Research, 113(C11), C11014, doi: 10.1029/2007JC004614.

Thibodeau, B., Bauch D., Kassens, H., Timokhov, L. A. (2014): Interannual variations of river water content and distribution over the Laptev Sea between 2007 and 2011: Arctic Dipole connection. Geophysical Research Letters, 41(20), 7237-7244, doi: 10.1002/2014GL061814.

Thomson, R. E., Emery, W. J. (2014): Data analysis methods in physical oceanography. 3rd edition, Elsevier, Amsterdam.

Topham, D. R., Perkin, R. G. (1988): CTD sensor characteristics and their matching for salinity calculations. IEEE Journal of Oceanic Engineering, 13(3), 107-117, doi: 10.1109/48.564.

Visser, A. W., Souza, A. J., Hessner, K., Simpson, J. H. (1994): The effect of stratification on tidal current profiles in the region of freshwater influence. Oceanologica Acta, 17(4), 369-381.

Wang, J., Mizobata, K., Bai, X., Hu, H., Jin, M., Yu, Y., Ikeda, M., Johnson, W., Perie, W., Fujisaki, A. (2014): A modeling study of coastal circulation and landfast ice in the nearshore Beaufort and Chukchi seas using CIOM. Journal of Geophysical Research Oceans, 119(6), doi: 10.1002/2013JC009258.

Wegner, C., Bauch, D., Hölemann, J., Janout, M. A., Heim, B., Novikhin, A., Kassens, H., Timokhov, L. (2013): Interannual variability of surface and bottom sediment transport on the Laptev Sea shelf during summer. Biogeosciences, 10, 1117-1129, doi: 10.5194/bg-10-1117-2013.

Wegner, C., Wittbrodt, K., Hölemann, J. A., Janout, M. A., Krumpen, T., Selyuzhenok, V., Novikhin, A., Polyakova, Y., Krykova, I., Kassens, H., Timokhov, L. (2017): Sediment entrainment into sea ice and transport in the Transpolar Drift: A case study from the Laptev Sea in winter 2011/2012. Continental Shelf Research, 141, 1-10, doi: 10.1016/j.csr.2017.04.010.

Weingartner, T. J., Danielson, S. L., Potter, R. A., Trefry, J. H., Mahoney, A., Savoie, M., Irvine, C., Sousa, L. (2017): Circulation and water properties in the landfast ice zone of the Alaskan Beaufort Sea. Continental Shelf Research, 148, 185-198, doi: 10.1016/j.csr.2017.09.001.

Yu, Y., Stern, H., Fowler, C., Maslanik, J. (2014): Interannual variability of Arctic landfast ice between 1976 and 2007. Journal of Climate, 27(1), 227-243, doi: 10.1175/JCLI-D-13-00178.1.